الجمهورية الجزائرية الديمقراطية الشعبية
République Algérienne Démocratique Et Populaire
وزارة التعليم العالي والبحث العلمي
Ministère de L'Enseignement Supérieur et de La Recherche Scientifique
جامعة فرحات عباس- سطيف1
Université Ferhat Abbas - Sétif 1

THÈSE

Présentée à l'Institut d'Optique et Mécanique de Précision pour l'obtention du Diplôme de

DOCTORAT 3ème Cycle LMD

Domaine : Sciences et Techniques
Filière : Optique et mécanique de Précision
Spécialité: Optique et Photonique Appliqué

Par
Abdeldjalil Benstiti

Thème

Etude du comportement de l'interaction d'un faisceau laser avec une onde acoustique

Soutenue, le: 24/06/2021 **Devant le jury composé de:**

Président du Jury	**B.Belloui**	**Prof**	**F.A.U Setif -1**
Directeur de thèse	**K. Ferria**	**Prof**	**F.A.U Setif -1**
Co-directeur de thèse	**A. Bencheikh**	**MCA**	**BBA.U**
Examinateur	**A.Guessoum**	**MCA**	**F.A.U Setif -1**
Examinateur	**A.Latreche**	**Prof**	**BBA.U**

PEOPLE'S DEMOCRATIC REPUBLIC OF ALGERIA

MINISTRY OF HIGHER EDUCATIONAND SCIENTIFIC RESEARCH

FERHAT ABBAS UNIVERSITY – SETIF -1-

THESIS

Submitted to Institute of Optics and Precision Mechanics
For the degree

Of Phd
In Applied Optics and Photonics

By

Abdeldjalil Benstiti

Title

Behavior Study of a laser beam interaction with acoustic wave

Defended on: 24/06/2021 **In front of the composed committee of**

Chairman	**B.Belloui**	**Professor**	**F.A.U Setif -1**
Supervisor	**K. Ferria**	**Professor**	**F.A.U Setif -1**
Co-Supervisor	**A. Bencheikh**	**Assistant Professor**	**BBA.U**
Examiners	**A.Guessoum**	**Assistant Professor**	**F.A.U Setif -1**
Examiners	**A.Latreche**	**Professor**	**BBA.U**

Abstract

In this thesis, an acousto-optic technique based-beam shaping is presented through an analytical and a numerical analysis, which converts an input Gaussian beam into different output beam shapes, such as Flat-top, Doughnut, and Airy-like beams. A deep characterization that reveals the generated beam properties is also performed and discussed. As a result, flexible converting a Gaussian beam into a defined shape will have a significant impact on a myriad of current laser applications.

Acknowledgements

A doctoral thesis is often described as a solitary endeavour; however the long list that follows definitely proves the opposite!

Firstly, All the praises and thanks be to ALLAH, the most beneficent and merciful, for his grace and giving me this opportunity to increase my scientific knowledge, and his help to give patience to complete my research after all the both academical and personal challenges I exceeded. ALLAH says: " For should you try to count Allah's blessings, you could never compute them" (An-Nahl 16:18).

At first, I would like to express my deepest gratitude for the continuous support, insight and patience of my supervisors: Pr.Kouider FERRIA and Dr. AbdelHalim BENCHEIKH; thank you so much for accepting to advisor me in my PhD. For their excellent guidance, support and valuable suggestions over the past years. Without their constant trust and gentle prodding, this thesis would have not been completed. For sharing me their time and guiding me through every step of my work. Their confidence in my work inspired me. Thanks also to their useful comments on my thesis.

Foremost, I am deeply grateful the local where the content of the thesis was realized; Institute of optics and precision mechanics (IOMP), for the technical assistance during the four years.

I wish to extend my heartfelt thanks to all our team members; special mention to Mr. Houcine BEKKIS, Mr. Ouis BOUMEDIEN, Ms. Saoussane CHABBOU, Ms. Ouided MOUSSAOUI and Ms. Laarfa BEDDIEF, I am grateful to all of them for their

moral support in moments of weakness.

I am extremely thankful to my professors of IOMP all the Ten years I have been there for teaching me new things, they kept me informed about topical research topics on optics and for those specific human qualities. Special mention to Pr.Nabil BELKHIR, Dr. Belkacem BAKHOUCHE, Dr. AbdelHak BELKHIR, Pr. Said BOUZID, Dr. Ahmed MANALLAH, Pr. NacerDin DEMEGH, Pr. Khaled IYADI, Pr. Mouhamed BOUAFIA and Dr. Aicha MEDJAHED. I learned from them how to behave in research life, Thanks to their many pieces of advice and discussion and their availability all the time that I need them, and the big encouragement they gave.

I am very grateful to Pr B.Belloui, professor at the University of Farhat ABBES, Sétif 1, I am sensitive to the honor he gave me by agreeing to read this manuscript and for agreeing to serve as president of the panel. I would like to thank all members of the examining committee of this PhD thesis. Thanks to Dr. A.Guessoum, MCA at the University of Farhat ABBES, Sétif 1 and Pr A.Latreche Professor at the University of Bordj Bou Arreridj. For accepting the evaluation of my work, and for the time they spent reading and commenting my thesis.

Thanks so much to all my colleagues in IOMP for cheering me this experience; I'm so thankful to the moments spent to gather.

Special thanks to my sincere wife, Meriem ALOUI has been a true and great supporter during my good and bad times. She has faith in me and my intellect even when I felt like digging hole and crawling into one because I didn't have faith in myself. These past several years have not been an easy ride, both academically and personally. I truly thank her for sticking by my side, even when I was irritable and depressed.

My endless gratitude goes to My hard-working parents have sacrificed their lives for us. their extreme attention to my education and their extreme emotional support,

encouragement, provided unconditional love and care for their endless support.

Also thanks so much for my beloved brothers; Mouhamed Amine, Lazhar, Adel , and Youcef. I love them and I thank them for all their advice, support, invocations and encouragement.

Dedication

To my princess; the joy of my life..
to my daughter "Ihssane" I dedicate this thesis.

AbdelDjalil

Contents

List of Figures

List of Tables

List of Publications

1. **Abdeldjalil Benstiti**, Kouider Ferria, and Abdelhalim Bencheikh. Generation of avariety of airy beams using a dynamic diffractive optical phase element.JOSA B,37(11):A45–A53, 2020.

2. Abdelhalim Bencheikh, Saoussene Chabou, Ouis Chouaib Boumeddine, Hocine Bekkis, **Abdeldjalil Benstiti**, Laarfa Beddiaf, and Widad Moussaoui. Cosine beam: diffraction-free propagation and self-healing.JOSA A, 37(11):C7–C14, 2020.

List of Conferences

International

1. **Abdeldjalil Benstiti**, Kouider Ferria, and Abdelhalim Bencheikh. "Airy beam generation using acoustooptical cell: Acoustic wavelength effect", CIPCQ'19, poster communication, Bejaia university, November, 04-06, 2019

2. **Abdeldjalil Benstiti**, Kouider Ferria, and Abdelhalim Bencheikh. "Propagation of truncated Gaussian beam through acousto-optic cell", ICIMM2018, poster communication, setif university, Octobre, 28-29, 2018.

3. **Abdeldjalil Benstiti**, Kouider Ferria, and Abdelhalim Bencheikh. "Interaction of a Gaussian laser beam with an acousto-optical cell", ICRA2017, oral communication, Algers university, November, 20-22, 2017

National

1. **Abdeldjalil Benstiti**, Kouider Ferria, and Abdelhalim Bencheikh. "Caractérisation paramétrique d'un faisceau Gaussien mise en forme par une cellule acousto-optique ", SENALAP8, poster communication, TAGHIT (5-9) Novembre 2017

General introduction

The perfect computer has been developed.
You just feed in your problems and they never come out again.
Al Goodman

NOWADAYS, lasers are every where, in our daily life, we use lasers in electronics devices remote control, in DVD lectures, etc.... Lasers are also are extensively used in industry, communication, meteorology and almost in every field. The main keys for the lasers usage are the intensity (power) and the spatial structure of the laser beam. For that reason the hot topic of structured light becomes of a big interest. As it is commonly known, the transverse profile of laser beams is theoretically modeled by the Gaussian function, hence its name the fundamental Gaussian beam[1]. Since lasers are applied in a variety of fields, the Gaussian beams model becomes less enough to achieve all laser's applications. For that reason, laser beams with customized profiles and structures are needed[2, 3], to be used in optical communication[4], optical tweezing [5], material processing [6, 7], and even in quantum experiments [8]. It is worth noting, that laser beam shaping consists on transforming a given Gaussian beam into a customized beam shape, using different techniques[9–15] The main technique used for shaping laser beams is based on diffractive optics[16–18], where an optical diffractive element (of phase or amplitude) is used to structure a given input Gaussian beam into another well shaped beam [19–21]. The present thesis is dedicated to a Gaussian laser beam shaping using another type of diffractive elements, here we use instead the usual

optical elements, we will use an acoustooptics cell to shape the laser beam[22–25]. The acoustic-optic cell consists on a liquid medium (water), in which an ultrasound wave is propagating and creating an elastic wave, the latter is manifested as a refractive index variation (sinusoidal). The phase transmittance created by the ultrasound wave allowed the manipulation of the input laser beam structure, by tuning the different parameters of the couple (laser beam and acousto-optic cell) we can shape the input laser beam at will. Throughout this thesis, we will demonstrate many beam shaping of an input Gaussian beam, into flat top, doughnut, and accelerated beams.
The thesis is organized as follows:

Chapter 1 is dedicated to Gaussian beam and acoustic waves theory, to understand the theoretical basics of acousto-optical interaction, the beam shaping and light guiding. Chapter 2 is reserved to the parametric characterization of the diffracted Gaussian beams by the acousto-optic cell. In this chapter we use mainly the Kurtosis parameter for the beam flatness characterization. Chapter 3 is dedicated to the theoretical study of the generation of hyperbolic tunable Airy-like beams using a truncated acousto-optical effect. Chapter 4 focuses on the generation of a variety of combined Airy beams (Dual and Quad) using a dynamic standing ultrasound wave.

The thesis is resumed by a general conclusion and future perspectives.

Bibliography

[1] Fred M Dickey. *Laser beam shaping: theory and techniques*. CRC press, 2018.

[2] LA Romero and FM Dickey. Lossless laser beam shaping. *JOSA A*, 13(4):751–760, 1996.

[3] David L Shealy and John A Hoffnagle. Laser beam shaping profiles and propagation. *Applied optics*, 45(21):5118–5131, 2006.

[4] Mona Mayeh and Faramarz Farahi. Laser beam shaping and mode conversion in optical fibers. *Photonic Sensors*, 1(2):187–198, 2011.

[5] Gavin Sinclair, Jonathan Leach, Pamela Jordan, Graham Gibson, Eric Yao, Zsolt John Laczik, Miles J Padgett, and Johannes Courtial. Interactive application in holographic optical tweezers of a multi-plane gerchberg-saxton algorithm for three-dimensional light shaping. *Optics Express*, 12(8):1665–1670, 2004.

[6] Anna Möhl, Sebastian Kaldun, Clemens Kunz, Frank A Müller, Ulrike Fuchs, and Stephan Gräf. Tailored focal beam shaping and its application in laser material processing. *Journal of Laser Applications*, 31(4):042019, 2019.

[7] Jiangning Li, Zheng Kuang, Stuart Edwardson, Walter Perrie, Dun Liu, and Geoff Dearden. Imaging-based amplitude laser beam shaping for material processing by 2d reflectivity tuning of a spatial light modulator. *Applied Optics*, 55(5):1095–1100, 2016.

[8] Philip Zupancic, Philipp M Preiss, Ruichao Ma, Alexander Lukin, M Eric Tai, Matthew Rispoli, Rajibul Islam, and Markus Greiner. Ultra-precise holographic beam shaping for microscopic quantum control. *Optics express*, 24(13):13881–13893, 2016.

[9] Fred M Dickey, Louis S Weichman, and Richard N Shagam. Laser beam shaping techniques. In *High-Power Laser Ablation III*, volume 4065, pages 338–348. International Society for Optics and Photonics, 2000.

[10] Tatiana Latychevskaia, Daniel Schachtler, and Hans-Werner Fink. Creating airy beams employing a transmissive spatial light modulator. *Applied optics*, 55(22): 6095–6101, 2016.

[11] GA Siviloglou, J Broky, A Dogariu, and DN Christodoulides. Observation of accelerating airy beam ballistics. In *Quantum Electronics and Laser Science Conference*, page QTuI4. Optical Society of America, 2008.

[12] Andreas Valdmann, Peeter Piksarv, Heli Valtna-Lukner, and Peeter Saari. White-light hyperbolic airy beams. *Journal of Optics*, 20(9):095605, 2018.

[13] Jianqiang Ma, Yan Li, Qizhi Yu, Zongfeng Yang, Yanlei Hu, and Jiaru Chu. Generation of high-quality tunable airy beams with an adaptive deformable mirror. *Optics letters*, 43(15):3634–3637, 2018.

[14] Don M Cottrell, Jeffrey A Davis, and Thomas M Hazard. Direct generation of accelerating airy beams using a 3/2 phase-only pattern. *Optics letters*, 34(17): 2634–2636, 2009.

[15] HT Dai, XW Sun, D Luo, and YJ Liu. Airy beams generated by a binary phase element made of polymer-dispersed liquid crystals. *Optics express*, 17(22):19365–19370, 2009.

[16] Sensen Li, Yulei Wang, Zhiwei Lu, Lei Ding, Pengyuan Du, Yi Chen, Zhenxing Zheng, Dexin Ba, Yongkang Dong, Hang Yuan, et al. High-quality near-field beam

achieved in a high-power laser based on slm adaptive beam-shaping system. *Optics Express*, 23(2):681–689, 2015.

[17] Sensen Li, Zhiwei Lu, Pengyuan Du, Yulei Wang, Lei Ding, and Xiusheng Yan. Beam shaping by using small-aperture slm and dm in a high power laser. In *Young Scientists Forum 2017*, volume 10710, page 107103Q. International Society for Optics and Photonics, 2018.

[18] Alexander B Stilgoe, Anatolii V Kashchuk, Daryl Preece, and Halina Rubinsztein-Dunlop. An interpretation and guide to single-pass beam shaping methods using slms and dmds. *Journal of Optics*, 18(6):065609, 2016.

[19] Michael Mazilu, Joerg Baumgartl, Tomas Čižmár, and Kishan Dholakia. Accelerating vortices in airy beams. In *Laser Beam Shaping X*, volume 7430, page 74300C. International Society for Optics and Photonics, 2009.

[20] Peter Muys and Eefje Vandamme. Direct generation of bessel beams. *Applied optics*, 41(30):6375–6379, 2002.

[21] Ming-Dar Wei, Wen-Long Shiao, and Yi-Tse Lin. Adjustable generation of bottle and hollow beams using an axicon. *Optics communications*, 248(1-3):7–14, 2005.

[22] NA Khilo, VN Belyi, NS Kazak, and PI Ropot. Acoustooptic refraction-influenced generation of tunable incomplete airy beams. *Journal of Optics*, 16(8):085702, 2014.

[23] Konstantin B Yushkov, Vladimir Ya Molchanov, Vladimir I Balakshy, and Sergey N Mantsevich. Acousto-optic transfer functions as applied to s laser beam shaping. In *Laser Beam Shaping XVIII*, volume 10744, page 107440Q. International Society for Optics and Photonics, 2018.

[24] Abdelhalim Bencheikh and Kouider Ferria. Gaussian laser beam tailoring using acoustooptic cell. *Optics & Laser Technology*, 44(4):806–809, 2012.

[25] K Ferria, A Bencheikh, and A Merabet. Doughnut beam generation using acousto-optic cell. In *2012 19th International Conference on Microwaves, Radar & Wireless Communications*, volume 2, pages 491–494. IEEE, 2012.

Chapter 1

Backgrounds and basics

I constantly sought knowledge and truth, and it became my belief that for gaining access to the effulgence and closeness to God, there is no better way than that of searching for truth and knowledge

Hasan Ibn al-Haytham

1.1 Introduction

ONE of the most important point in the laser science is the description of the spatial structure of laser beams. Which became opportunity for the theoretical and experimental scientific community. The usual starting point for the derivation of laser beam propagation modes is solving the scalar Helmholtz equation within the paraxial approximation[1, 2]. In this chapter, we start by describing the spatial profile of laser beams. Then, the derivation of the spatial profile of laser beams will be reviewed fundamental Gaussian beam profiles and its parameters. Secondly, fundamental principles of the ultrasound will take place. Where, the acoustic parameters will be well detailed in this section. Finally, acousto optic interaction theory will be illustrated by giving the theoretical and physical principles of the interaction between acoustic waves and laser beam in a liquid medium.

1.2 Gaussian beam theory

In this section, we will derive the governing equation for the electric field of a laser beam. A basic equations of electricity and magnetism can be used as a starting point for advanced development. The four Maxwell equations in vacuum are expressed as:

$$\vec{\nabla} \times \vec{E} + \frac{1}{c}\frac{\partial \vec{B}}{\partial t} = 0, \tag{1.1}$$

$$\vec{\nabla} \times \vec{H} - \frac{1}{c}\frac{\partial \vec{D}}{\partial t} = 0, \tag{1.2}$$

$$\vec{\nabla} \cdot \vec{D} = 0, \tag{1.3}$$

$$\vec{\nabla} \cdot \vec{B} = 0, \tag{1.4}$$

Where $\vec{E}$ and $\vec{H}$ are electric and magnetic fields. In addition, $\vec{D}$ and $\vec{B}$ are electric and magnetic flux densities defined as

$$\vec{D} = \epsilon_0 \vec{E} + 4\pi \vec{P} \text{ and } \vec{B} = \mu_0 \vec{H} + 4\pi \vec{M} \ . \tag{1.5}$$

Where ϵ_0 and μ_0 are the electric permittivity and the magnetic permeability respectively.

Polarization and magnetization densities $\left(\vec{P} \textit{ and } \vec{M}\right)$ are then introduced to define the electric and magnetic flux densities as follows:

$$\vec{P} = \chi \vec{E} \text{ and } \vec{M} = \eta \vec{H} \tag{1.6}$$

Where χ and η are the electric and the magnetic susceptibility

As such, the electric and magnetic flux densities can be simply expressed as

$$\begin{aligned} \vec{D} &= \epsilon_0 \vec{E} \\ \vec{B} &= \mu_0 \vec{H} \end{aligned} \tag{1.7}$$

The general wave equation for the electric field that governs the propagation of the electric field in free space. As for a linearly x-polarized electric field, the electric field propagating in the z-direction can be expressed in Cartesian coordinate as

$$\vec{E}\left(\vec{r}\right) = \hat{i} E_0\left(x, y, z\right) \exp\left(ikz\right). \tag{1.8}$$

We will only consider the electric field because all characteristics for the magnetic field are the same as those for the electric field, except for the magnitude of the field. Because the source-free region is considered, the divergence of the electric field is zero $\left(\vec{\nabla} \cdot \vec{E}\left(\vec{r}\right) = 0\right)$. Finally, the expression for the electric field is given by

$$\vec{\nabla} \cdot \vec{\nabla} \vec{E} + k^2 \vec{E}\left(\vec{r}\right) = 0. \tag{1.9}$$

Where k is light wave number.

By substituting Eq. (1.8) into Eq. (1.9), the equation becomes

$$\left(\frac{\partial^2}{\partial x^2}+\frac{\partial^2}{\partial y^2}+\frac{\partial^2}{\partial z^2}\right)\hat{i}E_0\left(x,y,z\right)\exp\left(ikz\right)+\hat{i}k^2E_0\left(x,y,z\right)\exp\left(ikz\right)=0. \tag{1.10}$$

Eq. (1.10) is referred to as a homogeneous Helmholtz equation, which describes the wave propagation in a source-free space. By differentiating the wave in the z-coordinate, we obtain

$$\frac{\partial}{\partial z}E_0\left(x,y,z\right)\exp\left(ikz\right)=ikE_0\left(x,y,z\right)\exp\left(ikz\right)+\frac{\partial E_0\left(x,y,z\right)}{\partial z}\exp\left(ikz\right), \tag{1.11}$$

and

$$\frac{\partial^2}{\partial z^2}E_0\left(x,y,z\right)\exp\left(ikz\right)=-k^2E_0\left(x,y,z\right)\exp\left(ikz\right)+2ik\frac{\partial E_0\left(x,y,z\right)}{\partial z}\exp\left(ikz\right)+\frac{\partial^2E_0\left(x,y,z\right)}{\partial z^2}\exp\left(ikz\right). \tag{1.12}$$

In many cases, the electric field slowly varies in the propagation direction (z-direction). The slow variation of the electric field in z-direction can make possible the following approximation (slowly varying approximation):

$$\left|\frac{\partial^2E_0\left(x,y,z\right)}{\partial z^2}\right|\ll 2\left|k\frac{\partial E_0\left(x,y,z\right)}{\partial z}\right| \tag{1.13}$$

By inserting Eq. (1.12) into Eq. (1.10) and using the assumption of Eq. (1.13), Eq. (1.10) becomes

$$\frac{\partial^2E_0\left(x,y,z\right)}{\partial x^2}+\frac{\partial^2E_0\left(x,y,z\right)}{\partial y^2}+2ik\frac{\partial E_0\left(x,y,z\right)}{\partial z}=0. \tag{1.14}$$

Scribes how the linearly polarized electric field propagates in the z direction in the Cartesian coordinate.

The solutions of the paraxial wave equation are known. This solution is as follows :

$$E_0(x,y,z) = A\exp\left[-i\left(\Delta\phi(z) + \frac{k}{2q(z)}\left(x^2+y^2\right)\right)\right] \tag{1.15}$$

$\Delta\phi(z)$ phase shift
$q(z)$ represents a radius of curvature, or the transverse variation of the amplitude and curvature of the wavefront.

This particular solution, called **« Gaussian fundamental mode »**. We substitute the expression E_0 in the paraxial wave equation, we get that for all (x,y):

$$\left[\frac{k^2}{q^2(z)}\left(x^2+y^2\right)\left(\frac{dq}{dz}-1\right) - 2k\left(\frac{d\Delta\phi}{dz}+\frac{i}{q}\right)\right]A = 0 \tag{1.16}$$

We deduce that $q(z)$ and $\Delta\phi(z)$ be verified :

$$\frac{dq}{dz} = 1 \Rightarrow q(z) = q_0 + z \tag{1.17}$$

With $q_0 = q(0)$.

If $\Delta\phi(0) = 0$, we find:

$$\frac{d\Delta\phi}{dz} = \frac{-i}{q} \Rightarrow \Delta\phi(z) = -i\ln\left(\frac{q_0+z}{q_0}\right) \tag{1.18}$$

Moreover, we pose

$$\frac{1}{q(z)} = \frac{1}{R(z)} - i\frac{\lambda}{\pi w^2(z)} \tag{1.19}$$

We then have:

$$\exp\left[-i\Delta\phi(z)\right] = \frac{1}{1+\frac{z}{q_0}} = \frac{1}{1+\frac{z}{R_0}-\frac{i\lambda z}{\pi w_0^2}} \tag{1.20}$$

Where the index 0 indicates the values in $z = 0$ and w_0 is the waist. If we choose at the origin an infinite radius of curvature (plane wave), we have $q_0 = i\frac{\pi w_0^2}{\lambda}$. We can then easily show that :

$$\frac{1}{q(z)} = \frac{1}{q_0+z} = \frac{1/q_0}{1+z/q_0} = \frac{1}{1+\left(\frac{\lambda z}{\pi w_0^2}\right)^2}\left[\frac{1}{z}\left(\frac{\lambda z}{\pi w_0^2}\right)^2 - i\frac{\lambda}{\pi w_0^2}\right] \tag{1.21}$$

On the other hand, where $\tan\theta(z) = \frac{z}{Z_R}$ and Z_R is the Rayleigh distance

$$\exp\left[-i\Delta\phi(z)\right] = \frac{1}{1-\frac{iz}{Z_R}} = \frac{1}{\sqrt{1+\left(\frac{z}{Z_R}\right)^2}}\exp\left(i\theta(z)\right) \tag{1.22}$$

Finally, we obtain the fundamental expression of the Gaussian spherical wave:

$$E(x,y,z) = \frac{Aw_0}{w(z)}\exp\left[-ikz\right]\exp\left[i\theta(z)\right]\exp\left[ik\frac{(x^2+y^2)}{2q(z)}\right] \tag{1.23}$$

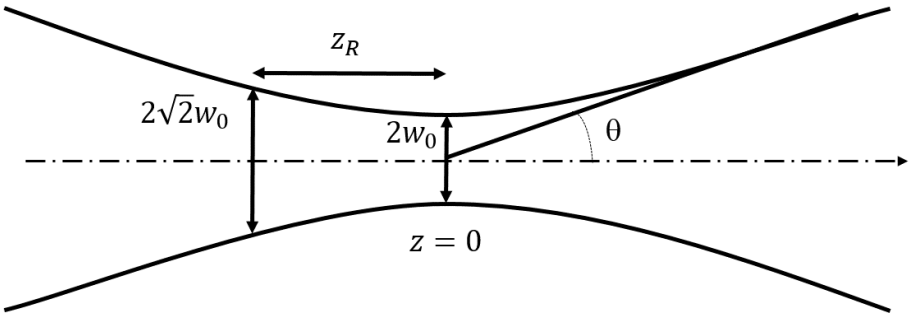

Figure 1.1: The Gaussian beam propagation parameters

The intensity profile of the Gaussian beam is :

$$I(x, y, z) = I_0 \exp\left[\frac{-2(x^2 + y^2)}{w^2(z)}\right] \tag{1.24}$$

The wave front curvature radius is:

$$R(z) = z\left[1 + \left(\frac{\pi w_0^2}{\lambda z}\right)\right] \tag{1.25}$$

The size of the Gaussian mode at any spatial plane is expressed as:

$$w(z) = w_0\sqrt{1 + \left(\frac{\lambda z}{\pi w_0^2}\right)^2} \tag{1.26}$$

1.3 Acoustic wave basics: fundamental principles of the ultrasound

The ultrasounds are acoustic waves,with a frequency greater than the upper limit of human hearing, about 15kHz[3].Ultrasound are mechanical vibrations that propagate, through various media including gases, liquids and solids, but cannot travel through a vacuum[4]. The ultrasonic wave propagates thanks to the elasticity of the medium that the propagation medium is submitted to a succession of pressure and depression[5].

1.3.1 Ultrasound parameters

Acoustic waves are governed by the same physical laws as electromagnetic waves. We consider an acoustic wave as the displacement of an infinitely small perturbation with respect to the conditions prevailing in the undisturbed medium. The particles move back and forth on either side of their position of equilibrium. They induce zones of compression and decompression moving through the elastic medium. An acoustic wave is characterized by many parameters:

1.3.1.1 Celerity and impedance

The celerity of the acoustic wave is the propagation speed of the pressure variation in the medium.The behavior of medium with respect to ultrasound is expressed by a constant called acoustic impedance Z. The acoustic impedance depends on the density and the compressibility of the medium or its ability to return to its original shape after deformation:

$$Z = \sqrt{\frac{\rho}{\chi_c}} \tag{1.27}$$

With Z , χ_c and ρ corresponding respectively to the mechanical impedance, the compressibility of the medium and the density.

The acoustic celerity is related to the mechanical impedance Z and the density of the medium by:

$$v = \frac{Z}{\rho_0} \tag{1.28}$$

1.3.1.2 Frequency and wavelength

Sounds are classified into four categories according to their frequency f_a or number of pressure per second $1Hz = 1cycle/s$:

Sounds	Frequency
infra-sound	0 to 20 Hz
audible sounds	20 Hz to 20 kHz
ultrasound	20 kHz to 1 GHz
hyper-sons	$>$ 1 GHz

Table 1.1: The range of sound according to their frequencies

The distance separating at a given moment two points of the path of the wave where the pressure is the same corresponds to the wavelength λ_a.that related to the frequency by the formula :

$$\lambda_a = \frac{v}{f_a} \tag{1.29}$$

With f_a and λ_a are respectively the frequency and the wavelength.

1.3.1.3 Pressure and intensity

At each point, the acoustic pressure p varies according to the frequency of the ultrasonic wave. The energy delivered depends on these pressure variations which subject the particles of the medium to vibratory movements. Ultrasonic intensity is the energy that crosses the unit area perpendicularly during the unit of time. It is related to the acoustic pressure by the formula :

$$I = \frac{p^2}{2\rho v} \tag{1.30}$$

1.3.2 Ultrasound propagation modes

Ultrasound energy used in flaw detection travels in different wave modes based on the direction of the wave and the corresponding motion of molecules in the test piece. The most commonly used modes are longitudinal waves, transverse waves, and surface waves(Rayleigh waves)

1.3.3 Propagation equation

In this development we use a sinusoidal plane ultrasonic wave which propagates in a medium along the x direction. The particles of the medium vibrate around an equilibrium position with the same frequency of ultrasonic wave . Differential equation that describes this vibration is:

$$\frac{\partial^2 X\left(x,t\right)}{\partial t^2} = v^2 \ \frac{\partial^2 X\left(x,t\right)}{\partial x^2} \tag{1.31}$$

Where: $X\left(x,t\right)$ is the position of the particle, x is the propagation direction, v is the celerity of ultrasonic wave.

The solution of equation Eq. (1.31) is:

$$X\left(x,t\right) = X_0 \ \sin\left(\Omega t - k_a x\right) \tag{1.32}$$

Where: X_0 the amplitude of vibration, k_a Ultrasonic wave module, Ω Ultrasonic wave pulsation.

The particle velocity is then given by:

$$X'\left(x,t\right) = \frac{dX\left(x,t\right)}{dt} = X_0 \ \Omega_0 \ \cos\left(\Omega t - k_a x\right) \tag{1.33}$$

The ultrasonic pressure variation in a given point is related to the particle velocity in the medium by equation:

$$\Delta p\,(x,t) = \rho_0\ v\ X'\,(x,t) \tag{1.34}$$

The ratio of the pressure to the velocity at a given point is then equal to the product of the initial density of the medium by the wave velocity, this ratio is constant

$$\frac{\Delta p\,(x,t)}{X'\,(x,t)} = \rho_0\ v \tag{1.35}$$

This equation is often called the Ohm law, in acoustics, and the preceding ratio is called the acoustic impedance Z of the medium

$$\Delta p\,(x,t) = Z\ X_0\ \Omega_0\ \cos\left(\Omega t - k_a x\right) \tag{1.36}$$

1.4 Acousto optic interaction theory

Propagation of an ultrasonic wave in a medium, creates zones of expansion and zones of compression which leads to a change in the refractive index of the medium. As a result an optical phase grating is created. The propagated light is then diffracted to different orders.

1.4.1 Diffraction regime

For acousto-optic interactions in liquids, an equation for the diffraction light intensity was obtained in terms of **Klein Cook parameter** Q[6, 7], in which an apprecia-

ble amount of light is transferred out of zero order into diffracted orders and can be examined by using the Kelin and Cook parameter, Eq. (1.37) shows the expression:

$$Q = \frac{k_a^2 L}{k} = \frac{2\pi\lambda L}{n_0 \lambda_a^2} \tag{1.37}$$

Where L and n_0 are the interaction distance and the medium index respectively.

1.4.1.1 Bragg Regime $Q > 1$

The Bragg regime is observed at high acoustic frequencies usually exceeding 100 MHz. The diffraction pattern of this regime even at large acoustic power, consists of two diffraction maxima of zero and first orders. At Bragg angle of incidence θ_B only one diffraction order is produced while the others are annihilated by destructive interference, the angle of deviation of the light beam is then equal to:

$$\theta = \arcsin\left(\frac{\lambda}{2n_0\lambda_a}\right) \tag{1.38}$$

1.4.1.2 Raman-Nath Regime $Q < 1$

The Raman-Nath regime is observed at relatively low acoustic frequencies at small acousto-optic interaction lengths. This type of diffraction takes place at an arbitrary incident angle of light roughly normal to the acoustic beam and the diffraction pattern contains many diffraction orders of symmetrically distributed light intensity given by Bessel functions, the diffraction angle of each order is given by:

$$\theta_m = m\frac{\lambda}{\lambda_a} \tag{1.39}$$

Fig. 1.2 shows the different regimes:

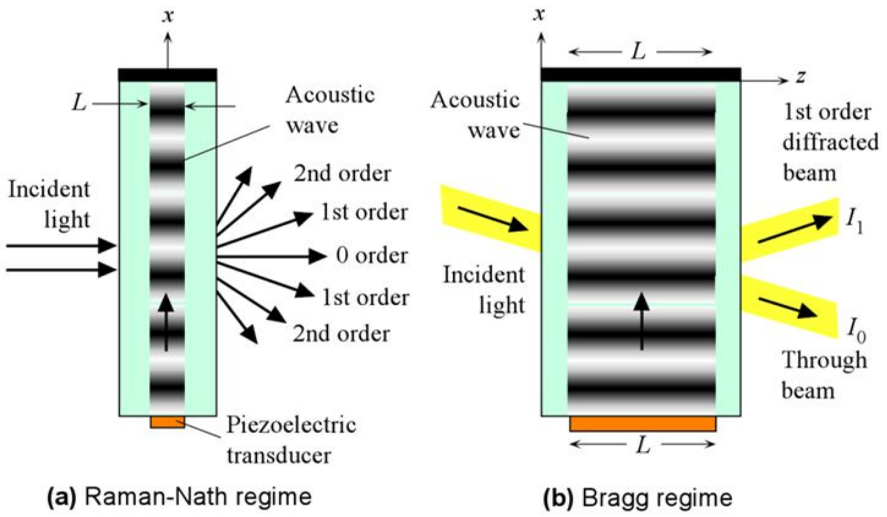

Figure 1.2: Illustration of Raman Nath and Bragg regimes

Bibliography

[1] FJ Duarte. *Laser Pulse Phenomena and Applications*. BoD–Books on Demand, 2010.

[2] Francesco Pampaloni and Jörg Enderlein. Gaussian, hermite-gaussian, and laguerre-gaussian beams: A primer. *arXiv preprint physics/0410021*, 2004.

[3] Jean-Pierre Lefebvre, Philippe Lasaygue, Catherine Potel, and Jean-François de Belleval. L'acoustique ultrasonore et ses applications (1re partie). *Acoustique & techniques*, 36:4–11, 2004.

[4] Warren Perry Mason and Robert N Thurston. *Physical Acoustics: Ultrasonic Instruments and Devices I*, volume 23. Academic Press, 1999.

[5] L Hallez. Caractérisation de transducteurs ultrasonores focalisés (hifu) dédiés à la sonochimie: application à l'irradiation de polymères. *Université de Franche Comté*, 2009.

[6] KAIL Wijewardena Gamalath and GLAU Jayawardena. Diffraction of light by acoustic waves in liquids. *International Letters of Chemistry, Physics and Astronomy*, 4:39–57, 2012.

[7] Adrian Korpel. *Acousto-optics*, volume 57. CRC Press, 1996.

Chapter 2

Parametric characterization

Finding the truth is difficult, and
the road to it is rough
Hasan Ibn al-Haytham

2.1 Introduction

INTERACTION of a Gaussian laser beam with an acoustic wave, could be evaluated by analytical methods as well as by numerical ones. However when an analytical solution is possible, it becomes more interesting, it allows the evaluation of the electric field distribution in the transverse and longitudinal directions. It is worth noting, that more we know about the beam, more we can use it in different fields. This chapter is dedicated to study analytically the interaction of an incident Gaussian beam with a dynamic transmittance. The latter is generated by an acoustic wave propagating in a liquid medium (water). By using the Kirchhoff-Fresnel diffraction integral, we demonstrate the analytic expression of the resulting field (of the Gaussian beam after diffraction by the transmittance) as well as the transverse intensity at any propagation distance z. In addition, by acting on the different parameters of the incident Gaussian beam and the acoustic wave, we demonstrated some beam shapes. Furthermore, based

on the intensity's expression of the output beam (shaped), we demonstrate a parametric characterization of the resulting beam using the famous statistical quantity, known as Kurtosis parameter. The latter is usually used in beam optics to assess the flatness of laser beam. In this chapter we demonstrate the analytic expression of the Kurtosis parameter for a given Gaussian beam, diffracted by an acoustic wave propagating in water. In addition, we use some numerical simulations to relate the Kurtosis to the corresponding intensity's distribution.

2.2 Beam's parameters

It is well known from the theory of laser beam that the beam propagation factor M^2 is a very useful parameter that characterizes the focusability of any laser beam. However, to achieve an optimum control of industrial processes accomplished by using higher power lasers, a precise description of laser beams is required. To this end, the kurtosis parameter is also employed to describe the flatness or the sharpness of such beams, it is given by the following expression[1–4]:

$$K = \frac{\langle x^4 \rangle}{\langle x^2 \rangle^2}. \tag{2.1}$$

where $\langle x^4 \rangle$ et $\langle x^2 \rangle$ are the irradiance moments, fourth and second order respectively, in the spacial domain, and are expressed as follows:

$$\left\langle x^4 \right\rangle = \frac{\int_{-\infty}^{+\infty} x^4 I\left(x\right) dx}{\int_{-\infty}^{+\infty} I\left(x\right) dx}. \tag{2.2}$$

$$\left\langle x^2 \right\rangle = \frac{\int_{-\infty}^{+\infty} x^2 I\left(x\right) dx}{\int_{-\infty}^{+\infty} I\left(x\right) dx}. \tag{2.3}$$

2.3 The field expression of the Gaussian laser beam intensity profile modified by the acoustic wave

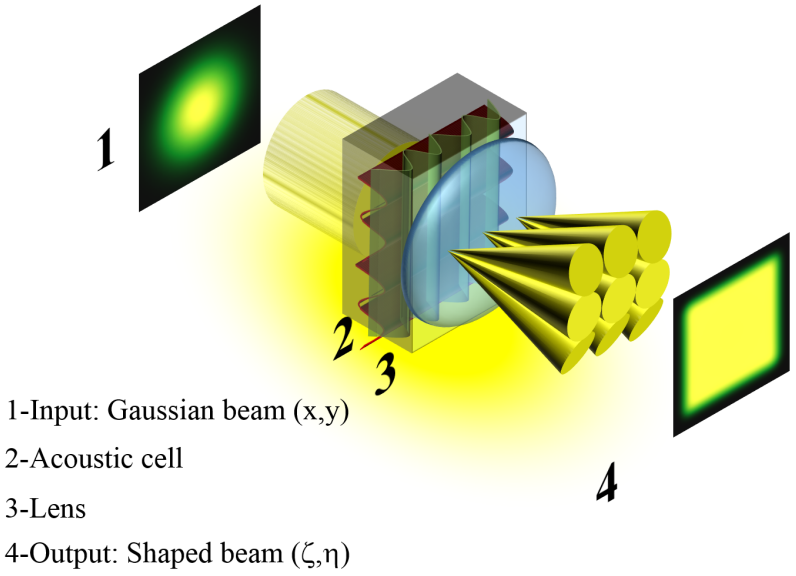

Figure 2.1: The optical layout of the transformation of an incident Gaussian beam into a Flat-top beam using an acousto-optical cell.

In this part we will present the expression of the intensity diffracted by an acoustic wave. Firstly, we present the expression of Gaussian beam Eq. (2.4), then the expression of the refractive index given by Eq. (2.5) created by the propagation of the acoustic wave[5, 6]:

$$E_0(x) = A.\exp\left[-\left(\frac{x}{w_0}\right)^2\right]. \tag{2.4}$$

In what follows the amplitude is normalized $A = 1$.

$$n(x,t) = n_0 + \Delta n \cdot \sin(\Omega t - k_a x). \tag{2.5}$$

The expression of the field before the lens,(the output face of the cell), is given by:

$$E_1(x,t,z=L) = E_0(x)\cdot\exp\left[-ikL\left(n_0+\Delta n\cdot\sin\left(\Omega t-k_a x\right)\right)\right], \tag{2.6}$$

Applying the Fresnel Kirchhoff integral[7]:

$$E_{out}(\zeta) = \frac{\exp(-ikz)}{\sqrt{i\lambda z}}\exp\left(-i\frac{k}{2z}\zeta^2\right) \times\int_{-\infty}^{+\infty} E_1(x)\cdot\exp\left(i\frac{k}{2f}x^2\right)\exp\left(-i\frac{k}{2z}x^2\right)\exp\left(i\frac{2\pi}{\lambda z}\zeta x\right)dx, \tag{2.7}$$

Using this transformation:

$$\exp\left\{-ikL\Delta n\cdot\sin\left(\Omega t-k_a x\right)\right\} = \sum_{m=-\infty}^{+\infty} J_m\left(kL\Delta n\right)\exp\left\{-im\left(\Omega t-k_a x\right)\right\}. \tag{2.8}$$

After some transformation the filed expression is given by:

$$E_{out}(\zeta) = \frac{\exp(-ikz)}{\sqrt{i\lambda z}}\exp\left[-im\Omega t\right]\exp\left[-ikLn_0\right]\exp\left(-i\frac{k}{2z}\zeta^2\right)\sum_{m=-\infty}^{+\infty} J_m(\psi) \times\int_{-\infty}^{+\infty}\exp-\left[\left(\frac{1}{{w_0}^2}+\frac{i\pi}{\lambda z}\left(1-\frac{z}{f}\right)\right)x^2-\left(\frac{i2\pi\zeta}{\lambda z}+imk_a\right)x\right]dx, \tag{2.9}$$

Where, $\psi = kL\Delta n$ is the Raman-Nath parameter.

$$\int_{-\infty}^{+\infty} e^{-\left(p^2x^2\mp qx\right)}dx = \frac{\sqrt{\pi}}{p}e^{\frac{q^2}{4p^2}}. \tag{2.10}$$

Using the expression given by Eq. (2.10),[8], ignoring all phase factors $\left(\exp\left(-ikz\right)\exp\left[-im\Omega t\right]\exp\left[-ikLn_0\right]\exp\left(-i\frac{k}{2z}\zeta^2\right)\right)$ not concerned by the integration and squaring the amplitude, We find the final expression of the transverse intensity at any propagation distance z [9, 10]:

$$I\left(\zeta\right)=\left(\frac{1}{\lambda \mathrm{z}}\right)\frac{\pi}{\left(\frac{1}{{w_0}^2}+\frac{\pi}{\lambda z}\left(1-\frac{z}{f}\right)\right)}\times\sum_{-\infty}^{+\infty}J_m^2\left(\psi\right)\exp\left[-\frac{\left(\left(\frac{\sqrt{2}\pi w_0}{\lambda \mathrm{z}}\right)\zeta+\frac{w_0}{\sqrt{2}}k_a\ m\right)^2}{\left(1+\left(\frac{\pi\left(1-{}^{z}/_{f}\right)}{\lambda \mathrm{z}}\right)^2{w_0}^2\right)}\right]. \quad (2.11)$$

With, $k_a=\frac{2\pi}{\lambda_a}$ is the acoustic wave number.

The transverse distribution of the intensity in the focal plane $z=f$ is given by:

$$I\left(\zeta,\ z=f\right)=\left(\frac{\pi w_0^2}{\lambda f}\right)\sum_{-\infty}^{+\infty}J_m^2\left(\psi\right)\exp\left[-\left(\left(\frac{\sqrt{2}\pi w_0}{\lambda f}\right)\zeta+\frac{w_0}{\sqrt{2}}k_a\ m\right)^2\right]. \quad (2.12)$$

To generalize the intensity expression to two dimensions we use the following equation:

$$E\left(\zeta,\eta\right)=E\left(\zeta\right)\times E\left(\eta\right) \quad (2.13)$$

2.4 The Kurtosis parameter K for a Gaussian beam shaped by an acousto-optic cell at a lens focal plane

In this section we will evaluate the Kurtosis parameter of an incident Gaussian beam shaped by an acoustic-optic cell, as it is well known that the Kurtosis parameter is z dependent, here we have fixed $z = f$ to obtain an analytical expression for the K in the focal plan.

To calculate the Kurtosis parameter, we firstly calculate the fourth and second moments of the intensity distribution.

2.4.1 Calculation of $\langle x^4 \rangle$

We begin by the calculation of the zero order moment of the intensity, which represents the intensity power.

To calculate the integral $\int_{-\infty}^{+\infty} I(x)\,dx$,The following relation was used [8]:

$$\int_{-\infty}^{+\infty} e^{-\left(p^2x^2+qx\right)}dx = \frac{\sqrt{\pi}}{p}e^{\frac{q^2}{4p^2}}. \tag{2.14}$$

Several changes should be made in order to apply the relation to the intensity equation:

$$\int_{-\infty}^{+\infty} e^{-\left(p^2x^2+qx\right)}dx = \int_{-\infty}^{+\infty} e^{-\left[\left(px+\frac{q}{2p}\right)^2-\frac{q^2}{4p^2}\right]}dx. \tag{2.15}$$

$$\int_{-\infty}^{+\infty} e^{-\left[\left(px+\frac{q}{2p}\right)^2\right]} dx = \frac{\sqrt{\pi}}{p}. \tag{2.16}$$

Where,

$p = \frac{\sqrt{2}\pi w_0}{\lambda f}$ and $\frac{q}{2p} = \frac{w_0}{\sqrt{2}} k_a\ m.$

Finally,

$$\int_{-\infty}^{+\infty} I\left(x\right) dx = \left(\frac{\pi w_0^2}{\lambda f}\right) \sum_{-\infty}^{+\infty} J_m^2(\psi) \frac{\sqrt{\pi}}{\left(\frac{\sqrt{2}\pi w_0}{\lambda f}\right)}. \tag{2.17}$$

To calculate the second part of the integral of the fourth moments of the intensity distribution, a variable change is necessary and we rename the parameters a and b :

$y = ax + b$ and $a = \frac{\sqrt{2}\pi w_0}{\lambda f}$ and $b = \frac{{w_0}^2 m}{\sqrt{2}\lambda_a}$.

$$\int_{-\infty}^{+\infty} x^4 I\left(x\right) dx = \left(\frac{\pi w_0^2}{\lambda f}\right) \sum_{-\infty}^{+\infty} J_m^2(\psi) \int_{-\infty}^{+\infty} x^4 e^{-(ax+b)^2} dx, \tag{2.18}$$

Then,

$$\int_{-\infty}^{+\infty} x^4 I\left(x\right) dx = \left(\frac{\pi w_0^2}{\lambda f}\right) \sum_{-\infty}^{+\infty} J_m^2(\psi) \frac{1}{a^5} \int_{-\infty}^{+\infty} (y-b)^4 e^{-y^2} dy, \tag{2.19}$$

After some algebra we have obtained the expression shown in Eq. (2.20):

$$\int_{-\infty}^{+\infty} x^4 I(x)\,dx = \left(\frac{\pi w_0^2}{\lambda f}\right) \sum_{-\infty}^{+\infty} J_m^2(\psi) \frac{1}{a^5} \times \int_{-\infty}^{+\infty} \left(b^4 - 4b^3 y + 6b^2 y^2 - 4by^3 + y^4\right) e^{-y^2} dy, \quad (2.20)$$

Using the formulas [8]:

$$\int_0^{\infty} x^h e^{-cx^2} dx = \frac{\Gamma\left[(h+1)/2\right]}{2c^{(h+1)/2}}. \quad (2.21)$$

Where, Γ represents the Gamma function.

$$\int_0^{\infty} e^{-gx^2} dx = \frac{1}{2}\sqrt{\frac{\pi}{g}}. \quad (2.22)$$

If h is an odd number the result of integral from $(-\infty\ to + \infty)$ is equal to zero

If h is an even number the result of integral from $(-\infty\ to + \infty)$ is equal to $2 \times \frac{\Gamma\left[\frac{h+1}{2}\right]}{2c^{\frac{h+1}{2}}}$

We obtain,

$$\int_{-\infty}^{+\infty} x^4 I(x)\,dx = \left(\frac{\pi w_0^2}{\lambda f}\right) \sum_{-\infty}^{+\infty} J_m^2(\psi) \left[\frac{\Gamma\left(\frac{5}{2}\right)}{a^5} + \frac{b^4}{a^5}\sqrt{\pi} + \frac{6b^2\Gamma\left(\frac{3}{2}\right)}{a^5}\right], \quad (2.23)$$

Finally, the fourth order intensity moment $\langle x^4 \rangle$ is given by the expression

$$\left\langle x^4 \right\rangle = \frac{\sum_{-\infty}^{+\infty} J_m^2(\psi) \left[\frac{\Gamma\left(\frac{5}{2}\right)}{a^5} + \frac{b^4}{a^5}\sqrt{\pi} + \frac{6b^2\Gamma\left(\frac{3}{2}\right)}{a^5} \right]}{\sum_{-\infty}^{+\infty} J_m^2(\psi) \frac{\sqrt{\pi}}{\left(\frac{\sqrt{2}\pi w_0}{\lambda f}\right)}}. \tag{2.24}$$

2.4.2 Calculation of $\left\langle x^2 \right\rangle$

As well in this part we exploit the same variable change used in the last part (calculate the fourth moments), We began by Eq. (2.25):

$$\int_{-\infty}^{+\infty} x^2 I\left(x\right) dx = \left(\frac{\pi w_0^2}{\lambda f}\right) \sum_{-\infty}^{+\infty} J_m^2(\psi) \frac{1}{a^3} \int_{-\infty}^{+\infty} (y-b)^2 e^{-y^2} dy \tag{2.25}$$

Then,

$$\int_{-\infty}^{+\infty} x^2 I\left(x\right) dx = \left(\frac{\pi w_0^2}{\lambda f}\right) \sum_{-\infty}^{+\infty} J_m^2(\psi) \frac{1}{a^3} \int_{-\infty}^{+\infty} \left(y^2 + b^2 - 2yb\right) e^{-y^2} dy \tag{2.26}$$

Finally, we find the expression of integral:

$$\int_{-\infty}^{+\infty} x^2 I\left(x\right) dx = \left(\frac{\pi w_0^2}{\lambda f}\right) . \sum_{-\infty}^{+\infty} J_m^2(\psi) \left[\frac{\Gamma\left(\frac{3}{2}\right)}{a^3} + \frac{b^2}{a^3}\sqrt{\pi} \right] \tag{2.27}$$

The final equation of the integral will be represented for $\left\langle x^2 \right\rangle$ in the above formula :

$$\left\langle x^2 \right\rangle = \frac{\sum_{-\infty}^{+\infty} J_m^2(\psi) \left[\frac{\Gamma\left(\frac{3}{2}\right)}{a^3} + \frac{b^2}{a^3}\sqrt{\pi} \right]}{\sum_{-\infty}^{+\infty} J_m^2(\psi) \frac{\sqrt{\pi}}{p}} \tag{2.28}$$

Finally, the expression of the kurtosis parameter is given as follows:

$$K = \frac{\frac{\sum_{-\infty}^{+\infty} J_m^2(\psi)\left[\frac{\Gamma\left(\frac{5}{2}\right)}{a^5}+\frac{b^4}{a^5}\sqrt{\pi}+\frac{6b^2\Gamma\left(\frac{3}{2}\right)}{a^5}\right]}{\sum_{-\infty}^{+\infty} J_m^2(\psi)\frac{\sqrt{\pi}}{p}}}{\left[\frac{\sum_{-\infty}^{+\infty} J_m^2(\psi)\left[\frac{\Gamma\left(\frac{3}{2}\right)}{a^3}+\frac{b^2}{a^3}\sqrt{\pi}\right]}{\sum_{-\infty}^{+\infty} J_m^2(\psi)\frac{\sqrt{\pi}}{p}}\right]^2} \tag{2.29}$$

2.5 The kurtosis for the transverse distribution of the intensity at any point of propagation z

In this section, we consider the generalization of the previous one, where we demonstrate a more general expression for the Kurtosis parameter K as a function of the propagation distance. So, we can follow the intensity profiles along z axis. Following the same step as in the previous section, and after a lengthy but straightforward algebra, the final expression of K is given by:

$$K = \frac{\frac{\sum_{-\infty}^{+\infty} J_m^2(\psi)\left[\frac{\Gamma\left(\frac{5}{2}\right)}{a1^5}+\frac{b1^4}{a1^5}\sqrt{\pi}+\frac{6b1^2\Gamma\left(\frac{3}{2}\right)}{a1^5}\right]}{\sum_{-\infty}^{+\infty} J_m^2(\psi)\frac{\sqrt{\pi}}{a_1}}}{\left[\frac{\sum_{-\infty}^{+\infty} J_m^2(\psi)\left[\frac{\Gamma\left(\frac{3}{2}\right)}{a1^3}+\frac{b1^2}{a1^3}\sqrt{\pi}\right]}{\sum_{-\infty}^{+\infty} J_m^2(\psi)\frac{\sqrt{\pi}}{a_1}}\right]^2} \tag{2.30}$$

Where the parameters a_1 and b_1 are given by:

$$a_1 = \frac{\left(\frac{\sqrt{2}\pi w_0}{\lambda z}\right)}{\sqrt{\left(1+\left(\frac{\pi\left(1-{}^{z}/_{f}\right)}{\lambda z}\right)^{2} {w_0}^2\right)}} \quad \text{and} \quad b_1 = \frac{\frac{w_0}{\sqrt{2}} k_a \; m}{\sqrt{\left(1+\left(\frac{\pi\left(1-{}^{z}/_{f}\right)}{\lambda z}\right)^{2} {w_0}^2\right)}} \tag{2.31}$$

2.6 Numerical simulation

In this section we present the numerical simulation of the Gaussian laser beam interaction with an acoustic wave. By considering a laser wavelength of $\lambda = 633nm$ and a beam waist of $w_0 = 1mm$. The lens back focal length used is $f = 100mm$. We start by presenting the result of the Flat top beam then the Doughnut beam and finally Doughnut beam with a flat inside. All the results presented in this section are obtained by considering 2D acousto-optic interaction where the laser beam interacts with two orthogonal acoustic beams in the medium A.O cell.

2.6.1 Flat top beams generation

In this section, we demonstrate the generation of different shapes of Flat-top beams by adjusting the acoustic power, so the effect of the Raman-Nath parameter ψ variation is given. We present the intensity patterns and profiles of each output beam as a function of the Raman Nath parameter ψ. Fig. 2.2 shows the intensity patterns (a, b, c, d) and their corresponding profiles (a1, b1, c1, d1) of the generated Flat-top beam, at the plane $z = f$, for different Raman-Nath parameters ψ ($\psi = 60$ in Fig. 2.2(a) and (a1), $\psi = 70$ in Fig. 2.2(b) and (b1), $\psi = 80$ in Fig. 2.2(c) and (c1), $\psi = 90$ in Fig. 2.2(d) and (d1)) with an acoustic wave number $k_a = 0.5m^{-1}$. It's obvious from Fig. 2.2 (a1, b1, c1, d1) that the flatness of the obtained beam is improved by the increasing of the Raman-Nath parameters ψ. And that's also clear from the 3D representation shown in Figs. 2.3 and 2.4, which represent the 3D intensity distribution of the generated

Flat-top beam in the plane $\zeta - \eta$ and the plane $\zeta - z$, respectively. Furthermore, Fig. 2.4 illustrates that the Flat-top beam is generated only close to (around) the focal plane of the lens ($z = f$), where $z = 100mm$.

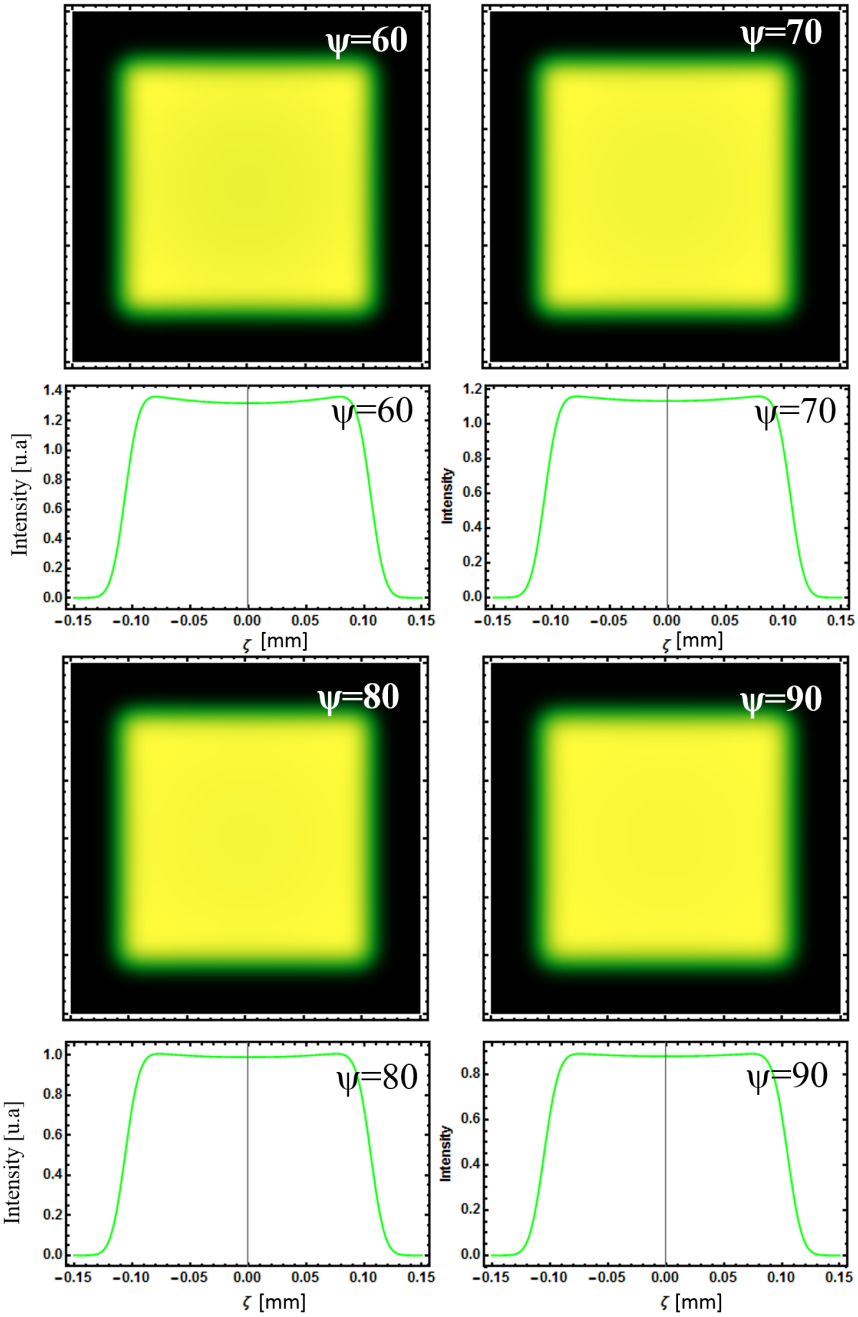

Figure 2.2: The intensity patterns (a, b , c, d) and profiles (a1, b1, c1, d1) of the generated Flat top beams, at the plane $z = f$, for different Raman-Nath parameters ψ with an acoustic wave number $k_a = 0.5m^{-1}$.

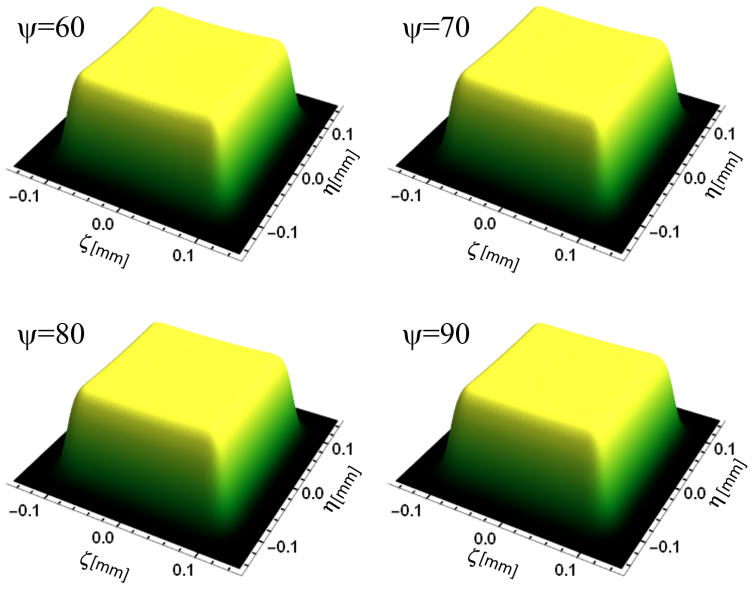

Figure 2.3: 3D intensity distribution in the plane $\zeta - \eta$ of the generated Flat top beams, at the plane $z = f$, for different Raman-Nath parameters ψ with an acoustic wave number $k_a = 0.5m^{-1}$.

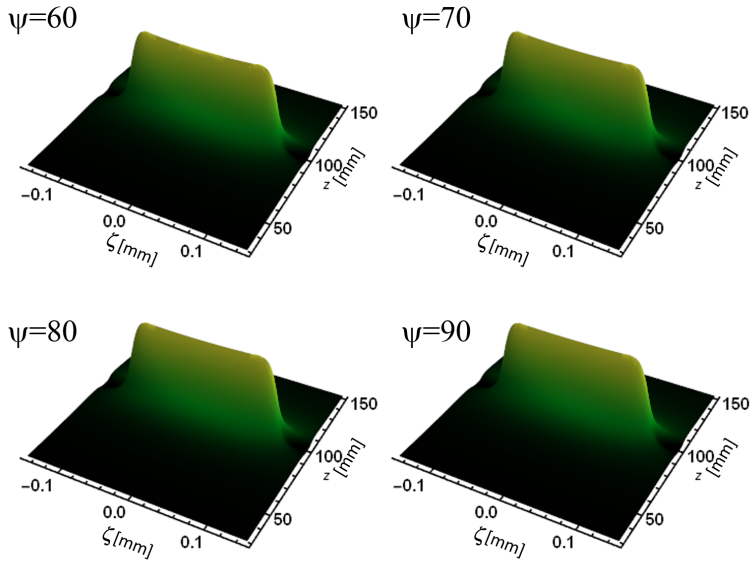

Figure 2.4: 3D intensity distribution in the plane $\zeta - z$ of the generated Flat top beams, at the plane $z = f$, for different Raman-Nath parameters ψ with an acoustic wave number $k_a = 0.5m^{-1}$.

2.6.2 Doughnut (petal) beams generation

In this section, we show the generation of different shapes of Doughnut (petal) beams for different acoustic wave number k_a and with a Raman-Nath parameter ψ equal to 2.3, the value for which the zero order (the central lob) of the Bessel function is disappeared. We present the intensity patterns and profiles of each shape as a function of the acoustic wave numberr k_a.

Fig. 2.5 displays the intensity patterns (a, b, c, d) and their corresponding profiles (a1, b1, c1, d1) of the different generated Doughnut (petal) beam, at the plane $z = f$, for different acoustic wave number k_a ($k_a = 1.2m^{-1}$ in Fig. 2.5(a) and (a1), $k_a = 2m^{-1}$ in Fig. 2.5(b) and (b1), $k_a = 2.6m^{-1}$ in Fig. 2.5(c) and (c1), $k_a = 4m^{-1}$ in Fig. 2.5(d) and (d1)) with a Raman-Nath parameter $\psi = 2.3$. It can be seen from Fig. 2.5 that the Doughnut (petal) beam can be generated by the increasing of the acoustic wave number k_a, which means increasing the shifts between the orders. And that's evident from the 3D representation shown in Figs. 2.6 and 2.7, which represent the 3D intensity distribution of the generated Doughnut (petal) beam in the plane $\zeta - \eta$ and the plane $\zeta - z$, respectively. Fig. 2.4 illustrates that the Doughnut beam is also generated close to (around) the focal plane ($z = f$).

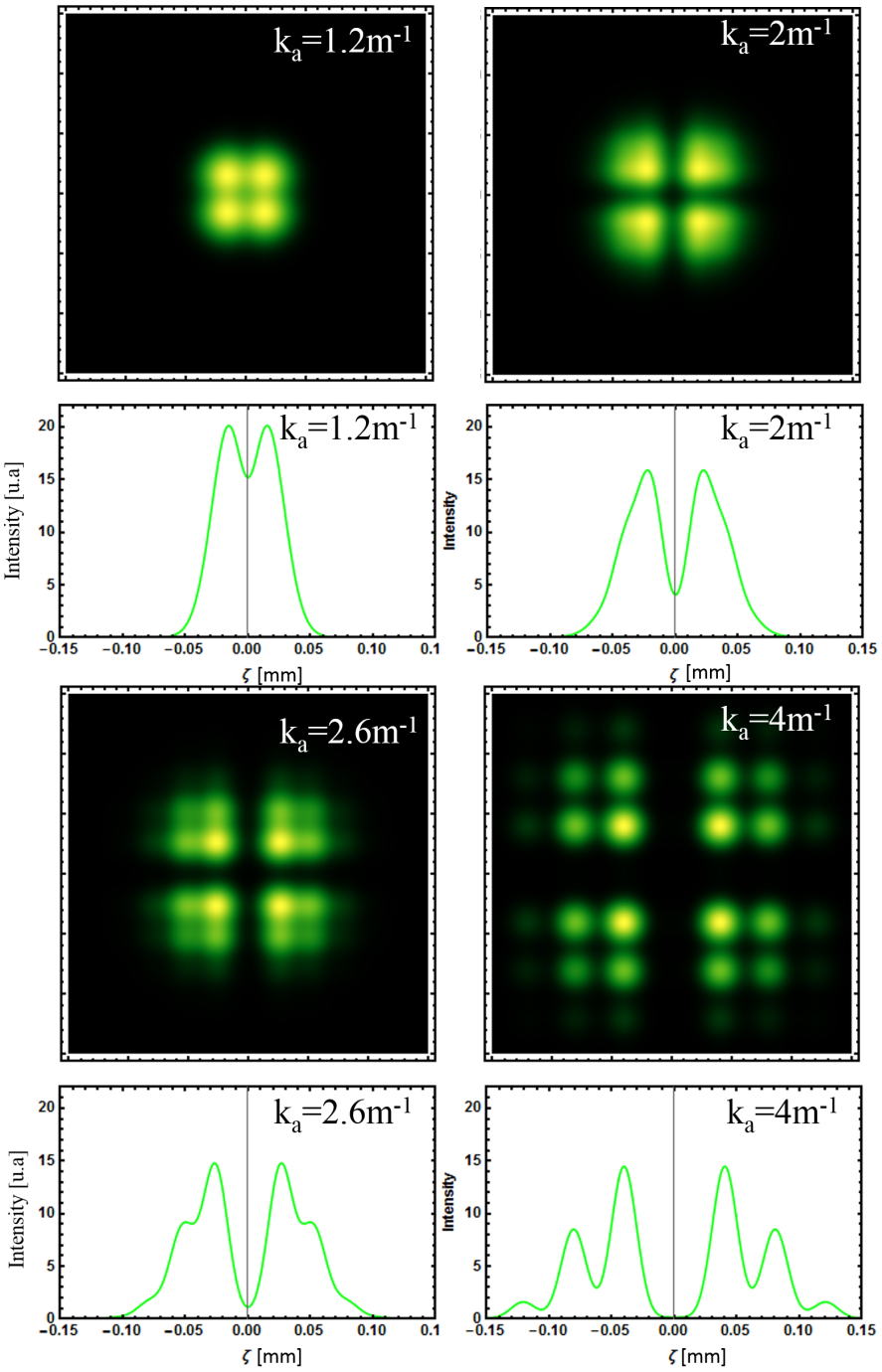

Figure 2.5: The intensity patterns (a, b, c, d) and profiles (a1, b1, c1, d1) of the generated Doughnut (petal) beams, at the plane $z = f$, for different acoustic wave number k_a with a Raman-Nath parameter $\psi = 2.3$.

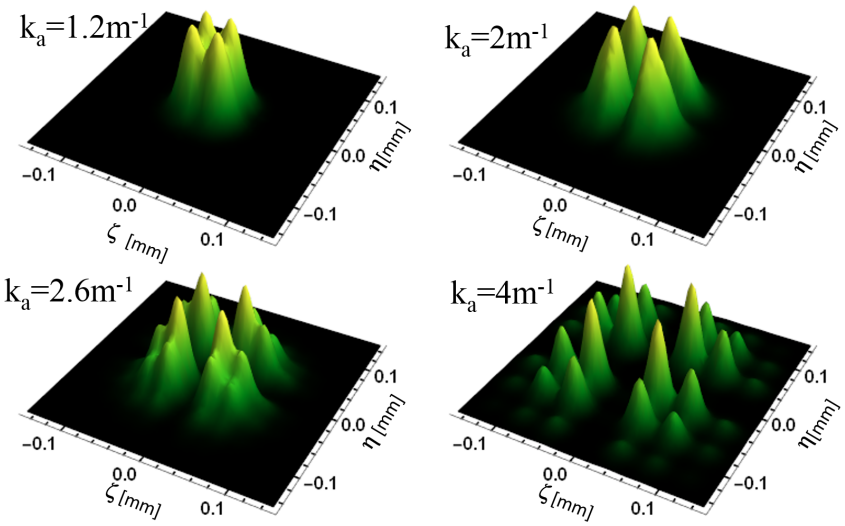

Figure 2.6: 3D intensity distribution in the plane $\zeta - \eta$ of the generated Doughnut (petal) beams, at the plane $z = f$, for different acoustic wave number k_a with a Raman-Nath parameter $\psi = 2.3$.

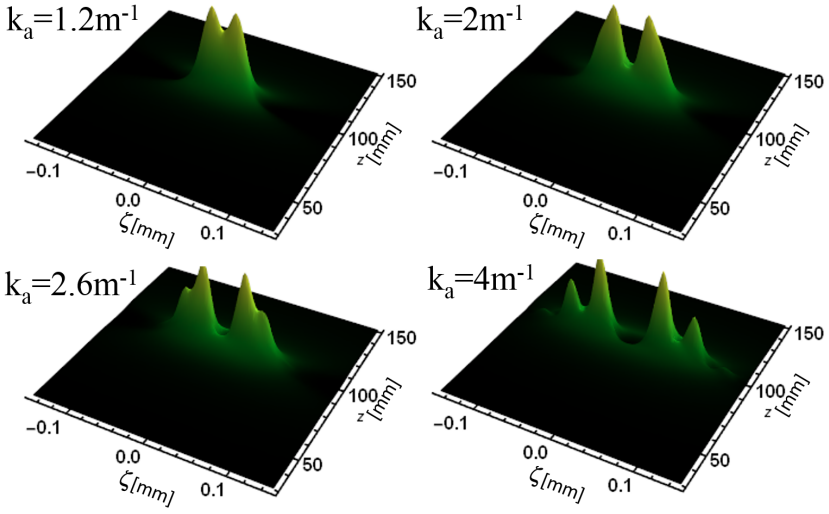

Figure 2.7: 3D intensity distribution in the plane $\zeta - z$ of the generated Doughnut (petal) beams, at the plane $z = f$, for different acoustic wave number k_a with a Raman-Nath parameter $\psi = 2.3$.

2.6.3 Doughnut (petal) beams with a flat inside generation

In this section, we present the intensity patterns and profiles of the generated Doughnut (petal) beam, with a certain flatness degree inside, as a function of the Raman Nath parameter ψ.

Fig. 2.5 shows the intensity patterns (a, b, c, d) and their equivalent profiles (a1, b1, c1, d1) of the different generated Doughnut (petal) beam that showing a flatness inside, at the plane $z = f$, for different Raman-Nath parameters ψ ($\psi = 10$ in Fig. 2.8(a) and (a1), $\psi = 15$ in Fig. 2.8(b) and (b1), $\psi = 20$ in Fig. 2.8(c) and (c1), $\psi = 25$ in Fig. 2.8(d) and (d1)) with an acoustic wave number $k_a = 0.5m^{-1}$. It can be seen that the flatness degree inside the generated Doughnut (petal) beam increases as the Raman-Nath parameter ψ increases.

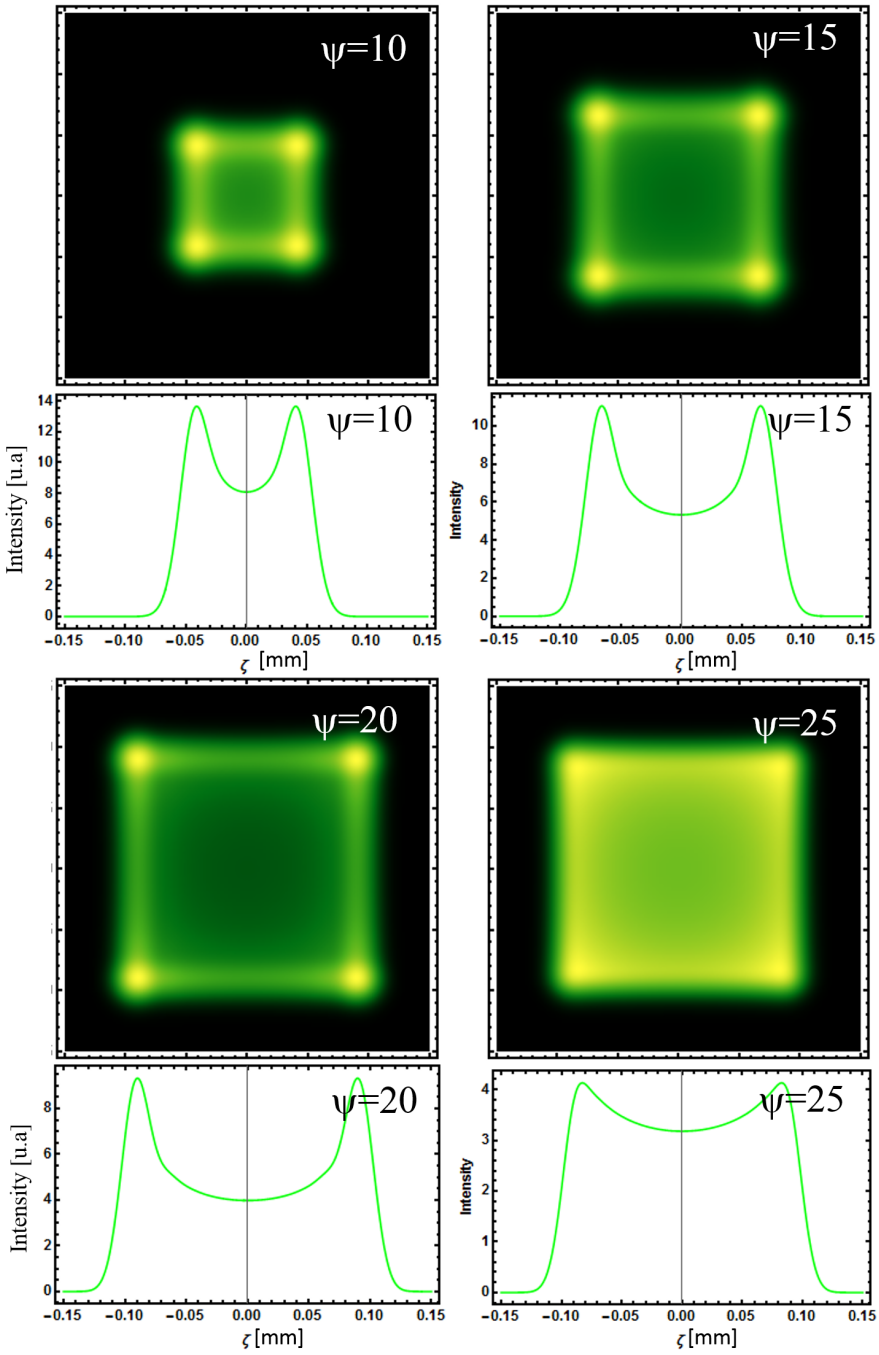

Figure 2.8: The intensity patterns (a, b , c, d) and profiles (a1, b1, c1, d1) of the generated Doughnut (petal) beams that showing a flatness inside, at the plane $z = f$, for different Raman-Nath parameters ψ with an acoustic wave number $k_a = 0.5m^{-1}$.

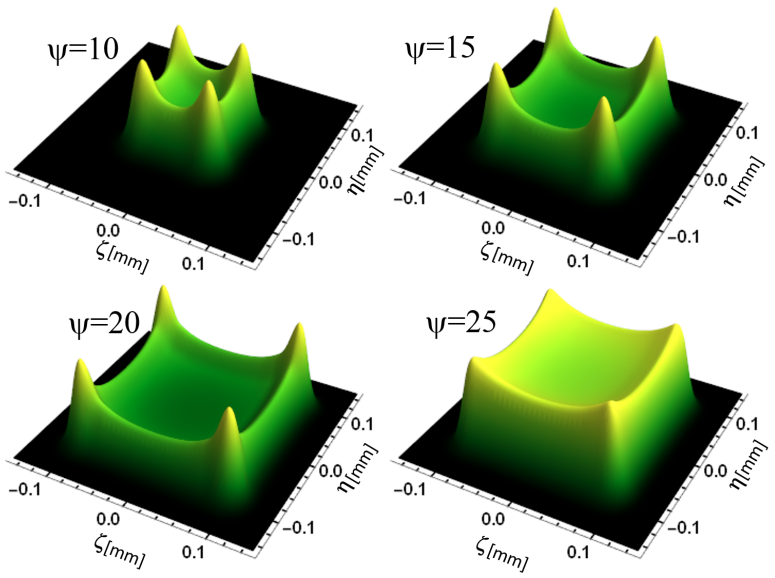

Figure 2.9: 3D intensity distribution in the plane $\zeta - \eta$ of the generated Doughnut (petal) beams that showing a flatness inside, at the plane $z = f$, for different Raman-Nath parameters ψ with an acoustic wave number $k_a = 0.5m^{-1}$.

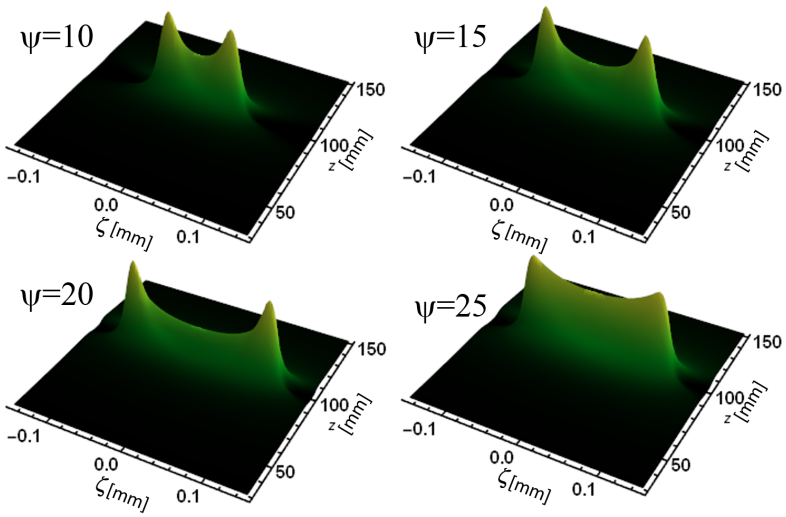

Figure 2.10: 3D intensity distribution in the plane $\zeta - z$ of the generated Doughnut (petal) beams that showing a flatness inside, at the plane $z = f$, for different Raman-Nath parameters ψ with an acoustic wave number $k_a = 0.5m^{-1}$.

2.6.4 Analysis of the obtained shapes using the Kurtosis parameter

We recall that the Kurtosis parameter allows to characterize the flatness of surfaces, it was used also extensively to characterize laser beam shapes [11, 12]. In this section we will numerically simulate the results of the equation Eq. (2.30). To relate the obtained shaped beams (using the acousto-optic cell) to the Kurtosis parameter, we will use as a reference for a flat top beams, a super Gaussian beam with different orders n. It is worth noting that more n increases more the super Gaussian becomes a perfectly flat-topped. The ideal value of the kurtosis parameter that we will take as a reference is $K = 1.81$ corresponding to an index of the super Gaussian $n = 100$.

Fig. (2.11) shows the standard curve we designed to relate the profiles to their Kurtosis degree. We have considered the case of the Super-Gaussian profile with $n = 100$ as a reference for flat-topped shape, corresponding to $K = 1.8$. However, it seems that more the profile becomes non flat, more the Kurtosis becomes greater than the standard value.

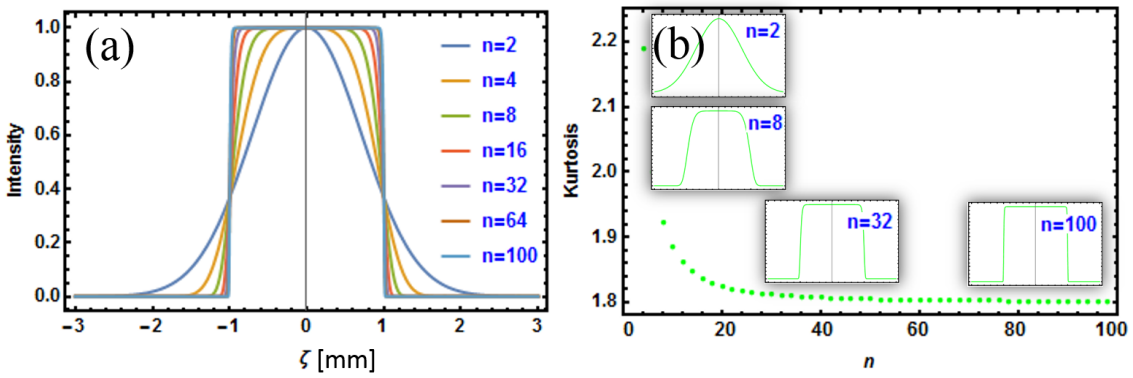

Figure 2.11: The Standard curve for the Kurtosis parameter. (left) Profiles of the super-Gaussian profile for different orders s, here more the order n increases more the profile becomes a perfect flat-topped. (Right) The Kurtosis curve corresponding to different profiles, from Gaussian to super-Gaussian $n = 100$.

Fig. (2.12) presents the evolution of the Kurtosis parameter as a function of the Raman-Nath parameter in Fig. (2.12)(a) and of the truncated parameter in Fig. (2.12)(b). It can be seen from Fig. (2.12)(a) that the Kurtosis evolution is divided into two levels illustrated by the dashed lines, so for small values of Raman Nath parameter ($8 < \psi < 33$), where $K < 1.8$, the shape of the generated beam be a Doughnut (petal) showing a certain degree of flatness inside, then when the Raman Nath parameter increases, a perfect Flat-top shape is obtained and the Kurtosis degree keeps its value equal to 1.81. In Fig. (2.12)(b), for a Raman-Nath parameter $\psi = 2.3$, the kurtosis degree is > 1.8 and the shape of the obtained beam be a Doughnut (petal).

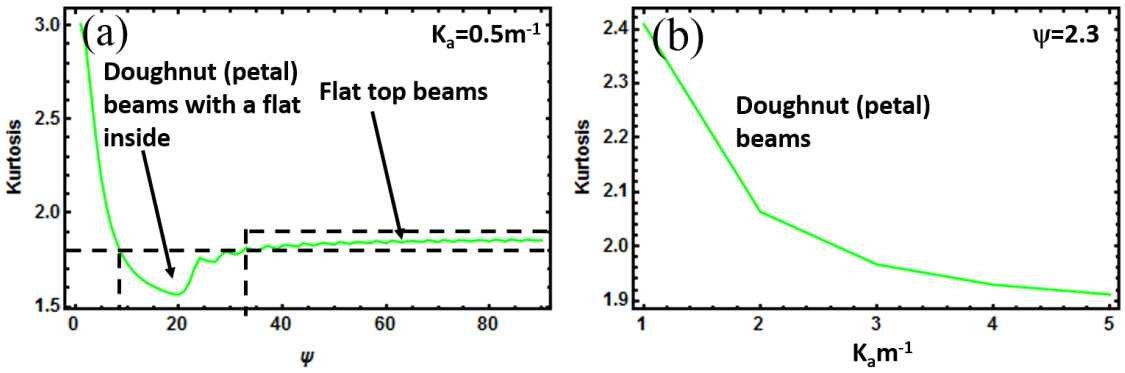

Figure 2.12: The Kurtosis parameter evolution (a) as a function of the Raman-Nath parameter ψ, for $k_a = 0.5m^{-1}$, and (b) as a function of the acoustic wave number k_a, for $\psi = 2.3$.

Fig. (2.13)-Fig. (2.15) show the evolution of the kurtosis parameter throughout the propagation for different interaction parameters. In each sub-figure, included on the corner, we present the transverse intensity distribution of the resulting beam after the interaction at the a specific position ($z = 100mm$), which corresponds to the focal of the lens ($z = f$). From Fig. (2.13)-Fig. (2.15), the beam shaping occurs around the focal plane of the lens, corresponding position to a minimum value of the kurtosis parameter. In Fig. (2.13), the kurtosis degree at the focal plane is approximately equal to 1.8, which corresponds to the super-Gaussian beam, and the generated beam after the interaction in the transverse direction ($z = 100mm$) has a Flat-top shape. While, in Fig. (2.14), the shape of the generated beam for a minimum values of the Kurtosis degree ($1.8 < K < 2.3$) transforms to a Doughnut(petal). In Fig. (2.15), the Doughnut (petal) shape shows a certain degree of flatness inside when $K < 1.8$.

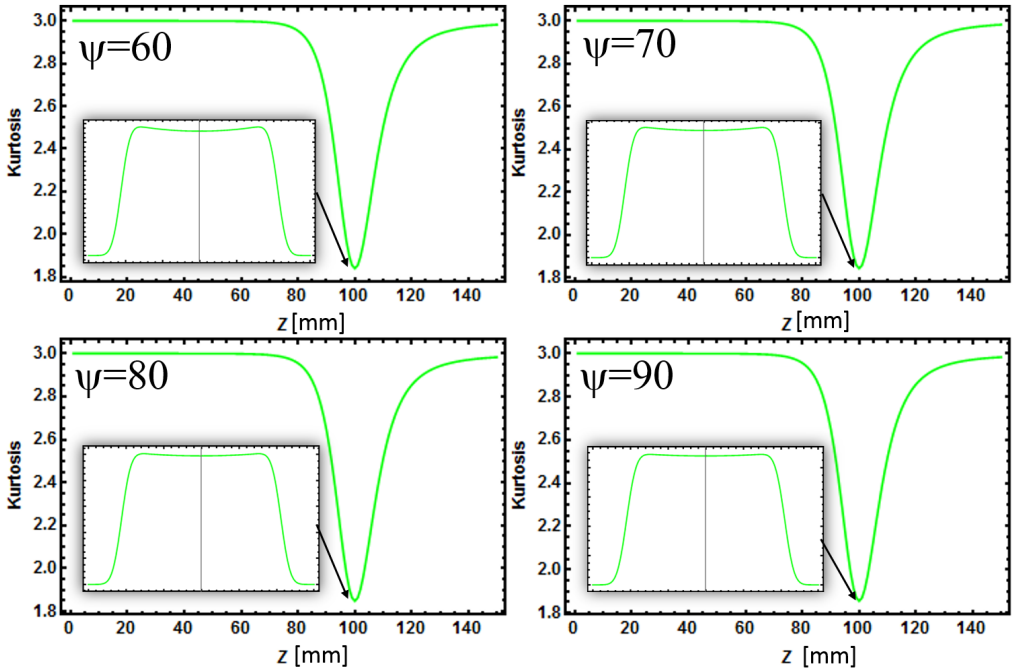

Figure 2.13: Kurtosis parameter for Flat top beams

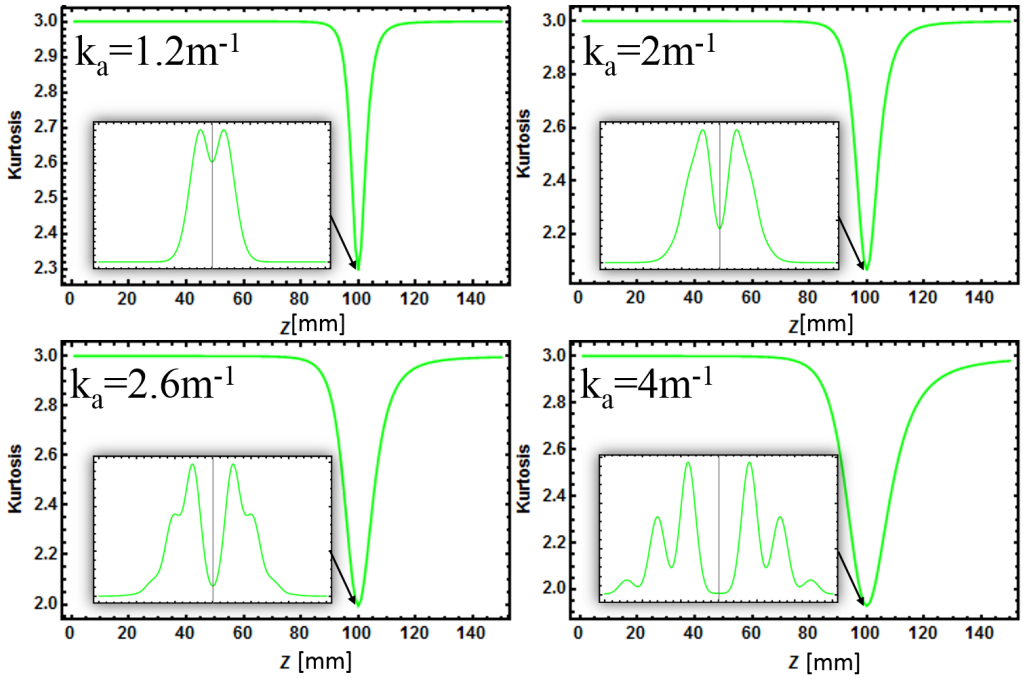

Figure 2.14: Kurtosis parameter for Doughnut(petal) beams

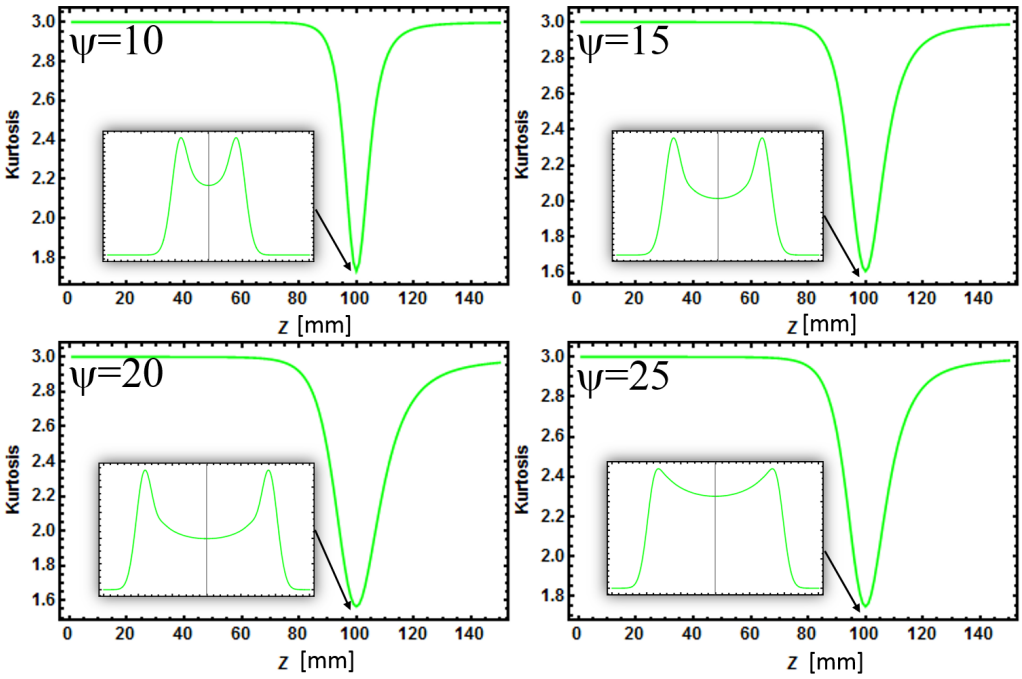

Figure 2.15: Kurtosis parameter for Doughnut(petal) beams with a flat inside

2.7 Conclusion

In this chapter, we have used the Kurtosis parameter to characterize the transverse intensity distribution, obtained after the diffraction of a Gaussian beam by an acousto-optic cell. We have derived the analytical expression that gives the propagation behavior of the interaction between the Gaussian beam and the acousto-optic cell, using the Kirchhoff-Fresnel integral. In addition, we have described analytically the Kurtosis parameter K starting from the second and fourth order intensity moments as a function of the laser beam-acousto-optic cell interaction. Furthermore, we have introduced a new standard curve for the Kurtosis parameter to characterize the flatness of laser beams. The obtained results show that for flat shapes the Kurtosis degree is approximately equal to 1.8, which is agree with that of the super Gaussian beam, while for Doughnut shapes with a flatness inside, the kurtosis value is < 1.8.

Bibliography

[1] G Piquero, PM Mejias, and R Martinez-Herrero. Sharpness changes of gaussian beams induced by spherically aberrated lenses. *Optics communications*, 107(3-4): 179–183, 1994.

[2] R Martinez-Herrero, PM Mejias, M Sanchez, and JLH Neira. Third-and fourth-order parametric characterization of partially coherent beams propagating throughabcd optical systems. *Optical and quantum electronics*, 24(9):S1021–S1026, 1992.

[3] Rosario Martínez-Herrero, G Piquero, and PM Mejias. On the propagation of the kurtosis parameter of general beams. *Optics Communications*, 115(3-4):225–232, 1995.

[4] L Ouahid, H Nebdi, and L Dalil-Essakali. Kurtosis factor of truncated and non-truncated simplified general-type beams. *Optical and Quantum Electronics*, 49(3): 91, 2017.

[5] Abdelhalim Bencheikh and Kouider Ferria. Gaussian laser beam tailoring using acoustooptic cell. *Optics & Laser Technology*, 44(4):806–809, 2012.

[6] K Ferria, A Bencheikh, and A Merabet. Doughnut beam generation using acousto-optic cell. In *2012 19th International Conference on Microwaves, Radar & Wireless Communications*, volume 2, pages 491–494. IEEE, 2012.

[7] Joseph W Goodman. *Introduction to Fourier optics*. Roberts and Company Publishers, 2005.

[8] Izrail Solomonovich Gradshteyn and Iosif Moiseevich Ryzhik. *Table of integrals, series, and products*. Academic press, 2014.

[9] Yoshihiro Ohtsuka and Aris Tanone. Acousto-optic intensity modification of a gaussian laser beam. *Optics Communications*, 39(1-2):70–74, 1981.

[10] Yoshihiro Ohtsuka, Yasutomo Arima, and Yoh Imai. Acoustooptic 2-d profile shaping of a gaussian laser beam. *Applied optics*, 24(17):2813–2819, 1985.

[11] Haotong Ma, Zejin Liu, Pu Zhou, Xiaolin Wang, Yanxing Ma, and Xiaojun Xu. Generation of flat-top beam with phase-only liquid crystal spatial light modulators. *Journal of Optics*, 12(4):045704, 2010.

[12] S Saghafi, MJ Withford, and Z Ghoranneviss. Characterizing flat-top laser beams using standard beam parameters. *Canadian journal of physics*, 84(3):223–240, 2006.

Chapter 3

Generation of hyperbolic tunable Airy-like beams using a truncated acousto-optical effect

The true Logic for this world
is the Calculus of Probabilities, which
takes account of the magnitude of the probability
James Clerk Maxwell

3.1 Introduction

In the previous chapter we have studied the diffraction of an input Gaussian beam with a sinusoidal ultrasound wave propagating in water. This latter creates a sinusoidal variation of the refractive index, giving rise to a sinusoidal phase transmittance. The latter diffracts the input Gaussian beam into many diffraction orders. We have shown in the previous chapter, that a good choice of the couple parameters of the Gaussian beam and the acoustic-optic cell allowed us to shape an input Gaussian beam into a flat top or doughnut beam. In this chapter, by considering some asymptotic ap-

proximation we will show a very interesting beam shaping, where a Gaussian beam is converted into a tunable Airy beam. The latter belongs to the family of nondiffracting beams, it propagates for a long distances without spreading. In addition to this features of free-diffraction, Airy beam propagates in a curved path, it belongs also to the family of accelerated beams. Accelerating Airy beams were introduced theoretically in the framework of quantum mechanics by Berry et all in 1979 [1]. In 2007, Siviloglou et al proposed Airy beams in the framework of optics, theoretically and observed them experimentally [2–4]. Since that time, the field of accelerating beams and especially Airy beams attracted many researchers' interest. They were studied in different linear [5–7] and nonlinear mediums [8, 9], and even in the turbulent atmosphere [10–12]. Many techniques were used for their generation [13–16]. They were applied in different fields, in plasma physics [17], guiding particles [18], microscopy [19–21], and in wireless communication [22, 23]. Throughout this chapter we demonstrate analytically and numerically the shaping of a given Gaussian beam into a tunable Airy-like beam using an acoustooptic cell. The latter is a glass cell filled with a water, in which an ultrasound wave propagates and creates a standing sinusoidal variation of the refractive index, giving rise to a truncated sinusoidal transparent transmittance. The good choice of the parameters related to the incident Gaussian beam and the acoustooptic cell allowed us to generate a tunable dynamic Airy-like beam with a hyperbolic path. Based on the Fresnel Kirchhoff diffraction integral, and the expansion of the truncation as a weighted sum of Gaussian functions, we demonstrate an analytic expression of the electric field amplitude, obtained after the diffraction of an incident Gaussian beam having a waist w_0 with the truncated sinusoidal transmittance of the acoustooptic cell having a square aperture width $2a$, a wavelength Λ, and an acousto-optic parameter ψ. The obtained analytic expression is a superposition of a weighted sum of shifted Airy-Complex-Gaussian functions. Based on numerical simulations, we study the effect of each parameter of the acousto-optic interaction on the behaviour of the resulting dynamic Airy-like beam.

3.2 Gaussian laser beam interaction by a truncated acoustic waves

In this chapter we demonstrate that under some conditions, a Gaussian beam could be converted into an Airy-like beam, using a truncated sinusoidal phase created by acoustic effect in a liquid medium (water). Fig. 3.1 shows the schematic description, of an incident Gaussian beam with a width $2w_0$. The latter passes through an acoustic cell, in which a sinusoidal phase mask is created. The spatial extent of the latter is truncated using a square aperture with $2a$ as a width, the resulting beam propagates in a curved path, where its transverse pattern could be described by the Airy function.

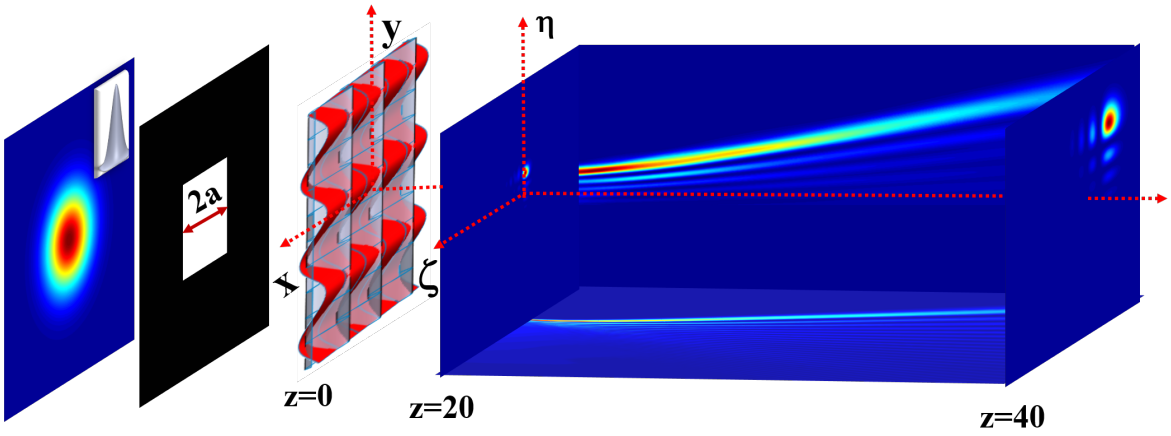

Figure 3.1: Interaction of an incident Gaussian beam with a truncated sinusoidal transmittance created par an acoustic wave propagating in a liquid medium (water)

The incident Gaussian beam is described by the electric field amplitude E_0 in 1-D Cartesian coordinates as follows

$$E_0(x) = A.\exp\left[-\left(\frac{x}{w_0}\right)^2\right]. \tag{3.1}$$

Where; w_0 is the Gaussian beam waist at the Acoustic cell plane, and the amplitude is normalized $A = 1$.

In the other hand, the acoustic cell is filled by a liquid (water) and excited by a standing acoustic wave, along the x axis, normal to the incident Gaussian beam. The resulting acoustic wave pressure is described by a sinusoidal variation as follows:

$$p_T(x,t) = p_0 + \Delta p\left[\sin(k_a x)\cos(\Omega t)\right], \tag{3.2}$$

Here P_0; is the average acoustic pressure, Δp; is the acoustic pressure amplitude, k_a; acoustic wave number and Ω is the angular frequency.

The sinusoidal variation of the pressure on water, creates a proportional elastic wave, giving rise to a sinusoidal variation of the refractive index as follows

$$n_T(x,t) = n_0 + \Delta n\left[\sin(k_a x).\cos(\Omega t)\right], \tag{3.3}$$

With n_0 is water refractive index, Δn is the refractive index amplitude owing to the acoustic pressure.

The refractive index variation is considered as a thin progressive sinusoidal phase grating given by

$$T(x,t) = \exp\left[-ikL\left(n_0 + \Delta n.\sin(k_a x).\cos(\Omega t)\right)\right], \tag{3.4}$$

Where L is the acoustic cell length, and k is the light wave number.

By choosing $w_0 < \lambda_a$, and considering the relative location of the incident Gaussian beam laying on the sinusoidal phase nodes, (generated by the piezoelectric transducer), the latter can be approximated by a cubic phase, using Taylor expansion of the sine function near zero ($\sin(x) \approx x - x^3/3!$). The phase transmittance function becomes

$$T(x,t) = \exp\left[-ikL\left(n_0 + \Delta n.\cos(\Omega t)\left(k_a x - \frac{(k_a x)^3}{6}\right)\right)\right]. \tag{3.5}$$

To evaluate the electric field amplitude of an incident Gaussian beam diffracted by a truncated progressive sinusoidal transmittance, we use the Fresnel-Kirchhoff diffraction integral given as follows[24]

$$\begin{aligned} E(\zeta,t) = \frac{\exp(-ikz)}{\sqrt{i\lambda z}}\exp(-ikLn_0)\exp\left(i\frac{k}{2z}\zeta^2\right) \\ \times \int_{-a}^{+a} \exp\left[-i\psi\left(k_a x - \frac{(k_a x)^3}{6}\right)\cos(\Omega t)\right]\exp\left[-\left(\frac{x}{w_0}\right)^2\right] \\ \times \exp\left(i\frac{k}{2z}x^2 - i\frac{k}{z}\zeta x\right)dx. \end{aligned} \tag{3.6}$$

With, $\psi = kL\Delta n$ is the Raman-Nath parameter.

After using a lens with a focal length f the previous integral becomes

$$\begin{aligned} E(\zeta,t) = \frac{\exp(-ikz)}{\sqrt{i\lambda z}}\exp(-ikLn_0)\exp\left(i\frac{k}{2z}\zeta^2\right) \\ \times \int_{-a}^{+a} \exp\left[-i\psi\left(k_a x - \frac{(k_a x)^3}{6}\right)\cos(\Omega t)\right]\exp\left[-\left(\frac{x}{w_0}\right)^2\right] \\ \times \exp\left(i\frac{k}{2z}x^2 - i\frac{k}{2f}x^2 - i\frac{k}{z}\zeta x\right)dx. \end{aligned} \tag{3.7}$$

Since the bounded integral of Eq. (3.7) has no analytical solution, we overcome this problem by expanding the aperture into a finite sum of weighted Gaussian function given as

$$A_p(x) = \sum_{n=1}^{N} A_n \exp\left(-\frac{B_n}{a^2}x^2\right), \tag{3.8}$$

Here A_n and B_n are complex coefficients that could be calculated using an optimization method like the Root Square Error method [25, 26]

By substituting Eq. (3.8) into Eq. (3.7) and ignoring all phase factors $\left(\exp(-ikz)\exp[-ikLn_0]\exp\left(-i\frac{k}{2z}\zeta^2\right)\right)$ not concerned by the integration, we obtain

$$\begin{aligned} E(\zeta,t) = \frac{\exp(-ikz)}{\sqrt{i\lambda z}}\exp(-ikLn_0)\exp\left(i\frac{k}{2z}\zeta^2\right)\sum_{n=1}^{N}A_n \\ \times\int_{-\infty}^{+\infty}\exp\left(-\frac{B_n}{a^2}x^2\right)\exp\left[-i\left(k_a x-\frac{(k_a x)^3}{6}\right)\right]\exp\left[-\left(\frac{x}{w_0}\right)^2\right] \\ \times\exp\left(-i\frac{k}{2f}x^2+i\frac{k}{2z}x^2-i\frac{k}{z}\zeta x\right)dx \end{aligned} \tag{3.9}$$

Using the variable change $h = \left(\sqrt[3]{\frac{\psi\cos(\Omega t)}{2}}k_a\right)x$, and after some algebra the integral of Eq. (3.9) is written in a more simplified form as follows

$$E(\zeta,t) = \frac{\exp(-ikz)}{\sqrt{i\lambda z}}\exp(-ikLn_0)\exp\left(i\frac{k}{2z}\zeta^2\right)\sum_{n=1}^{N}A_n\int_{-\infty}^{+\infty}\exp\left[i\left(\frac{h^3}{3}+qh^2+oh\right)\right]dh \tag{3.10}$$

Where

$$q = \frac{\left(-\frac{1}{iw_0{}^2} - \frac{B_n}{ia^2} - \frac{\pi}{\lambda z}\left(1 - \frac{z}{f}\right)\right)}{\left(\sqrt[3]{\frac{\psi\cos(\Omega t)}{2}}k_a\right)^2}, \quad o = \frac{\left(-\psi k_a + \frac{2\pi}{\lambda z}\zeta\right)}{\left(\sqrt[3]{\frac{\psi\cos(\Omega t)}{2}}k_a\right)}$$

The integral of Eq. (3.10) is a famous integral known as Airy integral given by [27]

$$\int_{-\infty}^{+\infty} \exp\left[i\left(\frac{h^3}{3} + ah^2 + bh\right)\right] dh = 2\pi e^{ia\left(\frac{2}{3}a^2 - b\right)} Ai\left(b - a^2\right). \tag{3.11}$$

Applying the integral formula of Eq. (3.11), the expression of the propagating electric field amplitude takes its final form as follows

$$E\left(\zeta, t\right) = \frac{exp\left(-ikz\right)}{\sqrt{i\lambda z}} \exp\left(-ikLn_0\right) \exp\left(i\frac{k}{2z}\zeta^2\right) \sum_{n=1}^{N} A_n \exp\left[iq\left(\frac{2}{3}q^2 - o\right)\right] Ai\left(o - q^2\right) \tag{3.12}$$

N.B : as the acoustic field propagates in 2D dimensions ζ, η we generalize our development to the y axis as follows:

$$E\left(\zeta, \eta, t\right) = E\left(\zeta\right) \times E\left(\eta\right) \tag{3.13}$$

3.3 Numerical simulation

In this section we study in detail the result shown by Eq. (3.12). Firstly we began by some numerical examples to check the analytical results of Eq. (3.12) with the numerical integral (numerical results) using a standing sinusoidal phase Eq. (3.4).

3.3.1 Acoustic wavelength parameter effect on the Airy beam intensity distribution: analytical versus numerical simulations

In this part we consider some numerical simulations, to check the validity of our analytical modeling versus the numerical calculation of the diffraction integral. We began by studying the effect of the acoustic wavelength on the profile of the resulting Airy beams. And we have fixed for the numerical simulations the following parameters; beam waist $w_0 = 1mm$, back focal length of the used lens $f = 200mm$, $L = 20mm$, $\psi = 20$ which corresponds to $\Delta n = 10^{-4}$, and different acoustic wavelengths ($\lambda_a = 2, 3, 4$ and $5mm$).

Figure 3.2 shows the different profiles of the generated Airy beams corresponding to different acoustic wavelengths ($\lambda_a = 2 - 3 - 4 - 5mm$). The shown Airy-like beams profiles obtained using a cubic phase overlap with those calculated using standing sinusoidal phase.

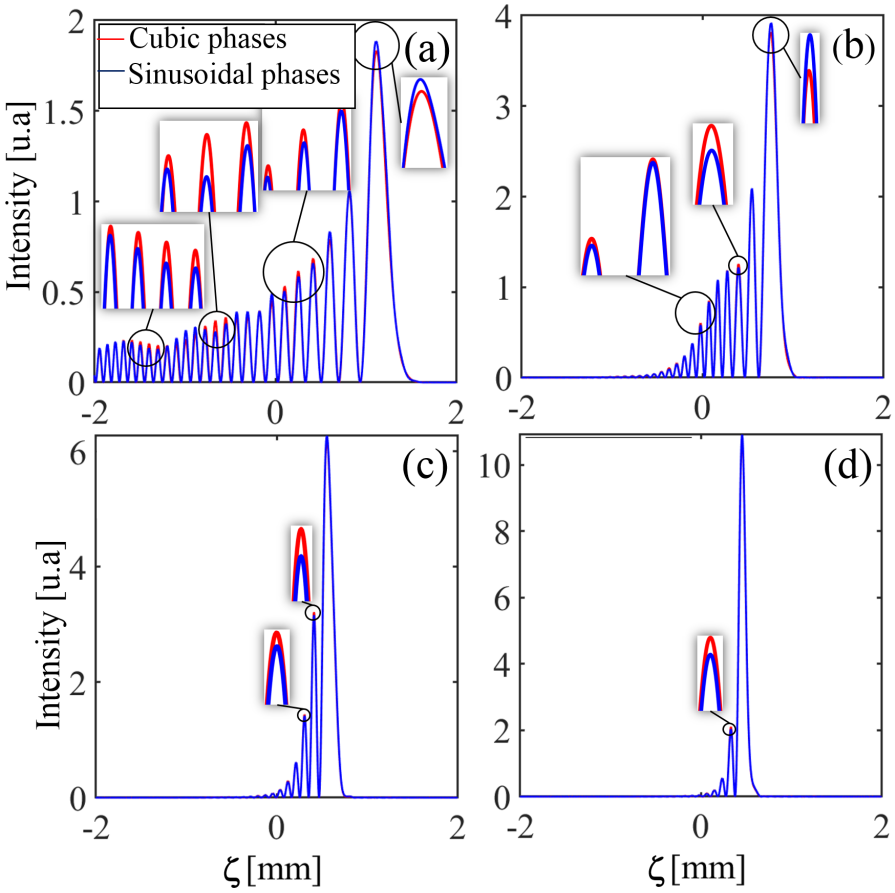

Figure 3.2: 1D Airy-beams using cubic and sinusoidal phases for different acoustic wavelengths: (a) $\lambda_a = 2mm$, (b) $\lambda_a = 3mm$, (c) $\lambda_a = 4mm$, (d) $\lambda_a = 5mm$. in the z plan: $z = f = 200mm$, $\Omega t = 0$ and $\Delta n = 10^{-4}$.

the obtained profiles by adopting a standing sinusoidal phase and a cubic phase seems overlapping, except a small variation in the amplitude without any significance influence on the expected results, this justify the approximation made.

The corresponding 2D longitudinal Airy beams propagation as a function of the applied acoustic wavelength are shown in Fig. 3.3. It is clear that the resulting Airy beams follow a curved trajectory, which is considerable when the ratio between the beam width and the acoustic wavelength decreases. By increasing the acoustic wavelength, the trajectory becomes less curved along the propagation path.

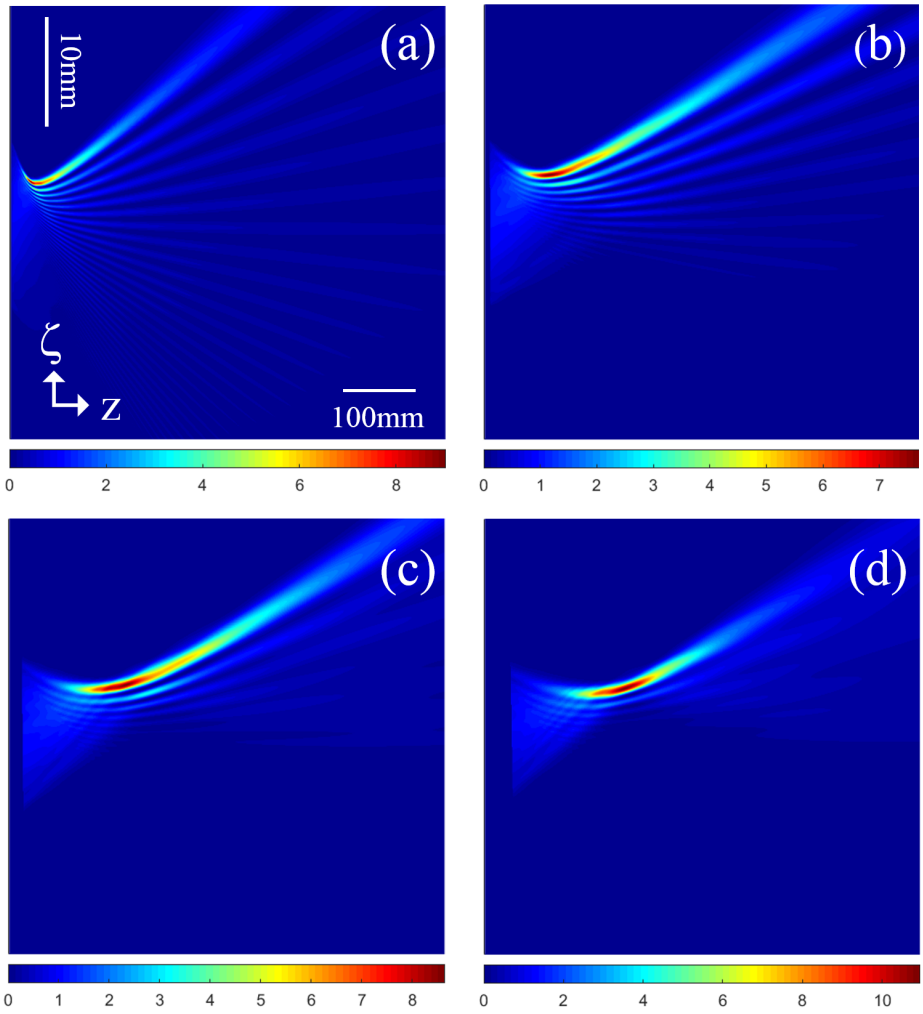

Figure 3.3: longitudinal Airy-beams in (ζ, z) plan for different acoustic wavelengths: (a) $\lambda_a = 2mm$, (b) $\lambda_a = 3mm$, (c) $\lambda_a = 4mm$, (d) $\lambda_a = 5mm$. for a beam width of $2w_0 = 1mm$

To have a clear idea in the transverse plan (ζ, η) we have done the following Figure 3.4; where the 2D transverse Airy beams at the back focal lens plane $(z = f = 200mm)$ are represented for different acoustic wavelengths.

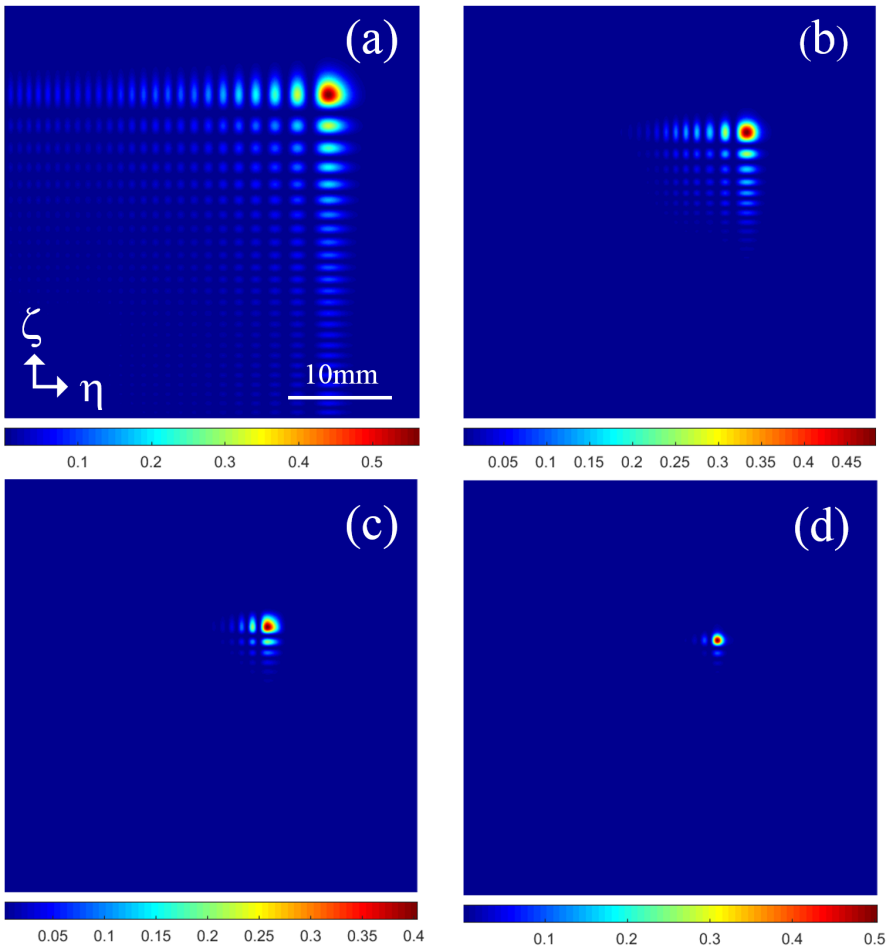

Figure 3.4: 2D Airy-beams (analytical results) for different acoustic wavelengths: (a) $\lambda_a = 2mm$, (b) $\lambda_a = 3mm$, (c) $\lambda_a = 4mm$, (d) $\lambda_a = 5mm$. in the z plan: $z = f = 200mm$, $\Omega t = 0$ and $\Delta n = 10^{-4}$.

It is to notice that increasing the acoustic wavelength leads to confine the beam energy on the central peak.

3.3.2 Effect of the coefficients truncation on the generated beams

In previous section (section 3.2) we have shown that the square aperture can be approximated to a finite sum of weighted Gaussian functions as represented in Eq. (3.8). So, we will study in this part the effect of the number of coefficient A_n and B_n on the generated beams. Fig. 3.5, Fig. 3.6 , Fig. 3.7 and Fig. 3.8 represent the transverse intensity diffracted for different coefficients A_n , B_n and for acoustic wavelengths taking the values of 2, 3, 4 and $5mm$.

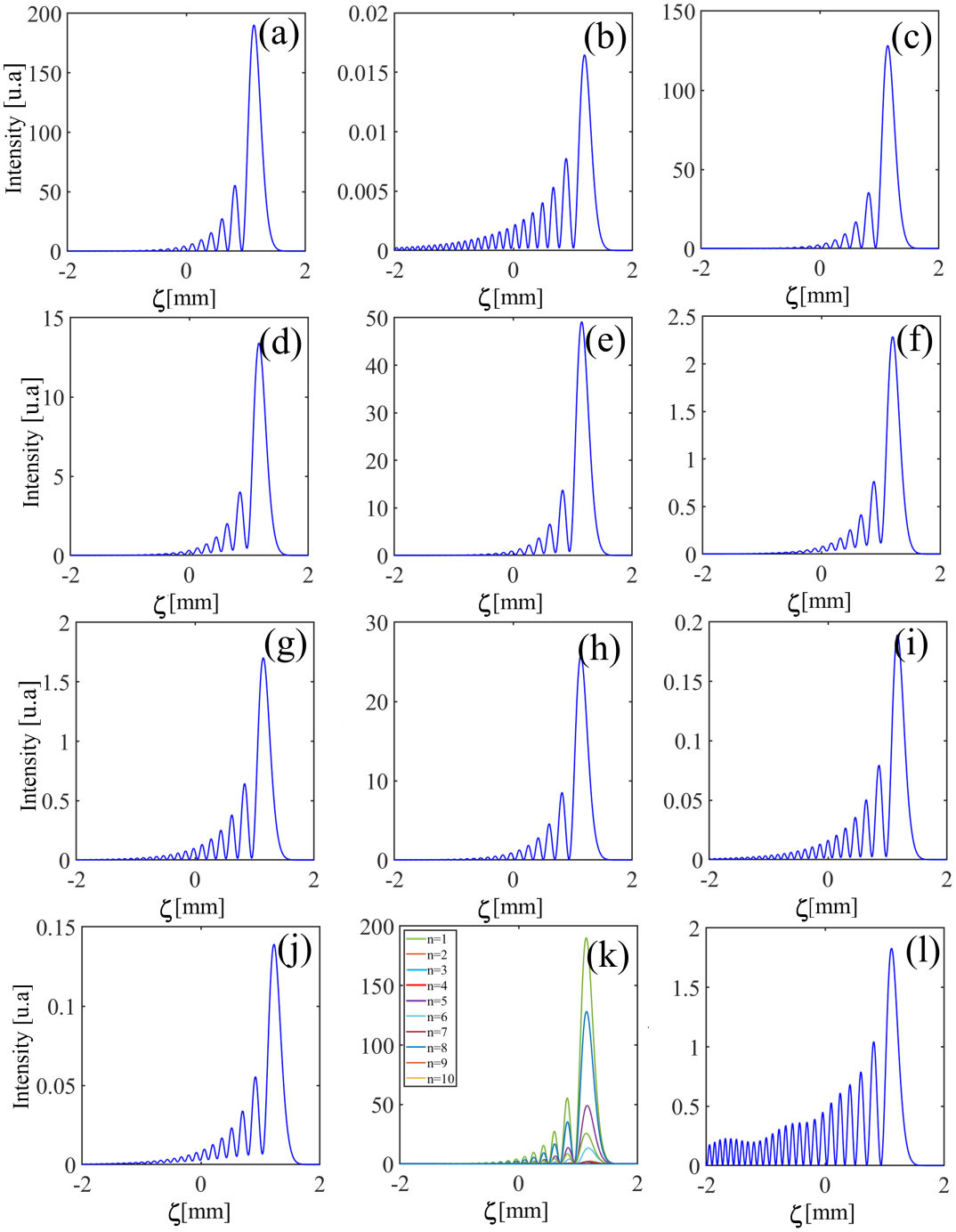

Figure 3.5: 1D Airy-beams (analytical results) for each coefficient A_n and B_n (a): n=1, (b): n=2, (c): n=3, (d): n=4, (e): n=5, (f): n=6, (g): n=7, (h): n=8, (i): n=9, (j): n=10. (k): represents the whole coefficients varying from $n = 1$ to 10. (l): represents the sum of the coefficients varying from $n = 1$ to 10. Acoustic wavelength $\lambda_a = 2mm$, representation plan $z = f = 200mm$, $\Omega t = 0$ and $\Delta n = 10^{-4}$.

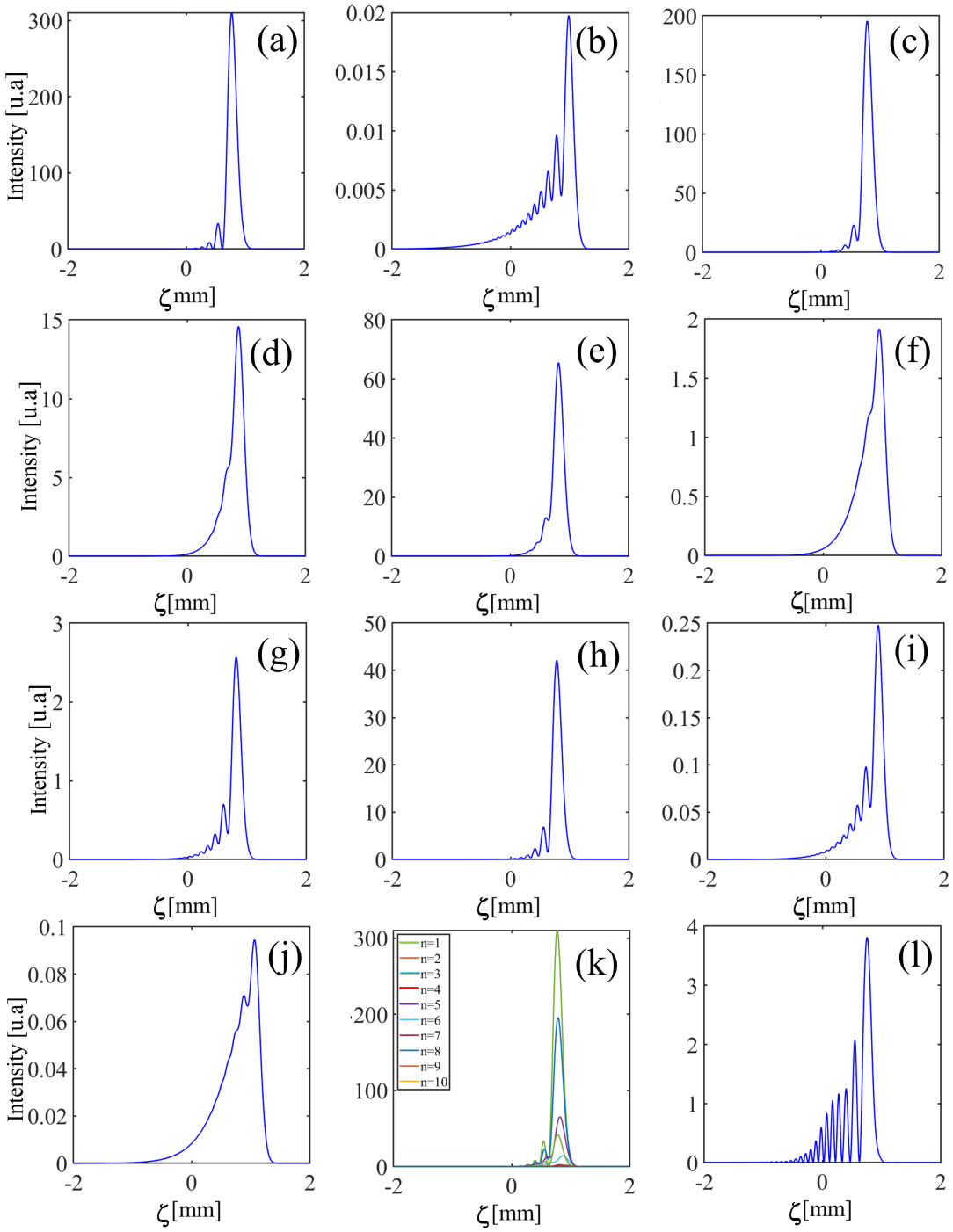

Figure 3.6: 1D Airy-beams (analytical results) for each coefficient A_n and B_n (a): n=1, (b): n=2, (c): n=3, (d): n=4, (e): n=5, (f): n=6, (g): n=7, (h): n=8, (i): n=9, (j): n=10. (k): represents the whole coefficients varying from $n = 1$ to 10. (l): represents the sum of the coefficients varying from $n = 1$ to 10. Acoustic wavelength $\lambda_a = 3mm$, representation plan $z = f = 200mm$, $\Omega t = 0$ and $\Delta n = 10^{-4}$.

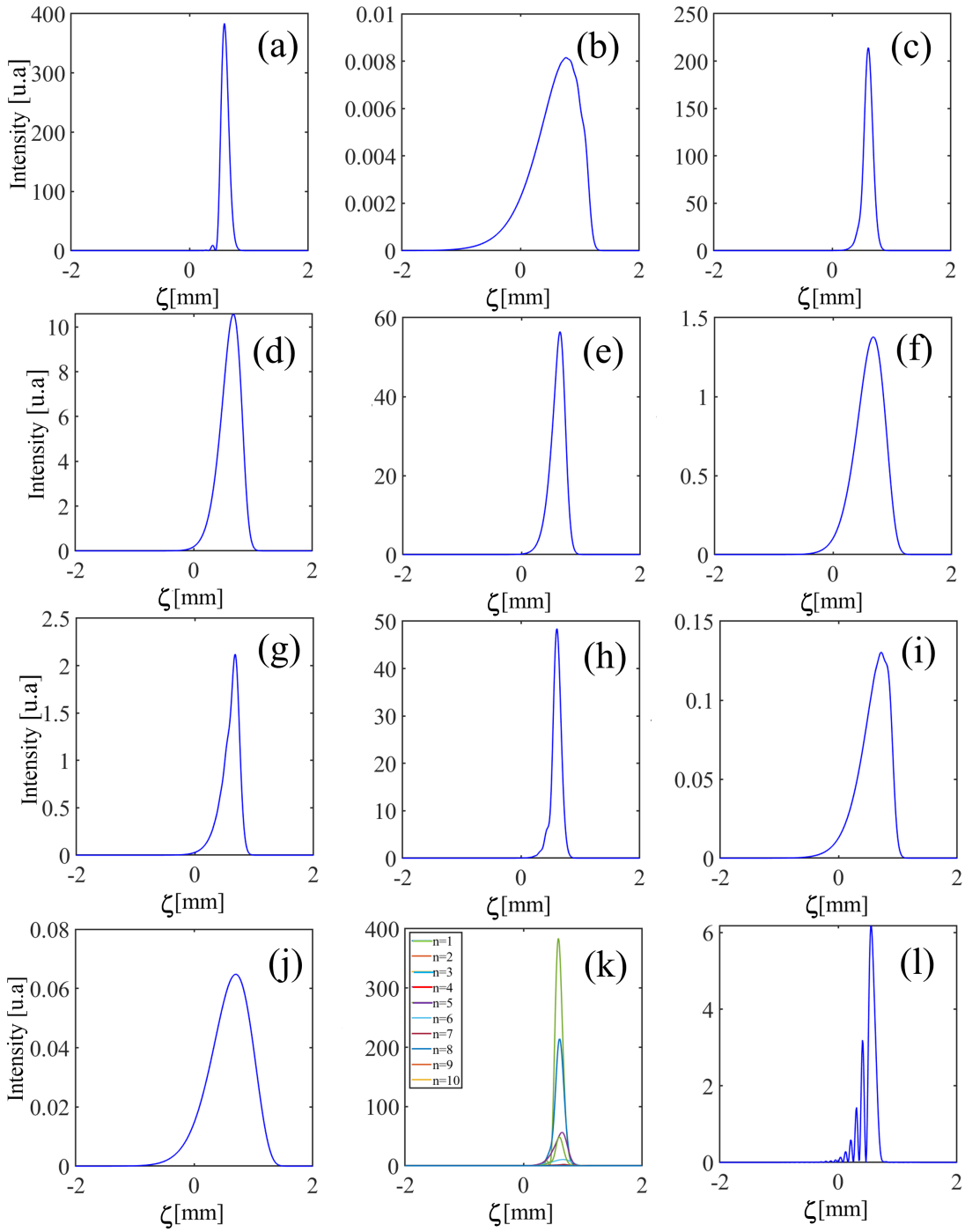

Figure 3.7: 1D Airy-beams (analytical results) for each coefficient A_n and B_n (a): n=1, (b): n=2, (c): n=3, (d): n=4, (e): n=5, (f): n=6, (g): n=7, (h): n=8, (i): n=9, (j): n=10. (k): represents the whole coefficients varying from $n = 1$ to 10. (l): represents the sum of the coefficients varying from $n = 1$ to 10. Acoustic wavelength $\lambda_a = 4mm$, representation plan $z = f = 200mm$, $\Omega t = 0$ and $\Delta n = 10^{-4}$.

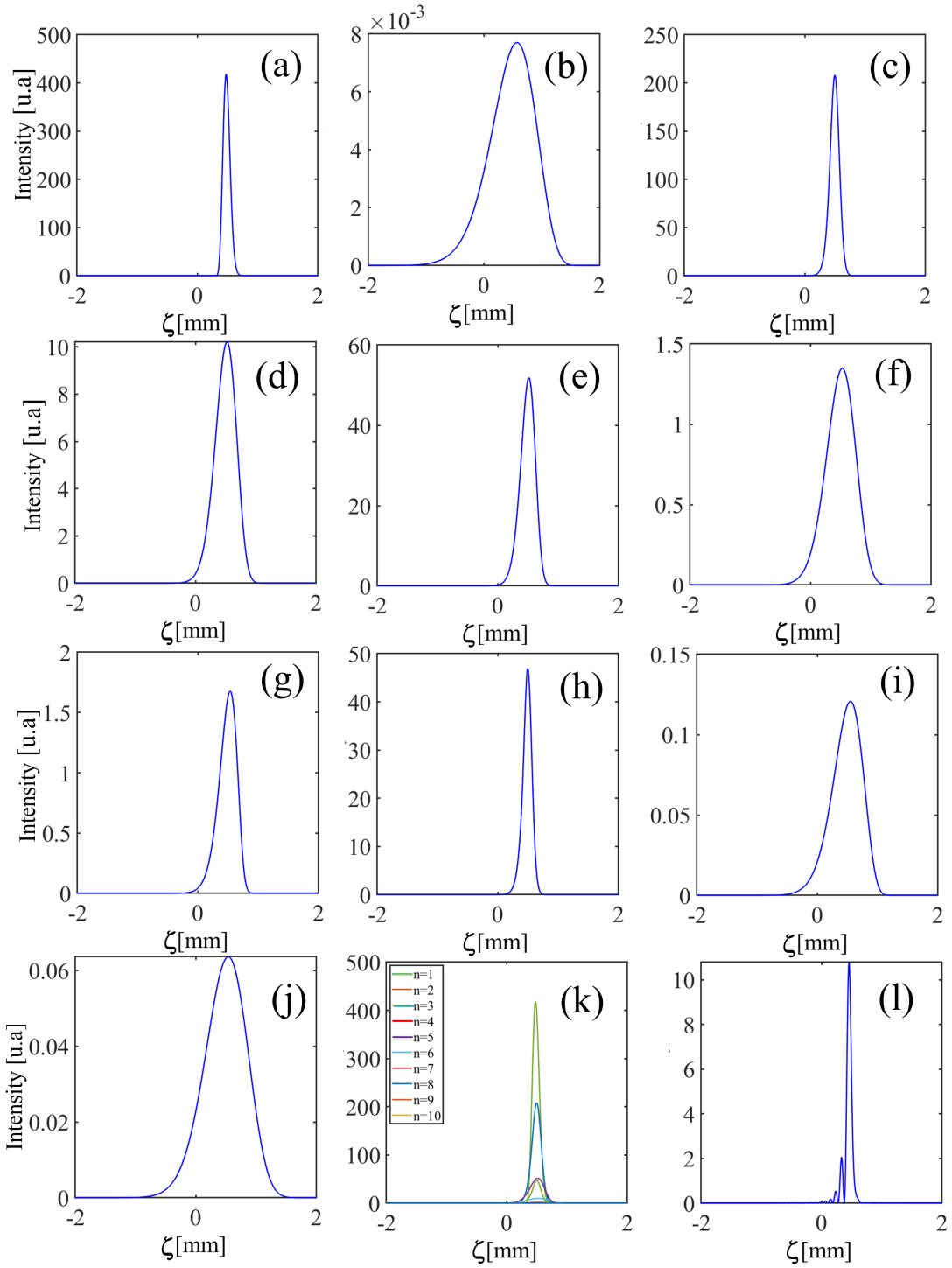

Figure 3.8: 1D Airy-beams (analytical results) for each coefficient A_n and B_n (a): n=1, (b): n=2, (c): n=3, (d): n=4, (e): n=5, (f): n=6, (g): n=7, (h): n=8, (i): n=9, (j): n=10. (k): represents the whole coefficients varying from $n = 1$ to 10. (l): represents the sum of the coefficients varying from $n = 1$ to 10.$\lambda_a = 5mm$ is the acoustic wavelength. The representation plan is $z = f = 200mm$, $\Omega t = 0$ and $\Delta n = 10^{-4}$.

From the above figures (Fig. 3.5 to Fig. 3.8), it is obvious that the contribution of the first and the third term in the summation are the most important, the remain terms are relatively weak. In addition, the intensities' zeroes of the different Airy-beams of each coefficient are almost the same, as it can be seen from the cited figures. These results help us to consider that the summation of many Airy-beams approximately as a single Airy-beam, which is especially true from a practical side of view.

3.3.3 Effect of the Expanding coefficients on the beam trajectory path as a function of acoustic wavelength

To study the trajectory of the resulting beam, which can be considered as a sum of many weighted and shifted Airy beams, we have plotted numerically the Airy beam paths corresponding to each couple of coefficient (A_n and B_n). Fig. 3.6 shows that all paths corresponding to all coefficient (A_n and B_n) overlap, and the whole beams propagates following only one path. The latter can be expressed analytically, by using some considerations as eliminated the imaginary part and by putting $w_0 = \infty$.

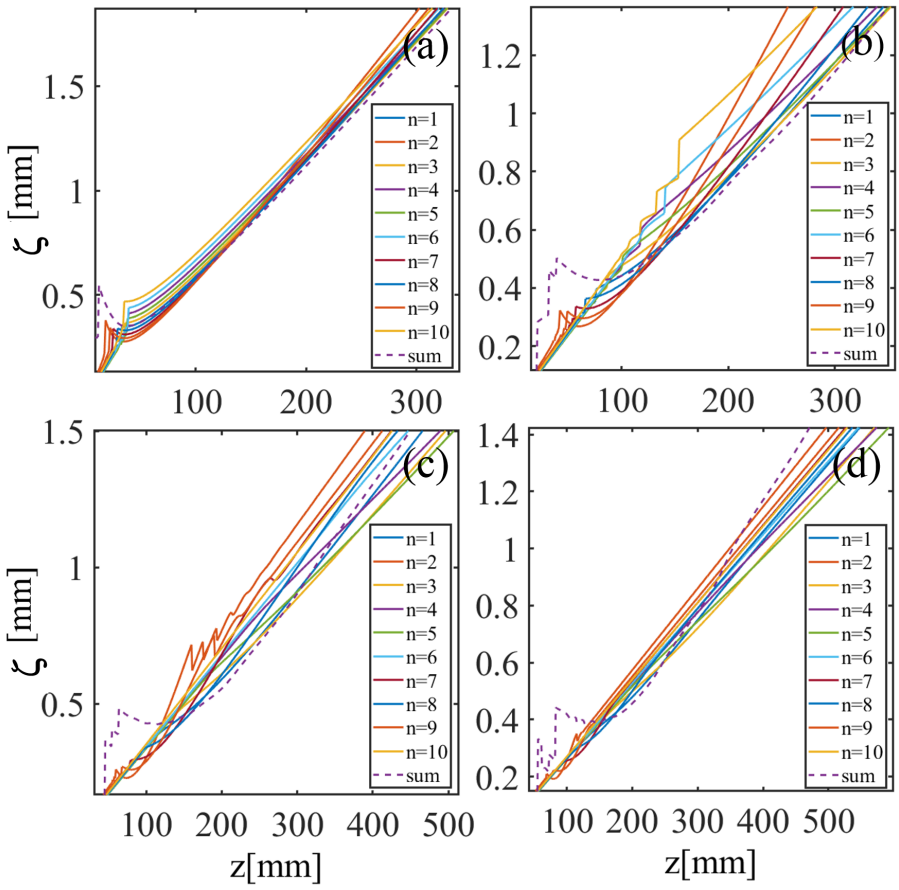

Figure 3.9: Airy beam paths (numerical results) corresponding to different coefficients A_n and B_n; (a): $\lambda_a = 2mm$, (b): $\lambda_a = 3mm$, (c): $\lambda_a = 4mm$ and (d): $\lambda_a = 5mm$. $\Omega t = 0$ and $\Delta n = 10^{-4}$.

-

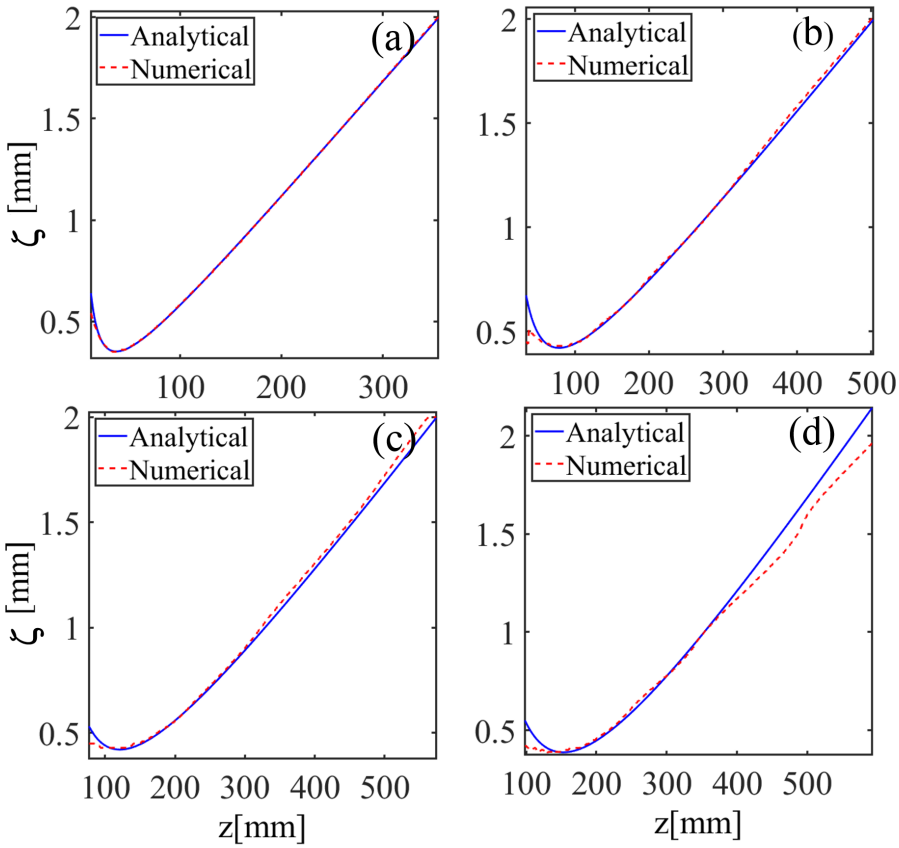

Figure 3.10: Airy beam paths (analytical and numerical results) ; (a): $\lambda_a = 2mm$, (b): $\lambda_a = 3mm$, (c): $\lambda_a = 4mm$ and (d): $\lambda_a = 5mm$. $\Omega t = 0$ and $\Delta n = 10^{-4}$.

3.3.4 The truncation effect on the path trajectory of the generated Airy beams

In this section we will demonstrate numerically the effect of the truncation (by an aperture or slit) on the path trajectory of the generated Airy beams. Figure 3.11(a-d) shows the obtained trajectories for different truncation widths (from $a = 0.4mm$ to $a = 0.8mm$) according to different acoustic wavelengths $\lambda_a = 2mm$, $\lambda_a = 3mm$, $\lambda_a = 4mm$ and $\lambda_a = 5mm$.

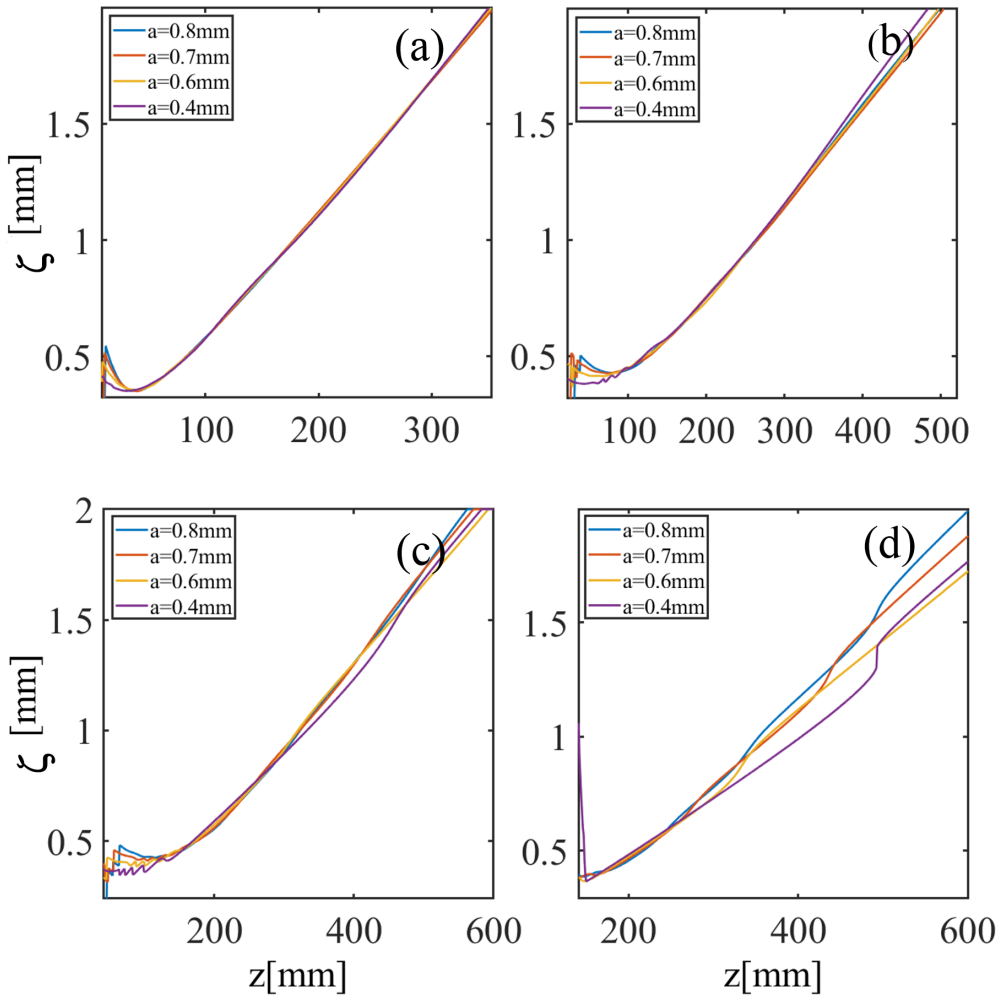

Figure 3.11: Airy beam paths (numerical results) corresponding to different truncated values a, wavelength (a): $\lambda_a = 2mm$, (b): $\lambda_a = 3mm$, (c): $\lambda_a = 4mm$ and (d): $\lambda_a = 5mm$. $\Omega t = 0$ and $\Delta n = 10^{-4}$.

It can be seen from the obtained curves that the aperture doesn't affect really the path trajectory. This can be explained physically as follows; as the ratio $\frac{w_0}{\lambda_a}$ (ratio between the Gaussian beam waist and the acoustic wavelengths) is smaller than the critical value which is 0.2 , so even we truncate the Gaussian beam, we are always in the region where the approximation (Sine function to cubic phase function) exists always, and consequently the output beam is an Airy-like beam. Small fluctuations in the near field due to diffraction are observed which disappear in the far-filed.

3.3.5 Effect of the refractive index increment Δn on the generated Airy beams

In this part we study the effect of the refractive index increment Δn on the generated Airy beam profiles and there trajectories along the propagation direction z. Fig. 3.12 shows the results of a numerical simulation, where the 2D transverse Airy beam distribution was presented within Fig. 3.12(a) to Fig. 3.12(c), and the 2D longitudinal Airy beam distribution from Fig. 3.12(d) to Fig. 3.12(f). As well, we present the 1D profile and the path trajectory respectively in Fig. 3.12(g) and Fig. 3.12(h).

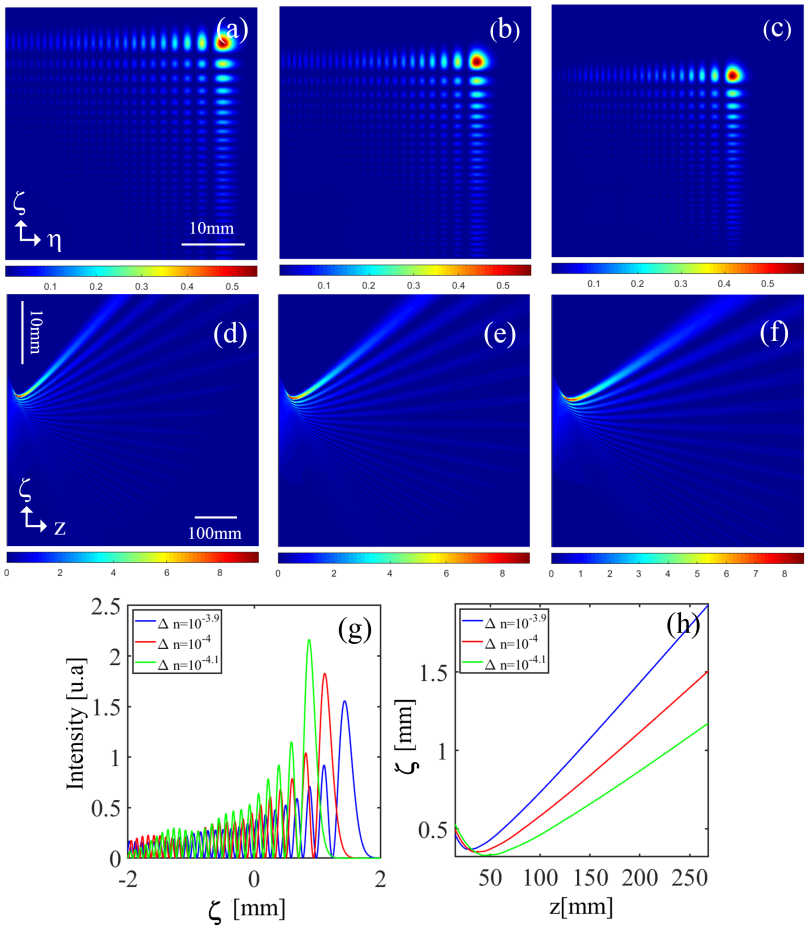

Figure 3.12: 2D transverse Airy beams in (ζ, η) plan; (a): $\Delta n = 10^{-3.9}$, (b): $\Delta n = 10^{-4.0}$ and (c): $\Delta n = 10^{-4.1}$, 2D longitudinal Airy beams in (z, ζ) plan; (d): $\Delta n = 10^{-3.9}$, (e): $\Delta n = 10^{-4.0}$ and (f): $\Delta n = 10^{-4.1}$, (g): 1D profile Airy beams for different Δn in the z plan $z = f = 200m$, (h): Airy beam path for different Δn. $\lambda_a = 2mm$

It seems clear, from Fig. 3.12(g), that the intensities of the Airy beams is increased and its distribution is shifted to left by decreasing the Δn parameter. However, the path trajectory became more curved by increasing Δn parameter, according to Fig. 3.12(h).

For this study we remark that the Airy beams are shifted towards x and y

directions as shown in the above figure Fig. 3.12(a)-Fig. 3.12(c) and Fig. 3.12(g). On the other hand the effect of Δn on the path trajectory is important, where the Airy beams are more curved when the Δn increases as shown in Fig. 3.12(d)-Fig. 3.12(f) and Fig. 3.12(h).

3.3.6 Effect of the time evolution of the ultrasound wave: the dynamic study

In this section, we exploit the dynamics property of the acousto-optic cell, where, we we study some additional cases as a function of the time evolution. Three values of Ωt $(\frac{\pi}{4}, \frac{3\pi}{4}, \pi)$ are chosen. Fig 3.13(a-c) shows the 2D transverse intensity of the obtained Airy beams. It seems clear that, when $\frac{\pi}{2} < \Omega t \leq \pi$, we are in the anti-symmetric case of the Airy beam and the intensity distribution becomes inverted. Fig 3.13(d-f) shows the 2D longitudinal Airy beams, while Fig. 3.13(h) shows the 1D path trajectory. It can be observed that the phase (due to time evolution) has a direct effect on the path trajectory. When, $0 < \Omega t \leq \frac{\pi}{2}$ the path is more curved if Ωt is smaller and when $\frac{\pi}{2} < \Omega t \leq \pi$ greater is the phase, more curved is the beam. Fig. 3.13(g) shows the intensity profile for different time phases, it can be seen that the profile is shifted with a decrease in intensity if we move from 0 to $\frac{\pi}{2}$ and from π to $\frac{\pi}{2}$, where the profile direction becomes inverted after $\frac{\pi}{2}$.

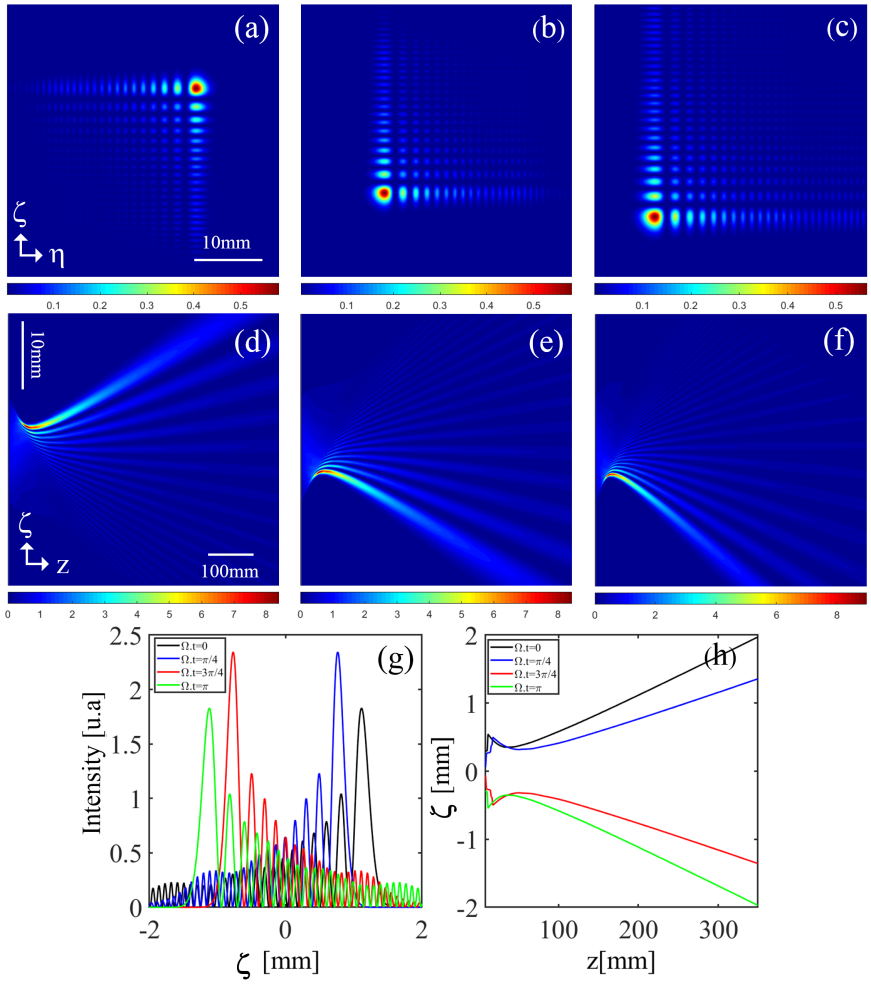

Figure 3.13: (a)-(b): 2D transverse Airy and (d)-(f): 2D longitudinal Airy beam beams for different time positions parameter $(\Omega t = \pi \setminus 4)$; $(\Omega t = 3\pi \setminus 4)$; $(\Omega t = \pi)$ respectively, (g): 1D profile Airy beams and (h): Airy beam path for different times position $(\Omega t = 0)$ $(\Omega t = \pi \setminus 4)$; $(\Omega t = 3\pi \setminus 4)$; $(\Omega t = \pi)$ respectively.

3.4 Conclusion

In summary, Airy-like beam through truncated acousto-optic cell was successfully generated. The resulted Airy beams are tunable with time characteristics. Which are

dependent on the acoustic parameters; Raman-Nath parameter and acoustic wavelength. The ideal intensity distribution was obtained in the focal plan. According to 2D energy distribution; higher is the Δn factor, higher is the curvature of the energy flux. However, larger is the acoustic wavelength, lower is the curvature of the energy. Further, Airy beam intensity shifted to right in transverse plane when the Δn parameter increases with decreasing in the maxima intensity . In the other hand, Larger is the acoustic wavelength, better is the system replay. Behinds, the intensity of maxima and specifically the main maximum increases and shifted to left in transverse plane by the acoustic frequency decreasing. Furthermore, hyperbolic trajectory has been successfully observed. In final step, temporal dynamic of the spatial structure was added, which is the main advantage for the acousto-optic technique. In time instant corresponding to the phase ($\Omega t = \pi$) the trajectory inverses its direction to the other side with perfect symmetric reflection of the beam distribution corresponding ($\Omega t = 0$) .

Bibliography

[1] Michael V Berry and Nandor L Balazs. Nonspreading wave packets. *American Journal of Physics*, 47(3):264–267, 1979.

[2] Georgios A Siviloglou and Demetrios N Christodoulides. Accelerating finite energy airy beams. *Optics letters*, 32(8):979–981, 2007.

[3] GA Siviloglou, J Broky, Aristide Dogariu, and DN Christodoulides. Observation of accelerating airy beams. *Physical Review Letters*, 99(21):213901, 2007.

[4] GA Siviloglou, J Broky, A Dogariu, and DN Christodoulides. Ballistic dynamics of airy beams. *Optics Letters*, 33(3):207–209, 2008.

[5] Xiuxiang Chu. Propagation of an airy beam with a spiral phase. *Optics letters*, 37(24):5202–5204, 2012.

[6] Dongmei Deng, Chidao Chen, Xin Zhao, and Huagang Li. Propagation of an airy vortex beam in uniaxial crystals. *Applied Physics B*, 110(3):433–436, 2013.

[7] Wei Wen and Xiuxiang Chu. Propagation of symmetric tunable dual airy beam through abcd optical system. *Optics Communications*, 333:38–44, 2014.

[8] Rui-Pin Chen, Chao-Fu Yin, Xiu-Xiang Chu, and Hui Wang. Effect of kerr nonlinearity on an airy beam. *Physical Review A*, 82(4):043832, 2010.

[9] Guoquan Zhou, Ruipin Chen, and Guoyun Ru. Propagation of an airy beam in a strongly nonlocal nonlinear media. *Laser Physics Letters*, 11(10):105001, 2014.

[10] Xiaoling Ji, Halil T Eyyuboğlu, Guangming Ji, and Xinhong Jia. Propagation of an airy beam through the atmosphere. *Optics express*, 21(2):2154–2164, 2013.

[11] Halil T Eyyuboğlu. Scintillation behavior of airy beam. *Optics & Laser Technology*, 47:232–236, 2013.

[12] Wei Wen and Xiuxiang Chu. Beam wander of an airy beam with a spiral phase. *JOSA A*, 31(4):685–690, 2014.

[13] Don M Cottrell, Jeffrey A Davis, and Thomas M Hazard. Direct generation of accelerating airy beams using a 3/2 phase-only pattern. *Optics letters*, 34(17): 2634–2636, 2009.

[14] Tal Ellenbogen, Noa Voloch-Bloch, Ayelet Ganany-Padowicz, and Ady Arie. Nonlinear generation and manipulation of airy beams. *Nature photonics*, 3(7):395–398, 2009.

[15] Xiuxiang Chu, Zejin Liu, and Pu Zhou. Generation of a high-power airy beam by coherent combining technology. *Laser Physics Letters*, 10(12):125102, 2013.

[16] Junxiao Zhou, Yachao Liu, Yougang Ke, Hailu Luo, and Shuangchun Wen. Generation of airy vortex and airy vector beams based on the modulation of dynamic and geometric phases. *Optics letters*, 40(13):3193–3196, 2015.

[17] Pavel Polynkin, Miroslav Kolesik, Jerome V Moloney, Georgios A Siviloglou, and Demetrios N Christodoulides. Curved plasma channel generation using ultraintense airy beams. *Science*, 324(5924):229–232, 2009.

[18] Jörg Baumgartl, Michael Mazilu, and Kishan Dholakia. Optically mediated particle clearing using airy wavepackets. *Nature photonics*, 2(11):675–678, 2008.

[19] Tom Vettenburg, Heather IC Dalgarno, Jonathan Nylk, Clara Coll-Lladó, David EK Ferrier, Tomáš Čižmár, Frank J Gunn-Moore, and Kishan Dholakia. Light-sheet microscopy using an airy beam. *Nature methods*, 11(5):541, 2014.

[20] Di Hu, Yao Liang, Yin Chen, Zan Hui Chen, and Xu Guang Huang. Autofocusing airy beam sted microscopy with long focal distance. *Optics Communications*, 404: 196–202, 2017.

[21] Zhengyi Yang, Martynas Prokopas, Jonathan Nylk, Clara Coll-Lladó, Frank J Gunn-Moore, David EK Ferrier, Tom Vettenburg, and Kishan Dholakia. A compact airy beam light sheet microscope with a tilted cylindrical lens. *Biomedical optics express*, 5(10):3434–3442, 2014.

[22] Yalong Gu and Greg Gbur. Scintillation of airy beam arrays in atmospheric turbulence. *Optics letters*, 35(20):3456–3458, 2010.

[23] Guoxuan Zhu, Yuanhui Wen, Xiong Wu, Yujie Chen, Jie Liu, and Siyuan Yu. Obstacle evasion in free-space optical communications utilizing airy beams. *Optics letters*, 43(6):1203–1206, 2018.

[24] Joseph W Goodman. *Introduction to Fourier optics*. Roberts and Company Publishers, 2005.

[25] JJ Wen and MA Breazeale. A diffraction beam field expressed as the superposition of gaussian beams. *The Journal of the Acoustical Society of America*, 83(5):1752–1756, 1988.

[26] JJ Wen and MA Breazeale. Computer optimization of the gaussian beam description of an ultrasonic field. *Computational Acoustics*, 2:181–196, 1990.

[27] Olivier Vallée and Manuel Soares. *Airy functions and applications to physics*. World Scientific Publishing Company, 2004.

Chapter 4

Generation of combined Airy beams using acousto-optic cell

Whosoever studies works of science must,
if he wants to find the truth,
transform himself into a critic of everything he reads
Hasan Ibn al-Haytham

4.1 Introduction

In the previous chapter, we have demonstrated analytically and numerically, under some asymptotic considerations, that an input Gaussian beam could be transformed into and interesting accelerated beams, which resembles to a single Airy-like beam. In this chapter we will extend the previous study to generate more complex Airy beams. We will show that under some practical considerations (the gaussian beam width is smaller enough than the ultrasound wavelength), that a couple of Gaussian beams could be transformed into a Dual-Airy beam (symmetric and anti-symmetric). In addition, we will demonstrate also, that a four symmetric Gaussian beams could be converted into a Quad-Airy beam under its two structures (Symmetric and anti-symmetric).

Throughout this chapter, we will demonstrate analytical expressions for the transverse intensities as well as for the path trajectories. All analytical expressions are validated using many numerical simulations. We use these simulations to demonstrate the effect of the acousto-optics interaction parameters (the Gaussian beam width, the acoustic wavelength, and the acoustic pressure or the Bessel parameter) on the generated Airy beams spatial properties such as; the curvature (acceleration), the launched angel (starting point), and the non diffracting range.

4.2 Theory

In this section, we provide some basics of the Gaussian beam diffraction by an ultrasonic standing wave. The ultrasonic wave propagating in a transparent medium (water) generates an elastic wave (wave pressure), the latter creates a variation of the liquid refractive index, which is proportional to the initial acoustic wave. The expression of the refractive index modulated by a standing ultrasonic wave is given as follows [1]

$$n_T(x,t) = n_0 + \Delta n\left[sin\left(k_a x\right).\cos\left(\Omega t\right)\right], \tag{4.1}$$

here n_0 represents the refractive index of the used liquid medium (water), Δn is the refractive index increment due to the acoustic pressure generated by the piezo-electric transducer on the liquid medium, k_a is the acoustic wave number in the liquid, x is the transverse spatial coordinate and Ω stays for the angular frequency. The refractive index given by Eq. (4.1) gives rise to a sinusoidal transmittance function, which is equivalent to a diffractive optical phase element (DOPE). By changing the different parameters of this latter, we will obtain a large interesting family of accelerated Airy beams.

In this chapter, the idea we used to generate Airy beams from Gaussian beams diffracted by a standing ultrasonic wave, is based on two considerations; Firstly, using the Airy function definition, $Ai(t) = \int \exp[xt - x^3/3]dx$, (The integral equation expresses a Fourier transform of a cubic phase). Secondly, using the asymptotic expression of the sinusoidal function near zero (using the Taylor series expansion of the sine function near zero), where $sin(x) \approx (x - x^3/3!)$. Based on these two considerations, the refractive index of the medium created by the ultrasonic wave becomes

$$n_T(x,t) = n_0 + \Delta n \left[\left(k_a x - \frac{(k_a x)^3}{6} \right) \cos(\Omega t) \right], \tag{4.2}$$

Consequently, the phase transmittance is written as

$$T(x,t) = \exp \left[-ikln_0 - i\psi \left(k_a x - \frac{(k_a x)^3}{6} \right) \cos(\Omega t) \right], \tag{4.3}$$

With $\psi = kl\Delta n$ is the Raman-Nath Parameter, k is the optical wave number, and l is the interaction length on the acousto-optic cell. In present study, we consider the case where the ultrasonic wave length is larger than the waist of the incident Gaussian laser beam $w_0 < \lambda_a$ (This is the main condition to consider the approximation of a sine function with a cubic term function).

Figure 4.1 shows the schematic layout for the Airy beams family generation. It is to notice, that the kind of the generated Airy beam depends on the number and the positions of input beams. To generate a Dual-Airy beam; two input symmetrically shifted Gauss beams are used. To generate a Quad-Airy beam; Four input symmetrically shifted Gauss beams are used (positioned on the vertices of a square or a lozenge).

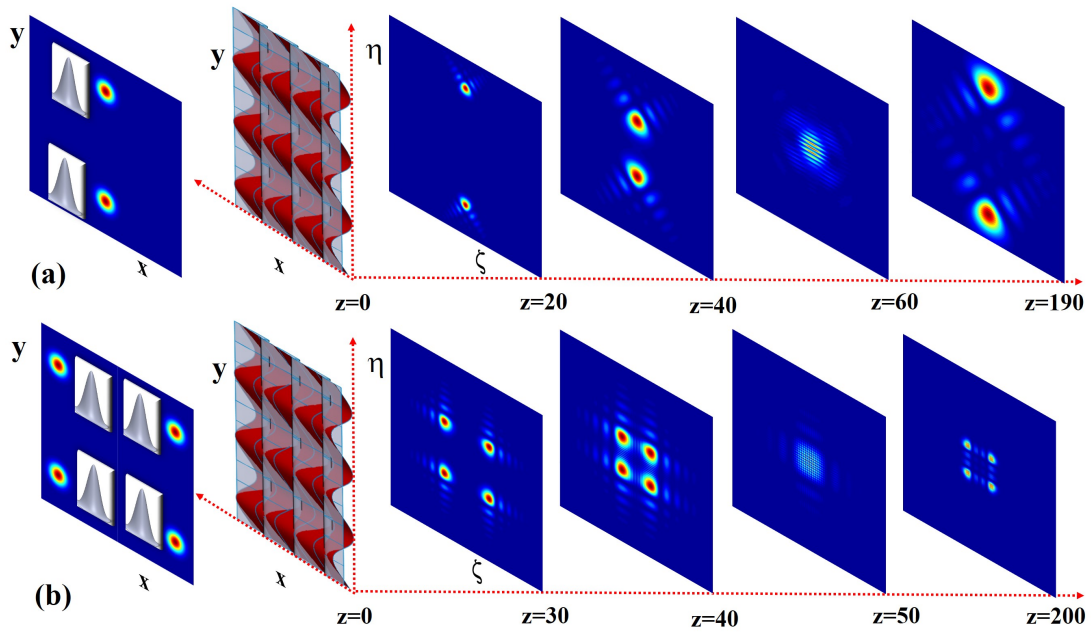

Figure 4.1: Optical layout showing the conversion of input Gaussian beams into combined Airy beam propagating along the z-axis.(a) Dual-Airy beam (b) Quad airy beam.

4.3 The diffraction of a Gaussian beam with a standing acoustic wave: Mathematical modelling

This section is dedicated to the modeling of the diffraction and propagation of some input Gaussian beams converted into some combined Airy beams using the cited acoustooptics cell. As it is well known, the diffraction and propagation of any optical beam could be described by the Fresnel-Kirchhoff diffraction integral, its expression in the 2-D Cartesian grid is given as follows [2]

$$E(\zeta,\eta,z)=\frac{1}{\sqrt{i\lambda z}}\int_{-\infty}^{+\infty}\int_{-\infty}^{+\infty}T(x,y) \times \exp\left(-i\frac{k}{2z}(\zeta-x)^2+i\frac{2\pi}{\lambda z}(\eta-y)^2\right)dxdy \quad (4.4)$$

By considering the input Gaussian beam and the transmittance function created by the acoustic wave, the above Fresnel-Kirchhoff integral becomes [2]

$$E(\zeta,\eta,z)=E(\zeta,z)\,E(\eta,z)=\frac{\exp(-ikz)}{i\lambda z}\exp\left(-i\frac{k}{2z}(\zeta^2+\eta^2)\right)\times \int_{-\infty}^{+\infty}E_0(x)T(x,t)\exp\left(-i\frac{k}{2z}x^2+i\frac{k}{z}\zeta x\right)dx\times \int_{-\infty}^{+\infty}E_0(y)T(y,t)\exp\left(-i\frac{k}{2z}y^2+i\frac{k}{z}\eta y\right)dy, \quad (4.5)$$

Here E_0 and E are the amplitudes for input and output beams respectively, and (x, y) and (ζ, η) stand for the coordinates of the input and output planes.

It is to notice that the present work is a plan for future experiments, so, we will consider the experimental conditions where the Gaussian beam size is small enough comparing to the ultrasonic wave wavelength. These considerations allow us to avoid truncated integrals, which becomes $-\infty$ to $+\infty$ allowing the analytical determination of the generated Airy beams spatial properties, such as the transverse intensity as well as the longitudinal one (on-axis intensity) .

4.3.1 Transformation of a Gaussian beam into an Airy beam

In this section, we demonstrate analytically how input Gaussian beams are converted into some combined Airy beams using a dynamic sinusoidal phase mask (the phase

mask is created by the propagation of the ultrasound wave on water). We began by the simplest case, we use 1-D counterpart of 2-D Airy beam, and applying the 1-D diffraction integral of Eq. (4.5), the 1-D electric field of the output beam is given by

$$E(\zeta,z,t)=\frac{1}{\sqrt{i\lambda z}}\int_{-\infty}^{+\infty}\exp\left[\left(-ikln_0-i\psi\left(k_a x-\frac{(k_a x)^3}{6}\right)\cos(\Omega t)\right)\right]\times\exp\left[-\left(\frac{x}{w_0}\right)^2\right]\exp\left(-i\frac{\pi}{\lambda z}x^2+i\frac{2\pi}{\lambda z}\zeta x\right)dx. \quad (4.6)$$

Using the scaling variable $h=k_a\sqrt[3]{\frac{\psi\cos(\Omega t)}{2}}x$ and ignoring all phase factors not concerned by the integration, Eq. (4.6) is reduced to the canonical Airy integral

$$E(\zeta,z,t)=\frac{1}{\sqrt{i\lambda z}}\int_{-\infty}^{+\infty}\exp\left[i\left(\frac{h^3}{3}+ah^2+(q\zeta-o)\,h\right)\right]dh, \quad (4.7)$$

Where

$$a=\frac{-\frac{1}{iw_0^2}-\frac{\pi}{\lambda z}}{\left(\frac{\psi\cos(\Omega t)}{2}\right)^{\frac{2}{3}}k_a^2},\ q=\frac{2\pi/\lambda z}{\sqrt[3]{\frac{\psi\cos(\Omega t)}{2}}k_a},\ o=\frac{\psi\cos(\Omega t)}{\sqrt[3]{\frac{\psi\cos(\Omega t)}{2}}}.$$

Using the following integral formula [3]

$$\int_{-\infty}^{+\infty}\exp\left[i\left(\frac{h^3}{3}+ah^2+bh\right)\right]dh=2\pi e^{ia\left(\frac{2}{3}a^2-b\right)}Ai\left(b-a^2\right). \quad (4.8)$$

After some algebra, we find the electric field expression of the generated 1-D Airy beam, in the (ζ,z) plane as follows

$$E(\zeta,z,t)=\frac{1}{\sqrt{i\lambda z}}\exp\left[ia\left(\frac{2}{3}a^2-(q\zeta-o)\right)\right]Ai\left((q\zeta-o)-a^2\right). \quad (4.9)$$

To check the validity of the approximations ($(sin(x) \approx (x - x^3/6)$ and the infinite integral), we used some simulations to compare the analytical results given by Eq. (4.9) and those solved numerically without any approximation given by Eq. (4.6), the results are shown in Fig. 4.2. The intensities' profiles are almost in perfect overlap. This result ensures us to continue using the same concept throughout the paper to generate all varieties of combined Airy beams.

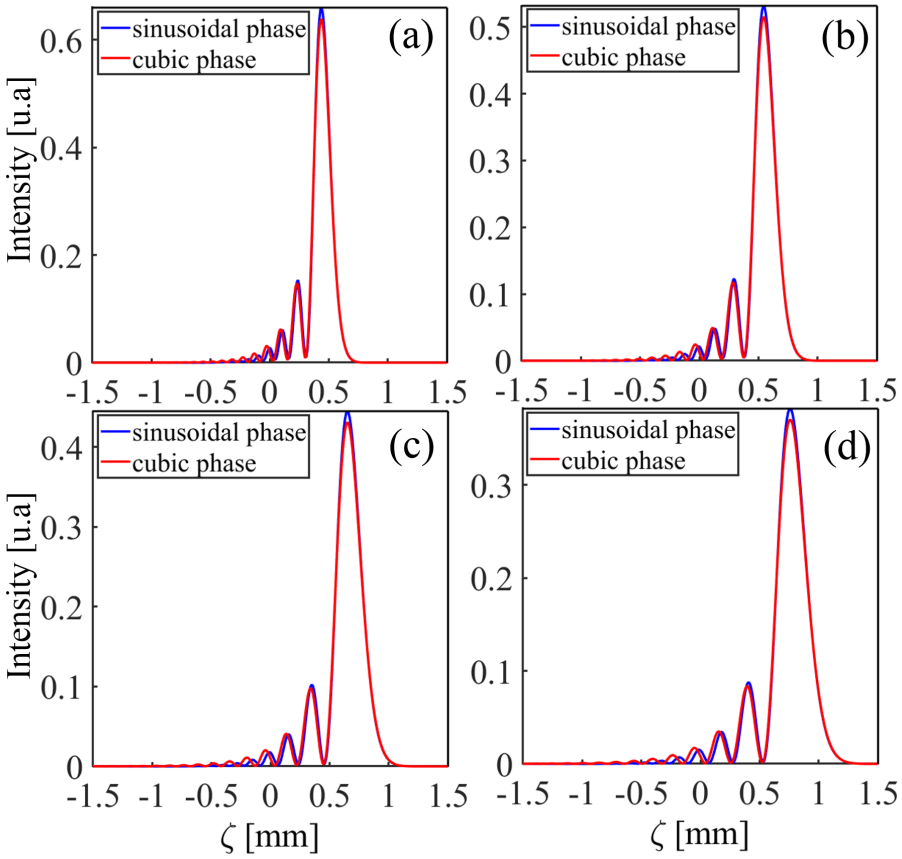

Figure 4.2: (a)..(d): Airy beams for different z positions; $z = 40mm, z = 50mm, z = 60mm, z = 70mm$ respectively at $t = 0$.

After showing the 1-D counterpart ($Ai(x)$) of the 2-D Airy beam ($Ai(x)Ai(y)$), we extend the previous development to the 2-D case. To generate 2-D Airy beams, we have to choose the meridian plane, where the 2-D Airy beam would propagate. By orienting the 2-D phase transmittance as shown in Fig. 4.3, the generated Airy beam

can propagate in 1-D geometry as shown in Fig. 4.3(a), or in 2-D square geometry as shown in Fig. 4.3(b), or in 2-D lozenge geometry as shown in Fig. 4.3(c). Furthermore, it is to notice that the phase shown in Fig. 4.3(b) is obtained by crossing two phases of Fig. 4.3(a), while the phase shown in Fig. 4.3(c) is obtained by rotating the phase shown in Fig. 4.3(b) by 45°.

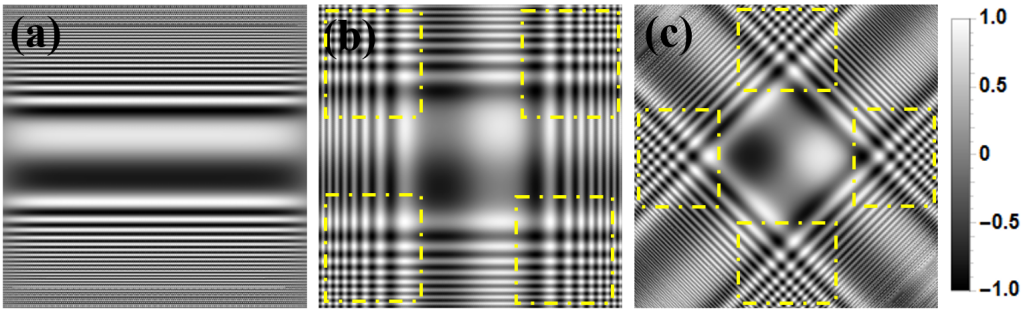

Figure 4.3: The periodic cubic phase transmittance used for the generation of all combined Airy beams: (a) 1-D geometry, (b) 2-D square geometry, and (c) 2-D lozenge geometry.

To generate the 2-D Airy beam we used the phase shown in Fig. 4.3(b). First, we consider the 2-D input Gaussian beam $E_0(x, y) = E_0(x)E_0(y)$, its field takes the following expression

$$E_0\left(x, y\right) = \exp\left[-\left(\frac{x - m\lambda_a}{w_0}\right)^2\right] \exp\left[-\left(\frac{y - m\lambda_a}{w_0}\right)^2\right]. \tag{4.10}$$

Here the shifts $m\lambda_a$ in x and y coordinates allow us to locate the input Gaussian beam where we want in the first quadrant.

To calculate the amplitude $E_{Square}(\zeta, \eta, z, t) = E(\zeta, z, t)E(\eta, z, t)$ of the generated 2-D Airy beam, we calculate separately $E(\zeta, z, t)$ and $E(\eta, z, t)$ following the same steps used before for 1-D Airy beam. Here we used the variable change:

$h = k_a \sqrt[3]{(\psi\cos(\Omega t)/2)}x$ and $g = k_a \sqrt[3]{(\psi\cos(\Omega t)/2)}y$. The two integrals we used to calculate $E(\zeta, z, t)$ and $E(\eta, z, t)$ are respectively

$$E\left(\zeta, z, t\right) = \frac{1}{\sqrt{i\lambda z}} \int_{-\infty}^{+\infty} \exp\left[i\left(\frac{h^3}{3} + a_1 h^2 + \left(q\zeta + o_1\right) h\right)\right] dh, \tag{4.11}$$

$$E\left(\eta, z, t\right) = \frac{1}{\sqrt{i\lambda z}} \int_{-\infty}^{+\infty} \exp\left[i\left(\frac{g^3}{3} + a_1 g^2 + \left(q\eta + o_1\right) g\right)\right] dg, \tag{4.12}$$

Where $a_1 = \dfrac{\frac{\psi\cos(\Omega t)3k_a {m_a k_a}^2}{6} - \frac{1}{iw_0^2} - \frac{\pi}{\lambda z}}{\left(\sqrt[3]{\frac{\psi\cos(\Omega t)}{2}} k_a\right)^2}$,

and

$o_1 = \dfrac{\frac{\psi 3k_a \left(k_a m \lambda_a\right)^2}{6} - \frac{2m\lambda_a}{iw_0^2} - \psi\cos(\Omega t)k_a}{\left(\sqrt[3]{\frac{\psi\cos(\Omega t)}{2}} k_a\right)}$.

Using the integral of Eq. (4.8), the expression of 2-D Airy beam amplitude in the square geometry is given by

$$\begin{aligned} E^{Ai}_{Square}\left(\zeta, \eta, z, t\right) = \frac{1}{i\lambda z} \exp\left[ia_1\left(\frac{2}{3}a_1^2 - \left(q\zeta - o_1\right)\right)\right] Ai\left(q\zeta - o_1 - a_1^2\right) \\ \times \exp\left[ia_1\left(\frac{2}{3}a_1^2 - \left(q\eta - o_1\right)\right)\right] Ai\left(q\eta - o_1 - a_1^2\right). \end{aligned} \tag{4.13}$$

The expression of the generated 2-D Airy beam amplitude given by Eq. (4.13), corresponds to an Airy beam generated by the geometry of Fig. 4.3(b). The initial beam position at the phase transmittance is located in the first quadrant highlighted by

the yellow dashed square. We mention that it is possible to deduce without calculation, the expression of the 2-D Airy beam corresponding to the other quadrants (2^{nd}, 3^{rd}, and 4^{th}). Moreover, since the optical components we used here have cylindrical symmetry, the diffraction integrals are invariant under rotations. Consequently, the 2-D Airy beam amplitude generated by the phase of Fig. 4.3(c), is obtained by rotating the coordinate system by 45°, where $\zeta = (1/\sqrt{2})(\eta - \zeta)$, and $\eta = (1/\sqrt{2})(\eta + \zeta)$. The final expression of 2-D Airy beam amplitude in the lozenge geometry is

$$\begin{aligned} E^{Ai}_{Lozenge}(\zeta,\eta,z,t) = \frac{1}{i\lambda z}\exp\left[ia_1\left(-\frac{q}{\sqrt{2}}(\eta-\zeta)+\frac{2}{3}a_1^2+o_1\right)\right] \\ \times Ai\left(\frac{q}{\sqrt{2}}(\eta-\zeta)-o_1-a_1^2\right)\exp\left[ia_1\left(-\frac{q}{\sqrt{2}}(\zeta+\eta)+\frac{2}{3}a_1^2+o_1\right)\right] \\ \times Ai\left(\frac{q}{\sqrt{2}}(\zeta+\eta)-o_1-a_1^2\right). \end{aligned} \tag{4.14}$$

4.3.2 Transformation of two Gaussian beams into a Dual-Airy beam

After generating the simplest case of 2-D Airy-like beams, we use two input symmetric Gaussian beams, which are converted into two types of Dual-Airy beams; the symmetric and anti-symmetric one. The mathematics behind this conversion could be deduced by symmetry of Eqs. (4.13-4.14) with respect to the origin $(x, y) = (0, 0)$ axis. The amplitude of the input field is given by

$$\begin{aligned} E_0(x,y) =& \exp\left[-\left(\frac{y+m\lambda_a}{w_0}\right)^2-\left(\frac{x+m\lambda_a}{w_0}\right)^2\right]+ \\ & \exp\left[-\left(\frac{y-m\lambda_a}{w_0}\right)^2-\left(\frac{x-m\lambda_a}{w_0}\right)^2\right]. \end{aligned} \tag{4.15}$$

Each Gaussian beam of Eq. (4.15) gives rise to 2-D Airy beam as described by the Eq. (4.13), without repeating the calculation from scratch, we deduce the 2-D Airy beam amplitude from Eq. (4.13), it is given in the square geometry as

$$\begin{aligned} E_{Square}^{DualAi}(\zeta,\eta,z,t) = \frac{1}{i\lambda z}\exp\left[ia_1\left(-q\zeta+o_1+\frac{2}{3}a_1^2\right)\right]Ai\left(q\zeta-o_1-a_1^2\right) \\ \times\exp\left[ia_1\left(-q\eta+o_1+\frac{2}{3}a_1^2\right)\right]Ai\left(q\eta-o_1-a_1^2\right) \\ +\frac{1}{i\lambda z}\exp\left[ia_1\left(q\zeta+o_1+\frac{2}{3}a_1^2\right)\right]Ai\left(-q\zeta-o_1-a_1^2\right) \\ \times\exp\left[ia_1\left(q\eta+o_1+\frac{2}{3}a_1^2\right)\right]Ai\left(-q\eta-o_1-a_1^2\right). \end{aligned} \quad (4.16)$$

The generated Dual-Airy beam in the Lozenge geometry could also be deduced from Eq. (4.14) without calculation using the symmetry with respect to the y-axis, the generated 2-D Dual-Airy beam amplitude is given by

$$\begin{aligned} E_{Lozenge}^{DualAi}(\zeta,\eta,z,t) = \frac{1}{i\lambda z}\exp\left[ia_1\left(-q(\eta-\zeta)+o_1+\frac{2}{3}a_1^2\right)\right]Ai\left(q(\eta-\zeta)-o_1-a_1^2\right) \\ \times\exp\left[ia_1\left(-q(\eta+\zeta)+o_1+\frac{2}{3}a_1^2\right)\right]Ai\left(q(\eta+\zeta)-o_1-a_1^2\right) \\ +\frac{1}{i\lambda z}\exp\left[ia_1\left(q(\eta+\zeta)+o_1+\frac{2}{3}a_1^2\right)\right]Ai\left(q(-\eta+\zeta)-o_1-a_1^2\right) \\ \times\exp\left[ia_1\left(q(\eta-\zeta)+o_1+\frac{2}{3}a_1^2\right)\right]Ai\left(q(-\eta+\zeta)-o_1-a_1^2\right). \end{aligned} \quad (4.17)$$

4.3.3 Transformation of four Gaussian beams into a Quad-Airy beam

In this section, the input beam is composed of four symmetric Gaussian beams positioned on the vertices of a square or a lozenge. This latter depends on the geometry of

the Quad-Airy beam we want to generate. As an example we have chosen the squared geometry shown in Fig. 4.3(b). The input Gaussian beams are shifted symmetrically with respect to the centre of the Quad-Airy beam, the amplitude of the input beam is written as

$$\begin{aligned} E_0(x,y) = \exp&\left[-\left(\frac{x-m\lambda_a}{w_0}\right)^2-\left(\frac{y-m\lambda_a}{w_0}\right)^2\right] \\ +\exp&\left[-\left(\frac{x+m\lambda_a}{w_0}\right)^2-\left(\frac{y+m\lambda_a}{w_0}\right)^2\right] \\ +\exp&\left[-\left(\frac{x-m\lambda_a}{w_0}\right)^2-\left(\frac{y+m\lambda_a}{w_0}\right)^2\right] \\ +\exp&\left[-\left(\frac{x+m\lambda_a}{w_0}\right)^2-\left(\frac{y-m\lambda_a}{w_0}\right)^2\right]. \end{aligned} \tag{4.18}$$

Without any further calculations, using just Eq. (4.14) and by symmetry, we can determine the four amplitude components of the generated Quad-Airy beam is a square geometry, given by

$$
\begin{aligned}
E_{Square}^{Quad}(\zeta,\eta,z,t) = \frac{1}{\sqrt{i\lambda z}} & \\
\times \exp\left[ia_1\left(-q\zeta + o_1 + \frac{2}{3}a_1^2\right)\right] & Ai\left(q\zeta - o_1 - a_1^2\right) \\
\times \exp\left[ia_1\left(-q\eta + o_1 + \frac{2}{3}a_1^2\right)\right] & Ai\left(q\eta - o_1 - a_1^2\right) \\
+ \frac{1}{\sqrt{i\lambda z}} & \\
\times \exp\left[ia_1\left(+q\zeta + o_1 + \frac{2}{3}a_1^2\right)\right] & Ai\left(-q\zeta - o_1 - a_1^2\right) \\
\times \exp\left[ia_1\left(+q\eta + o_1 + \frac{2}{3}a_1^2\right)\right] & Ai\left(-q\eta - o_1 - a_1^2\right) \\
+ \frac{1}{\sqrt{i\lambda z}} & \\
\times \exp\left[ia_1\left(q\zeta + o_1 + \frac{2}{3}a_1^2\right)\right] & Ai\left(-q\zeta - o_1 - a_1^2\right) \\
\times \exp\left[ia_1\left(-q\eta + o_1 + \frac{2}{3}a_1^2\right)\right] & Ai\left(q\eta - o_1 - a_1^2\right) \\
+ \frac{1}{\sqrt{i\lambda z}} & \\
\times \exp\left[ia_1\left(-q\zeta + o_1 + \frac{2}{3}a_1^2\right)\right] & Ai\left(q\zeta - o_1 - a_1^2\right) \\
\times \exp\left[ia_1\left(q\eta + o_1 + \frac{2}{3}a_1^2\right)\right] & Ai\left(-q\eta - o_1 - a_1^2\right). \quad (4.19)
\end{aligned}
$$

4.4 Analytical expression of the path trajectory of generated Airy beams

Determination of the Airy beams path trajectory is usually obtained by making the argument of the Airy function equals to its local maxima. In this study we follow this concept to determine the generated Airy beams trajectory. It is worth noting that the trajectory is the same for all combined Airy beams (Single, Dual- and Quad-Airy beams). For Dual-Airy beams, we just combine symmetrically the paths obtained in a

single Airy beam. For Quad-Airy beams, we combine the paths of two crossed Dual-Airy beams. For that reason, we limit the study for only one case to show the curved (accelerated) path of the different generated Airy beams. Taking the argument of Airy function given in Eq. (4.9), we can write

$$\begin{aligned}
\left[\frac{\left(\frac{2\pi}{\lambda z}\zeta - \psi k_a\right)}{\left(\sqrt[3]{\frac{\psi}{2}}k_a\right)} - \frac{\left(-\frac{1}{iw_0^2} - \frac{\pi}{\lambda z}\right)^2}{\left(\sqrt[3]{\frac{\psi}{2}}k_a\right)^4}\right] &= y_m, \\
\left[\frac{\left(-\psi k_a - \frac{2\pi}{\lambda z}\zeta\right)}{\left(\sqrt[3]{\frac{\psi}{2}}k_a\right)} - \frac{\left(-\frac{1}{iw_0^2} - \frac{\pi}{\lambda z}\right)^2}{\left(\sqrt[3]{\frac{\psi}{2}}k_a\right)^4}\right] &= y_m,
\end{aligned} \tag{4.20}$$

where y_m is the local maxima of the Airy function. After some algebra and using some approximations, we obtained the coordinates of Airy beam paths along the propagation axis z for the general case of two symmetric (Anti-symmetric) Dual-Airy beams. They are given by

$$\begin{aligned}
\zeta_1 &= \frac{\lambda z \psi k_a}{2\pi} + \frac{y_m \sqrt[3]{\frac{\psi}{2}} \lambda z k_a}{2\pi} + \frac{\pi}{\lambda z \psi {k_a}^3} - m\lambda_a, \\
\zeta_2 &= -\frac{\lambda z \psi k_a}{2\pi} - \frac{y_m \sqrt[3]{\frac{\psi}{2}} \lambda z k_a}{2\pi} - \frac{\pi}{\lambda z \psi {k_a}^3} + m\lambda_a,
\end{aligned} \tag{4.21}$$

where $m\lambda_a$ is the transverse shift.

4.5 Results and discussion

After modeling the interaction of one, two and four Gaussian beams with 2-D sinusoidal phase transmittance, the latter resulting from the propagation of crossed 2-D ultrasonic waves in water. We continue our investigation by simulating the different results presented in the previous section. We used a wavelength $\lambda = 633nm$, a Gaussian beam width $w_0 = 0.1mm$, an acoustic wavelength $\lambda_a = 0.5mm$, a cell width $l = 10mm$, $y_m = -1.01879$ and $m = 1.25$. We start our numerical simulation by a single-Airy beam, Dual-Airy beam and we finish by Quad-Airy beam.

4.5.1 Generated single-Airy beam

Based on the analytical models developed in the previous section, we simulated our results for an input 2-D Gaussian beam converted into an Airy-like beam, using a 2-D transmittance shown in Fig. 4.3(b).

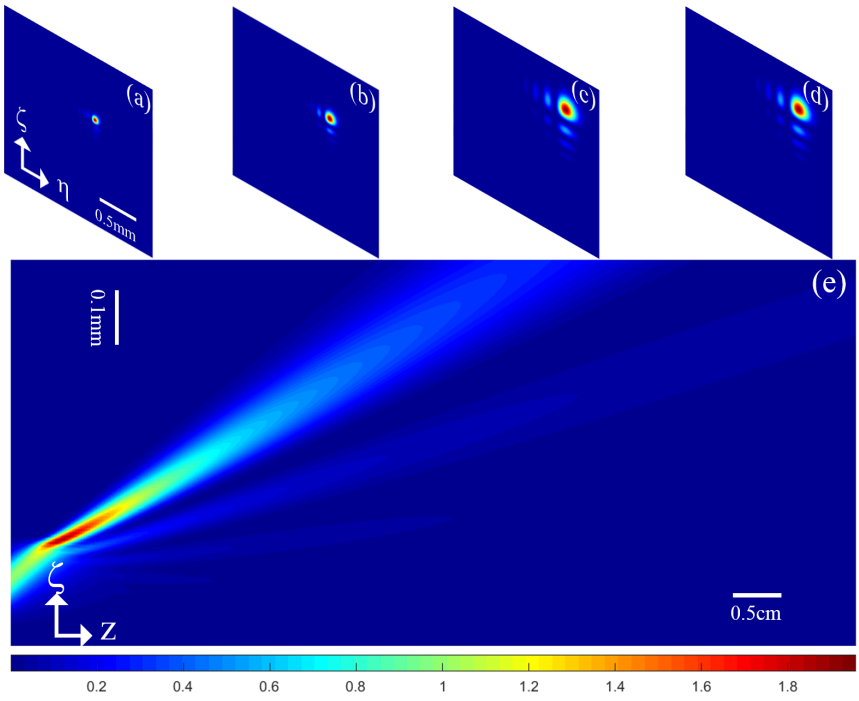

Figure 4.4: 2-D accelerated Airy-like beam: for different z positions; (a) $z = 20mm$, (b) $z = 30mm$, (c) $z = 40mm$, (d) $z = 50mm$ respectively at $t = 0$. (e): longitudinal accelerated Airy-like beam. $\lambda_a = 0.5mm$; $w_a = 0.1mm$.

The first results are shown in Fig. 4.4, where in the first row we presented cross-section of density plots at different propagation planes z. The obtained 2-D Airy beam structure is perfect. In the second row, the Airy beam propagation in the $(\zeta - z)$ plane is shown. The generated Airy beam follows a curved path. It is worth noting that the shift appearing in the direction of the two axis ζ and z, result from the shift that appears in the transmittance sine function, when the latter is expanded near zero (x is an extra term added to the cubic phase). For that reason, the generated Airy beam does not appear in the initial plane ($z = 0$) of the input Gaussian beam. The latter shifts by a given amount which depends on the transmittance parameters.

4.5.2 Generated Dual-Airy beam

In this section we extend our numerical simulations, we converted two input Gaussian beams into 2-D Dual-Airy beam with lozenge geometry, using the transmittance shown in Fig. 4.3(c).

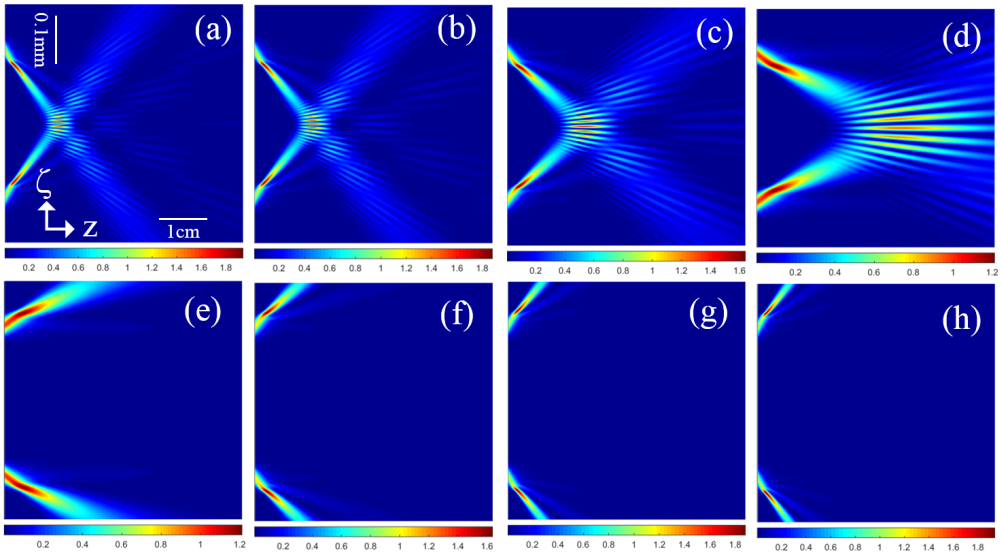

Figure 4.5: 2-D Dual-Airy beams in (ζ, z) plane for different time instants: (a) $t = 0$, (b) $t = 1/16f_a$, (c) $t = 1/8f_a$, (d) $t = 3/16f_a$, (e) $t = 5/16f_a$, (f) $t = 3/8f_a$, (g) $t = 7/16f_a$, (h) $t = 1/2f_a$.

In Fig. 4.5 we show density plots in $(\zeta - z)$ plane at different times t. The Dual-Airy beam evolves from symmetric structures as shown in Fig. 4.5(a)-4.5(d) into anti-symmetric ones as shown in Fig. 4.5(e)-4.5(h). In addition, the symmetric Dual-Airy beams exhibit a dynamic auto-focusing giving birth to interference patterns evolving with time.

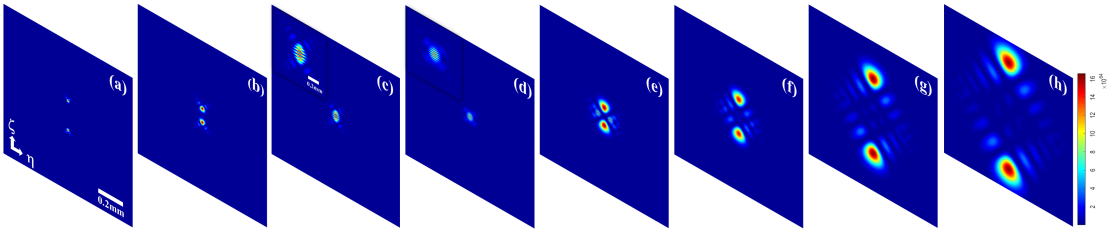

Figure 4.6: (a-h): Dual-Airy beams for different z positions; $z = 20mm, z = 40mm, z = 50mm, z = 60mm, z = 80mm, z = 100mm, z = 150mm, z = 190mm$ respectively at $t = 0$.

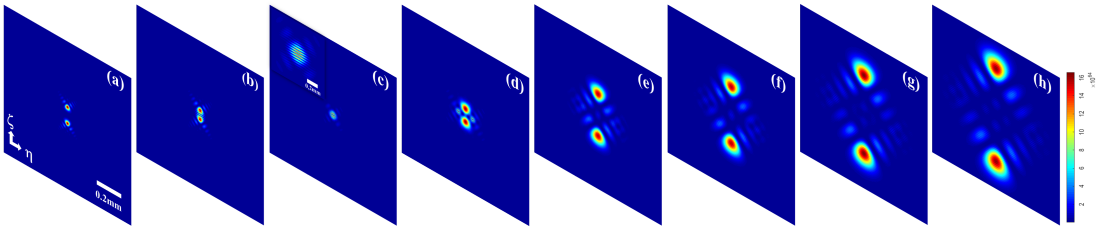

Figure 4.7: (a-h): Dual-Airy beams for different z positions; $z = 40mm, z = 50mm, z = 60mm, z = 80mm, z = 120mm, z = 140mm, z = 170mm, z = 190mm$ respectively at $t = 1/16f$.

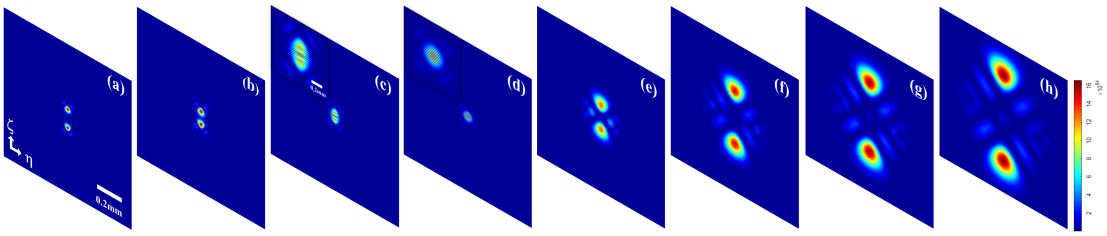

Figure 4.8: (a-h): Dual-Airy beams for different z positions; $z = 50mm, z = 60mm, z = 70mm, z = 80mm, z = 130mm, z = 180mm, z = 210mm, z = 240mm$ respectively at $t = 1/8f$.

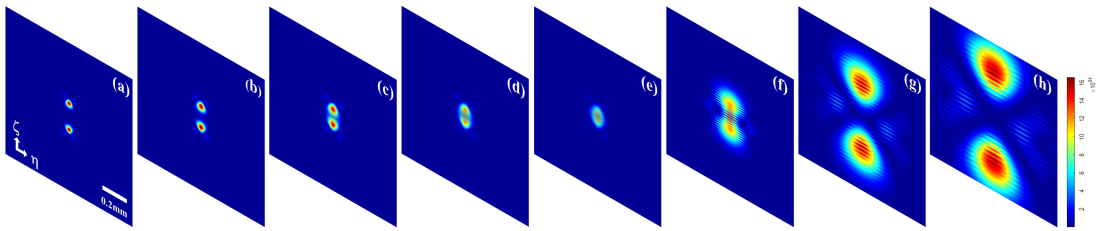

Figure 4.9: (a-h): Dual-Airy beams for different z positions; $z = 70mm, z = 90mm, z = 110mm, z = 120mm, z = 130mm, z = 250mm, z = 400mm, z = 500mm$ respectively at $t = 3/16f$.

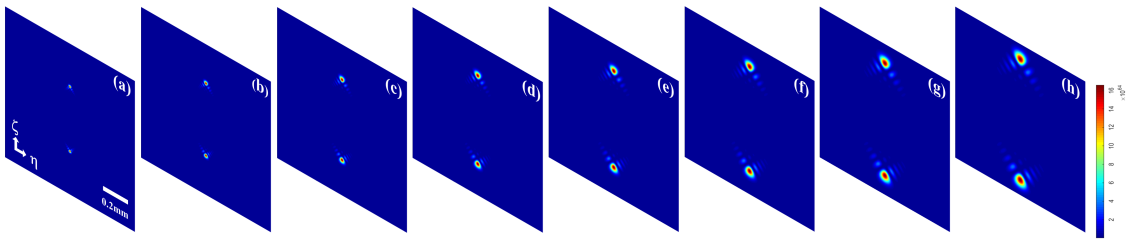

Figure 4.10: (a-h): Dual-Airy beams for different z positions; $z = 20mm, z = 30mm, z = 40mm, z = 50mm, z = 60mm, z = 70mm, z = 80mm, z = 90mm$ respectively at $t = \pi$.

In Fig. 4.6 we show density plots at the cross-section of a 2-D Dual-Airy beam for a fixed time and different z planes. During their propagation, they evolve from an anti-symmetric structure as shown in Fig. 4.6(a)-4.6(c), into auto-focusing as shown in Fig. 4.6(d), and then it inverts its structure to a symmetric one, as illustrated in Fig. 4.6(e)-4.6(h). For a fixed $z = 60mm$ plane and by varying time, t Fig. 4.11 shows the generated 2-D Airy beam cross-section density plots, its structure evolves during time evolution from anti-symmetric to symmetric patterns.

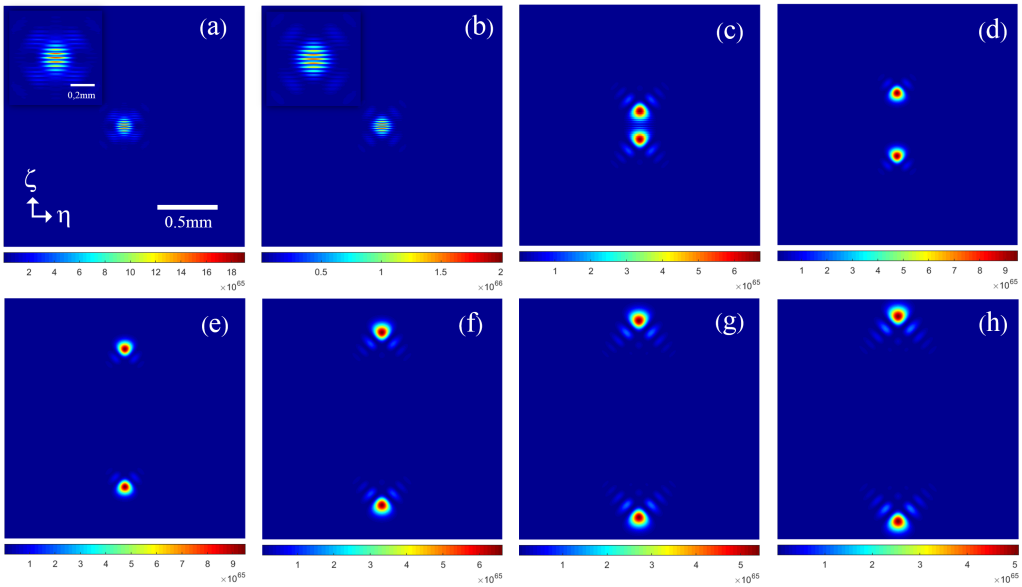

Figure 4.11: Dynamic Dual-Airy beams for different time instants; (a)-(h): $t = 0$, $t = 1/16f_a$, $t = 1/8f_a$, $t = 3/16f_a$, $t = 5/16f_a$, $t = 3/8f_a$, $t = 7/16f_a$, $t = 1/2f_a$ respectively at $z = 60mm$.

4.5.3 Generated Quad-Airy beam

We follow the same method, that we used for generating Dual-Airy beams. Quad-Airy beams are composed by two crossed Dual-Airy beams. The Quad-Airy beam is generated by the same 2-D standing ultrasonic wave, the only difference is the input beams, which have to be four symmetric Gaussian beams, located at vertices of a square or lozenge, it depends on the geometry we want for the generated Quad-Airy beam. In this work, we have chosen a square geometry as shown in Fig. 4.12. It is worth noting that increasing the number of input Gaussian beams will increase the intensity of the superposition of the four Airy beams. The path is the same as in a single Airy beam and Dual-Airy beam, the only difference is the 2-D lattice (structure) of the beam, it shows interesting periodic patterns. To illustrate the behavior of these Quad-Airy beams, which depends on the time evolution of the ultrasonic standing waves, we have

used density plots to show their spatial structure in the transverse plane, for a fixed time $t = 0$ and along propagation axis for different z planes. The resulting Quad-Airy beam shows at the beginning an anti-symmetric structure as shown in Figs. 4.12(a) and 4.12(b). During propagation it auto-focuses in a tight array of spots as shown in Fig. 4.12 (c), then, it auto-inverts its structure from anti-symmetric to symmetric as shown in Figs. 4.12(e)-4.12(h).

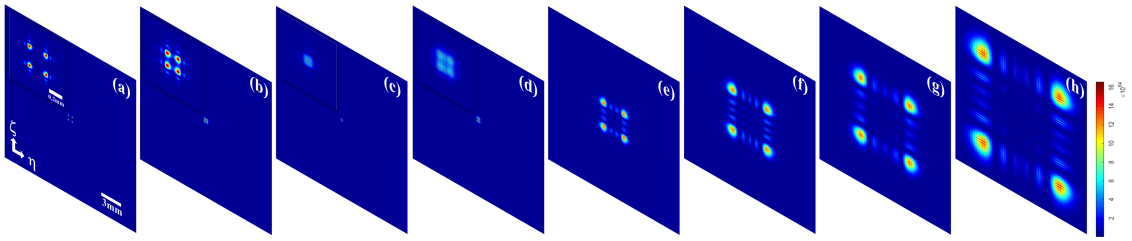

Figure 4.12: (a)-(h): Quad-Airy beams for different z positions;$z = 30mm$, $z = 40mm$, $z = 50mm$, $z = 70mm$, $z = 200mm$, $z = 300mm$, $z = 400mm$, $z = 600mm$ respectively at $t = 0$.

As mentioned before, we have dynamic phase transmittance depending on time. Fig. 4.13, shows cross-section patterns for a constant z and varying time. At fixed $z = 60mm$, we have the smallest array of spots resulting from the superposition of the four parts of the Quad-Airy beam at $t = 0$. After half a period the Quad-Airy beam structure is inverted, and then repeats the cycle each one time period.

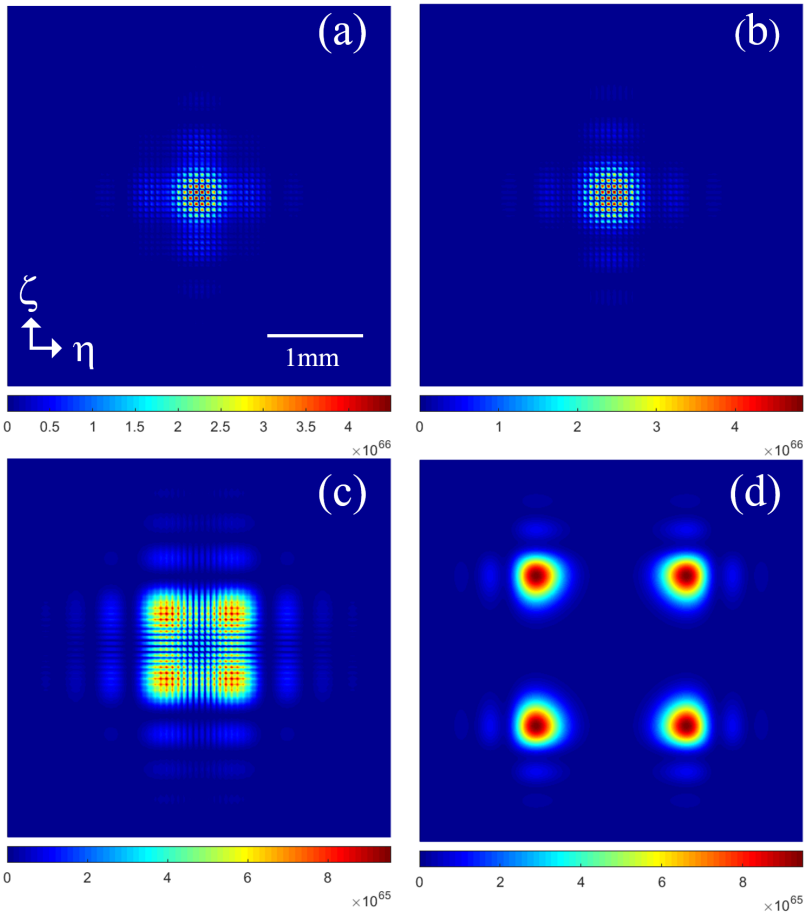

Figure 4.13: Dynamic Quad-Airy beams at fixed $z = 60mm$, and different time instants; (a)-(d): $t = 0$, $t = 1/16f_a$, $t = 1/8f_a$, $t = 3/16f_a$ respectively.

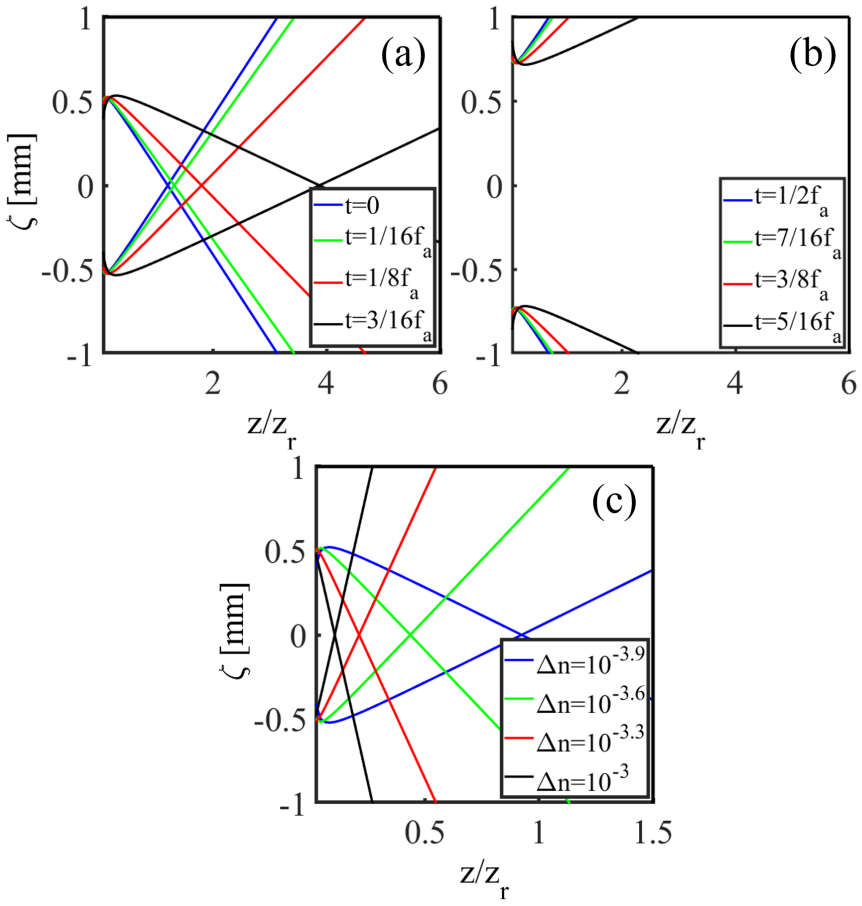

Figure 4.14: Dual-Airy beam paths corresponding to: (a)-(b) Fixed acoustic pressure and different times: $t = 0$, $t = 1/16f_a$, $t = 1/8f_a$, $t = 3/16f_a$, $t = 5/16f_a$, $t = 3/8f_a$, $t = 7/16f_a$, $t = 1/2f_a$. (c) Fixed time and different acoustic pressures giving rise to different refractive index increments Δn.

Finally, Fig. 4.14 shows Airy beam paths at different times t and for different refractive index increments Δn. Since, the generated Airy beams (single, Dual, and Quad) change their geometries from symmetric to anti-symmetric, when the transmittance evolves from one half period to another half period. We have plotted paths in Fig. 4.14(a) for the first half period showing symmetric geometries, and in Fig. 4.14(b) for the other half period showing the anti-symmetric geometries. An interesting result is shown in Fig. 4.14(a), it consists on the dynamic displacement of the crossed beams

giving rise to a dynamic longitudinal scanning, that could be controlled and tuned by acting on the acoustic pressure. In Fig. 4.14(c) we have plotted for a fixed time t, the trajectory of generated Airy beams for different acoustic pressures giving rise to different refractive index increments Δn. By increasing the acoustic pressure, the refractive index increment Δn increases and the crossed Airy beams displace in the propagation direction.

4.6 Conclusion

In this chapter we have proposed a theoretical framework for the generation of a variety of combined Airy beams; Single, Dual, and Quad Airy beams, using 2-D sinusoidal phase transmittance created by a standing ultrasonic wave, where the latter is generated by a piezo-electric transducer. By using the asymptotic expansion of the sine function of the transmittance, we have demonstrated analytically the amplitude expression of all generated Airy beams. We have verified our modeling using detailed numerical simulations, and the results are consistent. By tuning acousto-optic parameters (acoustic pressure and acoustic wavelength) we can change all Airy beam features, such as: curvature, path, and shape. These results could be extended using the same phase transmittance to generate different arrayed Airy beams. We believe that this work will serve as an applicable plan for future experiments involving accelerated beams and lasers beam scanning.

Bibliography

[1] Abdelhalim Bencheikh and Kouider Ferria. Gaussian laser beam tailoring using acoustooptic cell. *Optics & Laser Technology*, 44(4):806–809, 2012.

[2] Joseph W Goodman. *Introduction to Fourier optics*. Roberts and Company Publishers, 2005.

[3] Vallee Olivier and Soares Manuel. *Airy functions and applications to physics*. World Scientific Publishing Company, 2010.

Conclusion and Outlooks

In conclusion, the work presented throughout this thesis manuscript, is dedicated to study the interaction of an incident Gaussian laser beam with an acoustooptic cell. The used acousto optic cell consists on an ultrasound wave propagating in a liquid medium (here we have water), creating a sinusoidal variation on the medium refractive index, what leads to create a sinusoidal variation of the transmittance function (of the acoustooptic cell). Since this latter is tunable at will, we have exploited this feature for structuring and shaping Gaussian laser beam. So, the manuscript is composed of; an introduction, Four chapters, and a conclusion.

Chapter 1, The first part was reserved for the basic theory of Gaussian beams, how was dismantled from the four Maxwell equations, then we determined the parameters which characterize the Gaussian beam such as the radius and the waist. In the second part we have studied the theory of the propagation of the acoustic waves in an aqueous medium and we determine its properties and characteristics such as impedance, celerity, wavelength, frequency, pressure and intensity. once all the basic concepts have been presented, the acousto-optical interaction is set up, where we have defined the working regimes (Bragg regime and Raman-Nath regime). The Raman-Nath regime was chosen for our work due to the acoustic wavelength which is of the order of the input beam width. Over the course of Chapter 2, the intensity distribution diffracted by acoucto-optical cell was caracterizated using the Kurtosis parameter. A flat top beams were obtained successfully with high flatness degree. In the other hand, a Doughnut

beams with a flat inside were also achieved in this study. In Chapter 3, 2D Airy-like beam through truncated acousto-optic cell were successfully generated. Where, 2-D sinusoidal phase transmittance created by a standing ultrasonic wave is used. The final field equation has been developed analytically to have the distribution of the intensity thereafter. The truncation is expressed in the analytical computation by a finite sum of the Gaussian sheaves with the complex coefficients A_n and B_n. We also studied the effect of truncation on the trajectory, where a deviation has been noticed which is a very interesting result for future application in the precision industry. And as we used the acousto-optic cell as a diffracting element, the tunable study is highlighted. Additional parametric studies (effect of acoustic wavelength, and Raman-Nath parameter) were added to better understand the effect of truncation on the obtained Airy beam behavior details. In Chapter 4, the generation of a variety of combined Airy beams; Single, Dual, and Quad Airy beams was successfully obtained based on the same principle of interaction as the previous chapter by using the cell without truncation. The trajectory and the tunable study were controlled for each case as a function of the acoustic wavelength, and the Raman-Nath parameter.

Future work

Throughout this thesis, we studied the interaction between a Gaussian beam and an acoustic wave, to generate some interesting laser beam shapes such as; flat top and doughnut shapes as well as Accelerating beam shapes. The results achieved numerically are interesting to encourage us to verify them on a practical level. The experimental realization of the studies carried out will be our first next step. We would now like to generate also other types of non-diffracting beams such as the Bessel beam and the Mathieu beam by following the same acousto-optical principle. These results obtained for 2D dual and quad Airy beams could be generate different arrayed Airy beams with new distibutions. We believe that this work will serve as an applicable plan for future experiments involving accelerated beams and lasers beam scanning. In particular, we aim to implement using the same phase transmittance for shaping laser beams into

new shapes using a gradient index medium where the interaction takes place instead of the water we used. in the present work.

Abstract: Laser beam shaping technology becomes a hot topic in recent years, which acquired great importance for the scientific community as a result of technical and technological development that the world has known in many fields such; micro industries, military industries, telecommunications, medicine... In this thesis, an acousto-optic technique based-beam shaping is presented through an analytical and a numerical analysis, which converts an input Gaussian beam into different interesting output beam shapes, such as Flat-top, Doughnut, and Airy-like beams. A deep characterization that reveals the generated beam properties is also performed and discussed. As a result, flexible converting a Gaussian beam into a defined shape will have a significant impact on a myriad of current laser applications.

Key words: laser beam shapping, acousto optic interaction, gaussian beam.

Résumé: La technologie de mise en forme des faisceaux lasers est devenue un sujet d'actualité ces dernières années, elle a gagné une place importante au sein de la communauté scientifique, en raison du développement technique et technologique, que le monde a connu dans différents domaines tels que ; la micro industries, l'industrie militaires, les télécommunications, la médecine ... etc

Dans le travail présenté dans cette thèse, une technique de mise en forme de faisceaux lasers, basée sur l'interaction acousto-optique, est présentée à travers une analyse analytique et numérique, par laquelle on est arrivé à convertir un faisceau gaussien à des faisceaux de différentes formes, tels que le faisceau plat, le faisceau creux et le faisceau Airy. Une caractérisation approfondie qui révèle les propriétés du faisceau généré est également effectuée et discutée. En conséquence, la conversion dynamique d'un faisceau gaussien au moyen d'une phase active en des formes de faisceaux bien définie aura surement un impact significatif sur les applications futures des lasers.

Mots clés: la mise en forme des faisceaux laser, interaction acousto-optique, faisceau gaussien.